Robustness Verification and Optimization of Nonlinear Systems

by

Dongchan Lee

B.S., University of Toronto (2014)
S.M., University of Toronto (2016)

Submitted to the Department of Mechanical Engineering
in partial fulfillment of the requirements for the degree of

Doctor of Philosophy in Mechanical Engineering

at the

MASSACHUSETTS INSTITUTE OF TECHNOLOGY

May 2022

Author .....
Department of Mechanical Engineering
April 28, 2022

Certified by .....
Jean-Jacques E. Slotine
Professor of Mechanical Engineering, and Brain and Cognitive Sciences
Thesis Supervisor

Accepted by .....
Nicolas Hadjiconstantinou
Professor of Mechanical Engineering
Chairman, Department Committee on Graduate Theses

Robustness Verification and Optimization

of Nonlinear Systems

by

Dongchan Lee

Submitted to the Department of Mechanical Engineering
on April 28, 2022, in partial fulfillment of the
requirements for the degree of
Doctor of Philosophy in Mechanical Engineering

Abstract

Nonlinear systems allow us to describe and analyze physical and virtual systems, including dynamical systems, power grids, robots, and neural networks. The problems involving nonlinearity pose challenges in providing safety guarantees and robustness in the presence of uncertainty. This thesis provides methods to exploit knowledge on upper and lower bounds on the nonlinearity and solves problems related to robustness verification and optimization subject to uncertain parameters. The first half of the thesis develops the convex restriction of a non-convex feasibility set defined by a set of nonlinear equality and inequality constraints. Convex restrictions provide a closed-form convex quadratic condition that is sufficient for solving a system of nonlinear equations. By replacing the original constraints with the proposed conditions, a non-convex optimization problem can be solved as a sequence of convex optimization problems, with feasibility and robustness guarantees. We demonstrate its applications in Model Predictive Control (MPC), robustness verification of neural networks, robust Optimal Power Flow (OPF) problem, and motion planning in robotics. The second part of the thesis focuses on nonlinear dynamical systems and develops reachability analysis and constrained-input constrained-output analysis for verification problems. We provide an optimization-based method for computing reachable sets around a nominal trajectory. The proposed methods use contraction metrics to find templates for reachable sets. Additionally, we developed constrained-input constrained-output analysis to characterize the relationship between peak magnitudes of input and output signals. Numerical experiments were conducted to demonstrate their applicability to a broad class of nonlinear systems.

Thesis Supervisor: Jean-Jacques E. Slotine
Title: Professor of Mechanical Engineering, and Brain and Cognitive Sciences

Acknowledgments

I would like to express my sincere gratitude to many people who have helped and supported me throughout my graduate studies. Firstly, I am very grateful to my advisor, Professor Jean-Jacques Slotine for his support, motivation, and mentorship. His feedback was always constructive and helpful in shaping my research ideas, and it helped me think more deeply about the core research questions with a bigger picture in mind. I want to thank him for giving me the freedom to pursue my research interest and for always making time to discuss research ideas. I would like to thank my thesis committee members, Professor Domitilla Del Vecchio, Professor Alexander Rakhlin, and Dr. Konstantin Turitsyn for their valuable time and constructive comments.

I want to say a special thank you to Dr. Konstantin Turitsyn for advising me during the first half of my time at MIT, which provided the foundations for many of my research directions. I am grateful to Dr. Audun Botterud for welcoming me to the LIDS community and supporting me throughout the emergency control project. I was also very fortunate to have Prof. Line Roald and Prof. Dan Molzahn as encouraging and inspiring collaborators. I want to thank Dr. Yury Maximov for supporting my research and hosting me over the summer at Los Alamos National Laboratory.

I would like to acknowledge the Department of Energy, National Science Foundation, and Los Alamos National Lab for providing me with funding over the course of my graduate studies.

I would like to thank many friends and colleagues at MIT for being a great support and encouragement. I enjoyed many stimulating discussions with former Nexus members: Sam, Ashkan, Dan, Liviu, Hung, Petr, Katie, and Long. Special thanks to Sam for co-hosting sessions at INFORMS annual meeting with me and to Liviu for hosting me in Zurich. I was happy to find basketball and squash players at my level in my MechE cohort: Jaehyung, Jungki, Yoonho, and Youngsup. I also want to thank friends from Toronto who continued our journey together at MIT: Alex, Zheng, Jinsoo, and Shuvomoy. Special thanks to Alex for being a gym buddy to keep me in shape. I want to thank Suhyoun (Essie) Yu for always being there from the very

start of my doctoral studies.

Last but not least, I would like to thank my family. My parents and brother were always supportive throughout this long journey, and I am grateful for their love and encouragement.

Contents

List of Figures

List of Tables

Chapter 1

Introduction

1.1 Overview

Nonlinear systems are ubiquitous in describing physical phenomena and modeling mathematical problems, ranging from designing electric power grids to neural networks. Identifying and solving the set of equations is often at the core of mathematical analysis and engineering problems. For example, operating and designing electric power grids rely on nonlinear models to predict its reliability and safety. The power flow between nodes has a nonlinear relationship following Kirchoff's voltage and current laws. Delivering electricity from the point of generation to consumption involves feasibility to the power flow equations subject to operational constraints. Another example is designing and operating a robot with kinematic models described by a system of nonlinear equations. The solvability of the kinematic equations describes the feasible configurations of the robot. More recently, neural networks enabled breakthroughs in many domains such as image recognition, natural language processing, and perception. The layers of nonlinear activation functions in neural networks provide the expressive power as a nonlinear function approximator. Understanding the inherent robustness of prediction involves studying the equations involved in neural networks.

The underlying system model described in the above applications is written as a

system of equations denoted by

$$f(x, u) = 0.$$

The variables are partitioned into a parameter vector $u \in \mathbf{R}^m$ and the solution vector $x \in \mathbf{R}^n$. The vector of functions $f : (\mathbf{R}^n, \mathbf{R}^m) \to \mathbf{R}^n$ describes the relationship between x and u. This parameter vector u can describe either deterministic quantities that can be controlled or uncertain quantities that are unknown but have some known properties.

Systems involving dynamics can be described as an ordinary differential equation of the form

$$\dot{x} = f(x, u),$$

where x is the state, and u is the control parameter. The equilibrium (or fixed point) of the system corresponds to $f(x, u) = 0$, which is the nonlinear steady-state equation. The discrete-time version of the dynamical system $x_{t+1} = f(x_t, u_t)$ can be also analyzed by considering nonlinear equations in a finite-time horizon (i.e., $x_1 - f(x_0, u_0) = 0, \ldots, x_{N+1} - f(x_N, u_N) = 0.$)

1.2 Bounding Nonlinearities

A recurring theme throughout this thesis is the idea of bounding the nonlinearity by upper and lower estimators and deriving a result that holds for any function within the bounds. These nonlinear estimators are used to enforce the condition:

$$f(x) = 0,\ x \in \mathcal{D} \quad \Rightarrow \quad f^{\ell}(x) \leq f(x) \leq f^{u}(x).$$

The envelopes provide a necessary condition for satisfying the equality constraint. By enforcing either convexity or concavity to the upper and lower estimators, we develop methods that are computationally tractable. Figure 1-1 shows two examples of such envelopes.

There are a number of methods that exploit known bounds on nonlinearity in

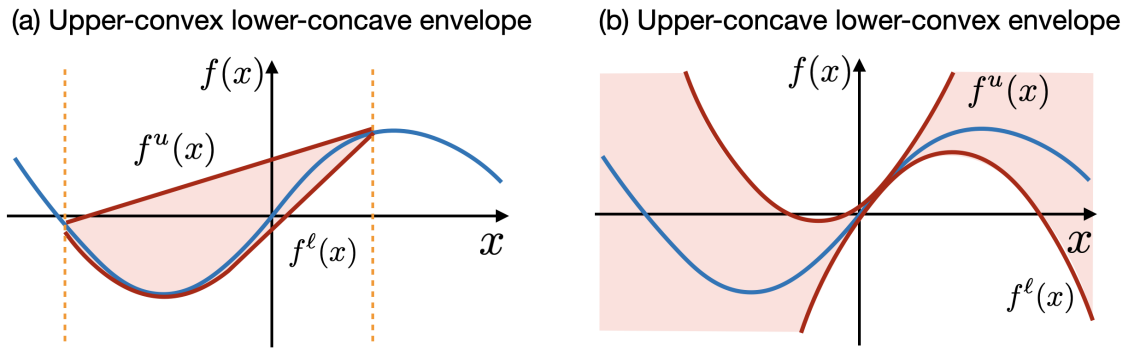

Figure 1-1: Examples of (a) Upper-convex lower-concave envelopes and (b) upper-concave lower convex envelopes denoted by red lines. The blue line is the considered nonlinear function, and the yellow dash line denotes the domain of the state space where the envelope is valid.

optimization and control applications.

The upper-concave lower convex envelope on the left of Figure 1-1 is widely used in *convex relaxation* of nonlinear equality constraints. The inequality constraints $f^\ell(x) \leq f(x) \leq f^u(x)$ is convex when the function f^ℓ is convex and f^u is concave with respect to x. McCormick envelopes for bilinear functions and quadratic envelopes for trigonometric functions are well-known examples in this category [68, 49]. The condition on the left forms a superset of the feasibility set, and solving a minimization problem replaced with convex relaxation finds a lower bound on the global optimal solution.

In control theory, *sector bounds* use a related approach by exploiting a conic bound on the nonlinearity [87, 54]. Absolute stability can be proven if the system is stable with respect to any nonlinear function that belongs to the sector. A one-dimensional sector bound is a special case of upper-convex lower-concave envelopes, but they are not equivalent to general high-dimensional systems. While sector bounds often result in linear matrix inequality constraints in the analysis, the proposed envelopes in this thesis can often yield less conservative results by expressing the bounds by a set of inequalities.

Lipschitz continuity of a function is widely used in proving the existence of a solution for nonlinear equations as well as the convergence of algorithms. The L-

smoothness of a function implies the existence of an upper-convex lower-concave envelope. We provide a lemma below to show how an upper-convex lower-concave envelope can be systematically derived from the L-smoothness of a function.

Quadratic Concave Envelopes

Definition 1. A function, $f : \mathbf{R}^n \to \mathbf{R}$ is called *L-smooth* if it is continuously differentiable and its gradient is Lipschitz continuous with Lipschitz constant L:

$$\|\nabla f(x) - \nabla f(y)\|_2 \leq L\|x - y\|_2, \quad \forall x,\, y \in \mathbf{R}^n. \tag{1.1}$$

If f is twice continuously differentiable, this is equivalent to $\|\nabla^2 f(x)\|_2 \leq L$ for all $x \in \mathbf{R}^n$.

Lemma 1. If $\nabla f(x)$ is uniformly Lipschitz in x with Lipschitz constant L and $x^{(0)} \in \mathbf{R}^n$ be any fixed point, then

$$\begin{aligned} f(x) &\leq f(x^{(0)}) + \nabla f(x^{(0)})^T(x - x^{(0)}) + \frac{L}{2}\|x - x^{(0)}\|_2^2, \\ f(x) &\geq f(x^{(0)}) + \nabla f(x^{(0)})^T(x - x^{(0)}) - \frac{L}{2}\|x - x^{(0)}\|_2^2. \end{aligned} \tag{1.2}$$

Proof. From calculus, $f(x) = f(y) + \int_0^1 \nabla f(z_\alpha)^T(x - y)$ where $z_\alpha = y + \alpha(x - y)$. Then,

$$\begin{aligned} |f(x) - f(y) - \nabla f(y)^T(x - y)| &= \left| \int_0^1 (\nabla f(z_\alpha) - \nabla f(y))^T(x - y) d\alpha \right| \\ \leq \int_0^1 \|\nabla f(z_\alpha) - \nabla f(y)\|_2 \|x - y\|_2 \, d\alpha &\leq L \int_0^1 \alpha \|x - y\|_2^2 \, d\alpha = \frac{L}{2} \|x - y\|_2^2 . \end{aligned}$$

By rearranging and letting $y = x^{(0)}$, we obtain (1.2). □

Equation 1.2 in Lemma 1 provide a upper-convex and lower-concave envelope just based on gradient and Lipschitz constant for any L-smooth function. Given more knowledge of the nonlinearity, a tighter bound can be derived to provide a less

conservative result. Examples of more general envelopes are provided in appendix A.1 for bilinear, trigonometric, and logistic functions.

Co-optimization of Domain

Another technique that utilized in this thesis is co-optimization of the domain,

$$\mathcal{D}(x^\ell, x^u) = \left\{ x \mid x^\ell \leq x \leq x^u \right\},$$

where the domain $\mathcal{D}$ is parametrized by x^ℓ and x^u, which are the upper and lower bounds on the state variable. In some applications, the description of the domain is generalized to a polytope $\mathcal{P}(z^\ell, z^u) = \left\{ x \mid z^\ell \leq Ax \leq z^u \right\}$ rather than a simple box.

The underlying idea is to restrict the domain of interest such that the result is applicable to systems that only exhibit local properties. By parametrizing the domain with the upper and lower bounds on state, we use optimization to search for the domain that satisfies the condition of interest. This is particularly useful when the system does not exhibit global property. Co-optimization of domain is used in Chapters 2, 3, and 6, and the detailed formulation and discussions can be found in the respective chapters.

Robustness to Uncertainty

This thesis deals with both *robustness verification* and *robust optimization* that involves nonlinear equations. We will consider the uncertainties that are unknown but bounded, and a system will be considered *robust* if there is no violation of safety constraints under all realizations within the uncertainty set.

1.3 Thesis Overview and Contributions

In this section, we provide an overview of the thesis structure and summarize the contributions of each chapter. We develop a variety of techniques that provide guarantees for optimization and robustness verification problems. Our approach consists

of exploiting knowledge about nonlinearity and using the information in computation and optimization to provide a provable guarantee.

Chapter 2 propose convex restriction of a feasibility set that is described by a system of nonlinear equations. Convex restriction provides a sufficient condition on the parameter space such that the solution to a system of nonlinear equations is feasible to a set of constraints. There has been a constant interest in finding an inner approximation of the feasibility set in the power systems community due to its importance in the safety of critical infrastructures. In this chapter, we present a convex condition that achieves (i) reduced conservativeness (ii) universality in its applications, and (iii) significant improvement in terms of scalability compared to the existing methods. We exploit sparse representation of nonlinear terms to control the trade-off between scalability and conservativeness of the proposed condition. By replacing the original constraint with the convex restriction, we propose sequential convex restriction to leverage convex optimization for solving non-convex problems. The result of the algorithm is guaranteed to produce a feasible path between the initial point to the final point and is useful for transitioning system settings without violating safety constraints. Related publications can be found in [64, 61].

Chapter 3 presents applications of convex restriction in optimization under uncertainty. We show that robustness can be guaranteed by ensuring that the uncertainty set resides inside of the convex restriction. The existing literature in robust optimization focused on inequality constraints and often neglected nonlinear equality constraints. By assuming that there are some quantities that can be controlled to satisfy equality constraints, equality constraints were solved with linear decision rules or bilevel optimization problems. In this chapter, we provide a method that can capture nonlinear relationships between decision variables in an optimization problem. While the solution of the proposed approach may not be globally optimal, the solution can be found with tractable methods by solving a sequence of convex optimization problems with the guarantee of robustness against the pre-specified uncertainty set Related publications can be found in [64, 65].

Chapter 4 shows applications of convex restriction in control, energy systems,

machine learning, and robotics. The first application considers robust model predictive control under uncertainty and safety constraints. Our framework considers a nonlinear dynamical system subject to disturbances from an unknown but bounded uncertainty set. By viewing the system as a fixed point of an operator acting over trajectories, we propose a convex condition on control actions that guarantee safety against the uncertainty set. Moreover, we consider the implicit time-discretization of system dynamics to increase the prediction horizon and enhance computational accuracy. The second application considers electric power grids with uncertain fluctuations from load demands and renewables. It considers the robust AC OPF problem that minimizes the generation cost while requiring a certain level of system security in the presence of uncertainty. We develop a convex restriction of the AC OPF problem that accounts for uncertainty in the power injections. The third application presents a convex condition that provides guaranteed upper and lower bounds on the outputs of a neural network. We propose a generalized fixed-point interpretation of deep neural networks and use it to derive a convex inner approximation of the feasible space defined by a trained neural network. The coefficients involved in the convex condition can be obtained by backpropagation, with the number of constraints and variables linearly proportional to the number of nodes in the neural network. The proposed condition is a set of linear constraints for a ReLU-activated neural network and a set of convex quadratic constraints for more general activation functions. The last application considers feasible path planning in robot manipulation. We show several test cases with potential failure modes. Related publications can be found in [66, 63, 65].

Chapter 5 presents a reachability analysis framework that utilizes contraction analysis. Reachability analysis is a formal verification method for satisfying safety constraints in discrete-time dynamical systems. In this chapter, we consider reachability analysis based on convex relaxation using upper-concave lower-convex envelopes. By exploiting the knowledge of nonlinearity involved in dynamics, the reachable set is computed by solving convex optimization problems. These bounds provide a guaranteed bound on all possible reachable trajectories given the initial condition. Moreover, the reachable sets are designed using contraction analysis in order to capture the dis-

tortion between neighboring trajectories. The templates for the reachable set can be computed by backpropagation of contraction condition in time. Related publications can be found in [62].

Chapter 6 presents input-output stability analysis of dynamical system around its equilibrium. This chapter develops a method to analyze the input to output relationship when the peak magnitude of the input is constrained by some quantity. We propose a certificate on the disturbance bound such that the output is guaranteed to be bounded by some pre-specified limit. The result guarantees that the system is robust against all possible realizations of magnitude-bounded disturbances. We present a method based on convex optimization to identify the peak magnitude that is tolerable by the system. We propose the concept of constrained-input constrained-output for locally stable systems and extend the bounded-input bounded-output stability result for globally stable systems. The related publication can be found in [60].

Chapter 7 summarizes the thesis contributions and discusses future directions.

Chapter 2

Convex Restriction

2.1 Introduction

This chapter studies methods for guaranteeing solvability and feasibility in the presence of nonlinear equality constraints. Consider the following optimization problem

$$\begin{aligned} \underset{u,x}{\text{minimize}} \quad & f_0(u) \\ \text{subject to} \quad & f(x,u) = 0, \\ & h(x,u) \leq 0, \end{aligned} \tag{2.1}$$

where $f : (\mathbf{R}^n, \mathbf{R}^m) \to \mathbf{R}^n$ and $h : (\mathbf{R}^n, \mathbf{R}^m) \to \mathbf{R}^s$ are vectors of continuous nonlinear functions. The decision variables are divided into $x \in \mathbf{R}^n$, referred to as implicit (decision) variables, and $u \in \mathbf{R}^m$, referred to as explicit (decision) variables. Explicit variables are a subset of decision variables that are independent of the uncertain variables, and implicit variables are a subset of decision variables that adapt to the uncertain variables according to the equality constraints. Note that the number of equality constraints and the number of implicit variables are the same, so the implicit variables can be solved by the system of equations if explicit variables are appropriately chosen. The objective function is $f_0 : \mathbf{R}^m \to \mathbf{R}$ and is a convex function of u without loss of generality. If the objective does not meet this condition, it can be rewritten in this form by adding $f_0(x,u) \leq u_{m+1}$ as a constraint and setting u_{m+1} as

the objective function. Consider the constraints involved in the optimization problem:

$$f(x,u) = 0 \tag{2.2a}$$

$$h(x,u) \leq 0. \tag{2.2b}$$

The feasible domain of explicit variables satisfying the nominal constraints is denoted by

$$\mathcal{U} = \{u \mid \exists\, x,\ f(x,u) = 0,\ h(x,u) \leq 0\}.$$

This notion implies that the solution manifold satisfying $f(x,u) = 0$ is projected onto the space of explicit variables. As an example, consider a quadratic equation, $f(x,u) = x^2 + u_1 x + u_2$. The projection of the manifold leads to the well-known solvability condition, $\mathcal{U} = \{u \mid u_1^2 - 4u_2 \geq 0\}$. The illustration of both manifold and its projection is shown in Figure 2-1. Notice that (a) finding a general solvability condition for a large system of nonlinear equations is generally difficult if possible, and (b) the solvability condition forms a non-convex set.

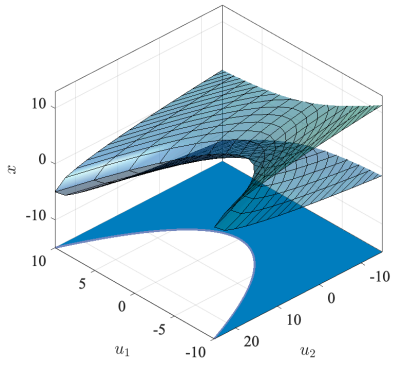

Figure 2-1: Projection of the manifold created by $x^2 + u_1 x + u_2 = 0$ onto the explicit variable space.

We considers the *convex restriction* of $\mathcal{U}$, which we denote by $\mathcal{U}^{\text{cvxrs}} \subseteq \mathcal{U}$. The convex restriction provides a convex sufficient condition for the feasibility of the explicit variable u and can be written with a closed-form expression based on the envelope over the nonlinear functions. We start with preliminaries and will show an extended analysis of the convex restriction and demonstrate its application.

2.2 Preliminaries

2.2.1 Fixed Point Theorems

Fixed point theorems have been widely used in game theory, economics, and dynamical systems [19, 18, 43]. In this chapter, Brouwer's fixed point theorem will be used in the proof to certify the existence of the implicit variable that satisfies the given constraints.

Theorem 1. (Brouwer's Fixed Point Theorem [19]) Let $\mathcal{P} \subseteq \mathbf{R}^n$ be a nonempty compact convex set and $G : \mathcal{P} \to \mathcal{P}$ be a continuous mapping. Then there exists some $x \in \mathcal{P}$ such that $G(x) = x$.

The convex restriction will be derived by designing the fixed-point equation from Newton's iteration and the self-mapping set $\mathcal{P}$ to be a polytope that is parametrized by its affine term. Using the sparse representation of the constraints, we will show that the number of constraints in convex restriction is linearly proportional to the number of constraints of the original problem.

Another well-known is the Banach Fixed Point Theorem, which relies on finding the contraction metric.

Theorem 2. (Banach Fixed Point Theorem [5]) Let $(\mathcal{P}, d)$ be a non-empty complete metric space with a contraction mapping $G : \mathcal{P} \to \mathcal{P}$. That is there exists $q \in [0, 1)$ such that $d(G(x), G(y)) \leq qd(x, y)$ for all x, y in $\mathcal{P}$. Then G admits a unique fixed-point x^*. Furthermore, x^* can be found as follows: start with an arbitrary element x_0 in $\mathcal{P}$ and define a sequence $\{x_n\}$ by $x_n = G(x_{n-1})$, then $x_n \to x^*$.

Moreover, consider the Implicit Function Theorem around some nominal point that satisfies $f(x^{(0)}, u^{(0)}) = 0$.

Theorem 3. (Implicit Function Theorem [36]) Suppose f is continuously differentiable. If $J_{f,0} = \nabla_x f \mid_{(x^{(0)}, u^{(0)})}$ is invertable, then there exists an open set $\mathcal{U}^{\text{cvxrs}} \subseteq \mathbf{R}^m$ containing $u^{(0)}$ such that there exists a unique continuously differentiable function such that $x = \varphi(u)$ and $f(x, u) = 0$ for all $u \in \mathcal{U}^{\text{cvxrs}}$.

The implicit function theorem states that the state x can be expressed as some function of u under the non-singular Jacobian condition, and its implications have been studied extensively [38]. The theorem states that there exists some open neighborhood around the nominal point where the implicit function exists, but it does not define the exact neighborhood. Unlike implicit function theorem, we are concerned with characterizing the domain where the solution is guaranteed to exist, and this is a much less restricted condition.

2.2.2 Decomposed Representation

The constraints in Equations (2.2a) and (2.2b) can be represented as linear combinations of continuous basis functions,

$$\begin{aligned} f(x,u) &= M\psi(z,u) \\ h(x,u) &= L\psi(z,u) \\ z &= Cx, \end{aligned} \tag{2.3}$$

where $\psi : (\mathbf{R}^q, \mathbf{R}^m) \to \mathbf{R}^p$ is a vector of nonlinear basis functions, and $M \in \mathbf{R}^{n\times p}$, $L \in \mathbf{R}^{s\times p}$ and $C \in \mathbf{R}^{q\times n}$ are constant matrices. The variable $z \in \mathbf{R}^q$ is a linearly transformed implicit variable and is assumed to satisfy the following condition.

Condition 1. $\mathbf{rank}(C) = n$. Equivalently, $\mathcal{P} = \{x \mid z = Cx,\ z^\ell \le z \le z^u\}$ is closed for some z^u, $z^\ell \in \mathbf{R}^q$.

The representation in Equation (2.3) satisfying Condition 1 always exists where a trivial example is setting M and C to be the identity matrix, and $\psi(z,u) = f(x,u)$ with $z = x$. The set of basis functions is not unique, and there is a natural trade-off between the complexity and conservatism based on the choice of the basis functions (see Example 3). In addition, the transformed implicit variable z needs to be chosen such that ψ_i is a function of only a finite subset of $\{z_1, ..., z_q\}$. To make this statement more precise, let $\mathcal{I}_k$ denote the set of indices of z that the basis function ψ_k depends on. That is, given $e_j \in \mathbf{R}^q$ is a unit vector with jth element equal to 1 and zero

otherwise,

$$\mathcal{I}_k = \{j \mid \exists\,(z,\, u,\, \varepsilon \neq 0),\quad \psi_k(z,u) \neq \psi_k(z + \varepsilon e_j, u)\}\,.$$

The degree of sparsity of the representation is defined as the worst-case cardinality of $\mathcal{I}_k$ and is denoted by $|\mathcal{I}|$ where

$$|\mathcal{I}| = \max_{k\in\{1,\ldots,p\}} |\mathcal{I}_k|.$$

It will be shown later that the number of constraints involved in the convex restriction grows exponentially with respect to $|\mathcal{I}|$, but there often exists a natural choice of z such that $|\mathcal{I}|$ does not grow with respect to the size of the problem. The following example in a network flow problem shows how these variables can be chosen.

Example 1. (Nonlinear Network Flow Problem) Consider a directed graph $G = (\mathcal{N}, \mathcal{A})$ with θ_i and b_i representing the internal state and external supply at each node $i \in \mathcal{N}$, and E denoting the incidence matrix of the graph. Suppose the flow model between node i and j is given by a nonlinear function $\sigma : \mathbf{R} \to \mathbf{R}$. The conservation of the flows at every node imposes the constraint,

$$b_i + \sum_{j\in I(i)} \sigma(\theta_j - \theta_i) = \sum_{j\in O(i)} \sigma(\theta_i - \theta_j), \qquad \forall i \in \mathcal{N},$$

where $I(i)$ is the set of start nodes of the edges that are incoming to, and $O(i)$ is the set of end nodes of the edges that are outgoing from, node i. Suppose that the supply b_i at node $i = \{2, \ldots, |\mathcal{N}|\}$ are controlled while b_1 balances the overall supply and demand. Then the explicit variables are $u = \begin{bmatrix} b_2 & \ldots & b_{|\mathcal{N}|} \end{bmatrix}^T$, and the implicit variables are $x = \begin{bmatrix} \theta^T & b_1 \end{bmatrix}^T$. Let the transformed variable be $z = \begin{bmatrix} E^T\theta & b_1 \end{bmatrix}$ by choosing $C = \mathbf{blkdiag}(E^T, 1)$. The equality constraint can be represented by $M = \begin{bmatrix} -E & I \end{bmatrix}$ with the basis function $\psi(z,u) = \begin{bmatrix} \sigma(z_1) & \ldots & \sigma(z_{|\mathcal{A}|}) & z_{|\mathcal{A}|+1} & u^T \end{bmatrix}^T$. Since ψ_i has only one variable as the argument for all i, the degree of sparsity is $|\mathcal{I}| = 1$ independent of the size of the network.

An important feature to notice is that the nonlinearity of ψ_k can be arbitrarily

bounded by constraining only $|\mathcal{I}_k|$ variables.

Lemma 2. For all $u \in \mathcal{U}$ and $\varepsilon > 0$, there exists some δ such that if $\mathcal{P}_k = \{x \mid z = Cx,\ z_i^\ell \leq z_i \leq z_i^u,\ \forall\, i \in \mathcal{I}_k\}$ with $z_i^u - z_i^\ell < \delta$ for all $i \in \mathcal{I}_k$, then

$$\max_{x \in \mathcal{P}_k} \psi_k(Cx, u) - \min_{x \in \mathcal{P}_k} \psi_k(Cx, u) < \varepsilon.$$

Proof. Suppose $\mathcal{P} = \{x \mid z = Cx,\ z^\ell \leq z \leq z^u\}$ with $z^u - z^\ell < \delta$. Since the basis functions are continuous, for all $u \in \mathcal{U}$ and $\varepsilon > 0$, there exists δ such that if $z^u - z^\ell < \delta$ then

$$\max_{x \in \mathcal{P}} \psi_k(Cx, u) - \min_{x \in \mathcal{P}} \psi_k(Cx, u) < \varepsilon.$$

Since the $\psi_k(x, u)$ is independent of z_j with $j \in \{1, ..., q\} \setminus \mathcal{I}_k$,

$$\max_{x \in \mathcal{P}_k} \psi_k(Cx, u) - \min_{x \in \mathcal{P}_k} \psi_k(Cx, u) = \max_{x \in \mathcal{P}} \psi_k(Cx, u) - \min_{x \in \mathcal{P}} \psi_k(Cx, u) < \varepsilon.$$

□

The effect of nonlinearity can be controlled by bounding a finite number of variables as we saw in Example 1. This property of the sparse representation will drastically reduce the complexity involved in convex restriction.

2.3 Convex Restriction

The convex restriction provides an analytical expression for a convex sufficient condition for feasibility in Equation (2.2) around some nominal point, $(x^{(0)}, u^{(0)})$. While convex relaxation has a globally optimal outer approximation (i.e., the convex hull of the feasible set,) the convex restriction can have many local regions where it cannot form a larger region due to the restriction as a convex set. We use the nominal point as the reference point around which the convex restriction is constructed. The nominal point is assumed to satisfy the following conditions.

Condition 2. The nominal point, $(x^{(0)}, u^{(0)})$, satisfies

(i) $f(x^{(0)}, u^{(0)}) = 0$ and $h(x^{(0)}, u^{(0)}) \leq 0$, and

(ii) If $f(x, u)$ is differentiable with respect to x, $\nabla_x f(x, u) \mid_{(x^{(0)}, u^{(0)})}$ is invertable.

Condition 2 is not strictly necessary in constructing convex restriction, but it will be used later in the analysis of the algorithm proposed based on the convex restriction. From the Implicit Function Theorem, it is known that there is a neighborhood of solutions where x can be expressed as a function of u if Condition 2 is satisfied. The convex restriction will provide the bounds on the implicit variable and an explicit description of a convex neighborhood where the existence of the implicit variable is guaranteed.

2.3.1 Fixed Point Representation

Here we present the fixed point representation of the equality constraint $f(x, u) = 0$. The equality constraint can be rewritten in the following fixed point form,

$$x = -(M\Lambda C)^{-1} M g(z, u), \tag{2.4}$$

where

$$g(z, u) = \psi(z, u) - \Lambda z,$$

with some matrix $\Lambda \in \mathbf{R}^{p \times q}$. The conservatism of the convex restriction depends on the choice of Λ. Finding the optimal Λ that maximizes the region for convex restriction is difficult, but the Jacobian evaluated at the base point gives a good approximate solution.

- If f is differentiable at the nominal point and $\nabla_x f(x_0, u_0)$ is non-singular, choose Λ as the Jacobian of the basis function with respect to z evaluated at the base point,

  $$\Lambda = \nabla_z \psi(z, u^{(0)}) \mid_{z = z^{(0)}} .$$

  Note that in this case $M\Lambda C = \nabla_x f(x, u^{(0)}) \mid_{x = x^{(0)}}$.

- If f is non-differentiable at the nominal point, choose each element of Λ as

$$\Lambda_{ij} = \partial_{z_j}\psi_i(z, u^{(0)}) \mid_{z=z^{(0)}},$$

where $\partial_{z_j}\psi_i(z,u)$ is the subgradient of ψ_i if ψ_i is locally convex with respect to z_j at the nominal point. If ψ_i is locally concave, then $\partial_{z_j}\psi_i(z,u)$ is the supergradient.

For differentiable functions, the fixed point form in Equation (2.4) is equivalent to a single step of Newton's method, $x = -J_f^{-1}\left(f(x,u) - J_f x\right)$, where $J_f = \nabla_x f(x,u)$.

Given the explicit variable u, Equation (2.4) defines a continuous nonlinear operator $G : \mathbf{R}^n \to \mathbf{R}^n$ that maps the implicit variable x to $-(M\Lambda C)^{-1}Mg(Cx,u)$. By iterating this operator, a sequence of approximate solutions can be generated with the initial condition $x = x^{(0)}$ for an arbitrary value of u. We will verify the existence of the implicit variable by studying this sequence of approximate solutions and inferring the existence of a fixed point of the sequence.

2.3.2 Self-mapping Polytope

Consider the following set of polytopes as a candidate for the self-mapping set in Brouwer's fixed point theorem,

$$\mathcal{P}(b) = \{x \mid Ax \leq b\}$$

where

$$A = \begin{bmatrix} C \\ -C \end{bmatrix}, \; b = \begin{bmatrix} z^u \\ -z^\ell \end{bmatrix}. \tag{2.5}$$

An alternative representation of this polytope is

$$\mathcal{P}(b) = \{x \mid z = Cx, \; z^\ell \leq z \leq z^u\}.$$

Since $\mathcal{P}(b)$ is a polytope satisfying Condition 1, the set is compact and convex. The set of polytopes parameterized by $b \in \mathbf{R}^{2q}$ will be used to guarantee the existence of an implicit solution using Brouwer's fixed point theorem.

Lemma 3. For a given explicit variable u, there exists an implicit variable x that satifies $f(x,u) = 0$ if and only if there exists $b \in \mathbf{R}^{2q}$ such that

$$\max_{x \in \mathcal{P}(b)} K_i g(Cx,u) \leq b_i, \qquad i = 1,\ldots,2q, \tag{2.6}$$

where $K_i \in \mathbf{R}^{1\times p}$ is the ith row of matrix K and

$$K = -A(M\Lambda C)^{-1}M.$$

Proof. The condition in Equation (2.6) implies that $-(M\Lambda C)^{-1}Mg(Cx,u) \in \mathcal{P}(b)$ for all $x \in \mathcal{P}(b)$. Then the set $\mathcal{P}(b)$ is self-mapping with the nonlinear map $G(x) = -(M\Lambda C)^{-1}Mg(Cx,u)$, so there exists an implicit variable $x \in \mathcal{P}(b)$ from Brouwer's fixed point theorem. To prove that this is a necessary condition, suppose there exists $(x^{(0)}, u^{(0)})$ satisfying Equation (2.2a). Choose $b = [(Cx^{(0)})^T\,(-Cx^{(0)})^T]^T$, then for $i = 1,\ldots,2q$, $\max_{x\in\mathcal{P}(b)} K_i g(x,u) = A_i x^{(0)} = b_i$, which satisfies the condition in Equation (2.6). □

2.3.3 Concave Envelopes

Suppose that the function g_k is known to be bounded by some analytical functions g_k^u and g_k^ℓ such that

$$g_k^\ell(z,u) \leq g_k(z,u) \leq g_k^u(z,u),$$

where the envelopes satisfy the following conditions.

Condition 3. g_k^u and g_k^ℓ are over- and under-estimators of g_k such that

(i) g_k^u is convex and g_k^ℓ is concave function of z and u,

(ii) g_k^u and g_k^ℓ are tight at the nominal point,

$$g_k^\ell(z^{(0)}, u^{(0)}) = g_k(z^{(0)}, u^{(0)}) = g_k^u(z^{(0)}, u^{(0)}),$$

(iii) if g is differentiable at the nominal point, the derivatives of estimators are tight,

$$\nabla_z g_k^\ell(z, u^{(0)})\big|_{z=z^{(0)}} = \nabla_z g_k^u(z, u^{(0)})\big|_{z=z^{(0)}},$$
$$\nabla_u g_k^\ell(z^{(0)}, u)\big|_{u=u^{(0)}} = \nabla_u g_k^u(z^{(0)}, u)\big|_{u=u^{(0)}}.$$

Similarly ψ_k^u and ψ_k^ℓ are the over- and under-estimators of ψ_k that satisfy Condition 3. We define the envelope such that the nonlinear function is bounded by a convex over-estimator and a concave under-estimator, which was discussed in Chapter 1. For any continuous function, there exists a concave envelope satisfying Condition 3.

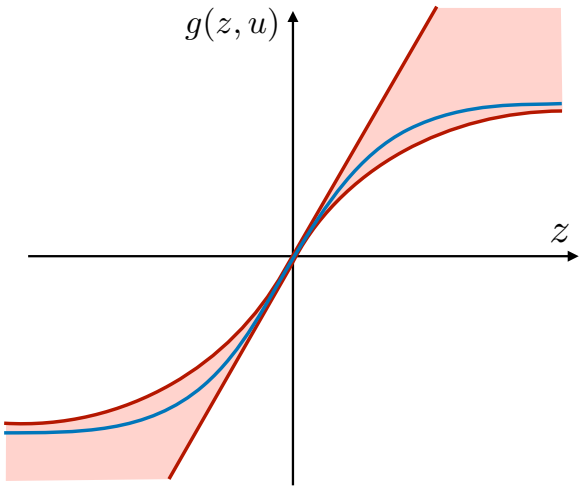

Figure 2-2: Illustration of a upper-convex lower-concave envelope.

An example of such an envelope is shown in Figure 2-2, which turns out to be necessary for enforcing convexity to a restricted set. These envelopes have flipped convexity and concavity compared to the envelopes used in convex relaxation [49, 70]. Given the model of the system, these envelopes are assumed to have a closed-form expression, and examples are provided in Appendix A.1.

2.3.4 Bounds over Intervals

Given the upper-convex lower-concave envelopes, the bound of g_k over the polytope $\mathcal{P}(b)$ can be defined as

$$g^{\ell}_{\mathcal{P},k}(u,b) \leq g_k(z,u) \leq g^{u}_{\mathcal{P},k}(u,b),$$

which is valid for all $z \in \{Cx \mid x \in \mathcal{P}(b)\}$. These bounds are defined as

$$g^{u}_{\mathcal{P},k}(u,b) = \max_{x \in \mathcal{P}(b)} g^{u}_{k}(Cx,u)$$
$$g^{\ell}_{\mathcal{P},k}(u,b) = \min_{x \in \mathcal{P}(b)} g^{\ell}_{k}(Cx,u).$$

Since $g^{u}_{k}(z,u)$ is a convex function, its maximum occurs at at least one of the vertices of the polytope $\mathcal{P}(b)$. Similarly, the minimum of concave $g^{\ell}_{k}(z,u)$ occurs at the vertex. The self-mapping condition in Brouwer's fixed point theorem can be viewed as solving a containment of the polytope $\mathcal{P}(b)$ into the inequality constrained sets Equations (2.6) and (2.2b). Solving the containment problem is generally hard, but it becomes tractable if the polytope is in the vertex representation contained in a convex set [53].

2.3.5 Vertex Tracking

By relaxing the equations with concave envelopes, the interval bound of $g_k(z,u)$ can be expressed by tracking all the vertices of the polytope

$$g^{u}_{\mathcal{P},k}(u,b) = \max_{x \in \partial\mathcal{P}(b)} g^{u}_{k}(Cx,u)$$
$$g^{\ell}_{\mathcal{P},k}(u,b) = \min_{x \in \partial\mathcal{P}(b)} g^{\ell}_{k}(Cx,u),$$

where $\partial\mathcal{P}(b)$ are the vertices of the polytope $\mathcal{P}(b)$. Although the number of vertices of the face-polytope $\mathcal{P}(b)$ grows exponentially with respect to the number of faces, the following lemma shows that only the vertices involved in $\mathcal{I}(k)$ need to be tracked.

Lemma 4. The interval bounds can be expressed with the inequalities

$$\begin{aligned} g^u_{\mathcal{P},k}(u,b) &\geq g^u_k(z,u), \quad \forall z \in \{z \mid z_i \in \{z^\ell_i, z^u_i\}, \forall i \in \mathcal{I}_k\} \\ g^\ell_{\mathcal{P},k}(u,b) &\leq g^\ell_k(z,u), \quad \forall z \in \{z \mid z_i \in \{z^\ell_i, z^u_i\}, \forall i \in \mathcal{I}_k\}, \end{aligned} \tag{2.7}$$

where these inequalities can be expressed by $2^{\mathcal{I}_k+1}$ inequalities by listing all possible vertices.

Lemma 2 from the previous section showed that the nonlinearity can be bounded by controlling $|\mathcal{I}_k|$ variables. Similarly, $g^u_{\mathcal{P},k}$ and $g^\ell_{\mathcal{P},k}$ can be expressed by inequalities involving $|\mathcal{I}_k|$ variables. If the nonlinearity is decomposed in a way such that $|\mathcal{I}_k|$ does not grow with the problem size, the number of constraints involved is also independent of the problem size.

2.3.6 Vertex Pruning

It is not necessary to track all the vertices in Equation (2.7) because the maximum or minimum never occurs at some of those vertices. As an example, consider the bilinear function in Appendix A.1.1. The maximum always occurs at vertices (x^u, y^u) or (x^ℓ, y^ℓ), and it is unnecessary to trace (x^u, y^ℓ) and (x^ℓ, y^u). Many of the vertices can be pruned from the candidates by exploiting this property.

2.3.7 Convex Restriction and its Properties

Given these considerations, the convex restriction of the feasibility set can be expressed as an explicit condition. This condition was first provided in [61].

Theorem 4. (Convex Restriction of Feasibility Set) For a given explicit variable u, there exists an implicit variable x that satisfies $f(x,u) = 0$ and $h(x,u) \leq 0$ if there exists $b \in \mathbf{R}^{2q}$ such that

$$K^+ g^u_{\mathcal{P}}(u,b) + K^- g^\ell_{\mathcal{P}}(u,b) \leq b \tag{2.8a}$$

$$L^+ \psi^u_{\mathcal{P}}(u,b) + L^- \psi^\ell_{\mathcal{P}}(u,b) \leq 0, \tag{2.8b}$$

where $K_{ij}^+ = \max\{K_{ij}, 0\}$ and $K_{ij}^- = \min\{K_{ij}, 0\}$ for each element of K.

Proof. From Condition (2.8a), for $i = 1, \ldots, 2q$,

$$\begin{aligned}
\max_{x \in \mathcal{P}(b)} K_i g(Cx, u) &\leq \max_{x \in \mathcal{P}(b)} \left(K_i^+ g^u(Cx, u) + K_i^- g^\ell(Cx, u) \right) \\
&\leq K_i^+ \max_{x \in \mathcal{P}(b)} g^u(Cx, u) + K_i^- \min_{x \in \mathcal{P}(b)} g^\ell(Cx, u) \\
&= K_i^+ \max_{x \in \partial\mathcal{P}(b)} g^u(Cx, u) + K_i^- \min_{x \in \partial\mathcal{P}(b)} g^\ell(Cx, u) \\
&= K_i^+ g_{\mathcal{P}}^u(u, b) + K_i^- g_{\mathcal{P}}^\ell(u, b) \leq b_i.
\end{aligned}$$

From Lemma 3, there exists a solution for the implicit variable, $x \in \mathcal{P}(b)$. Similarly, from the condition in Equation (2.8b),

$$\max_{x \in \mathcal{P}(b)} L_i \psi(x, u) \leq L_i^+ \psi_{\mathcal{P}}^u(u, b) + L_i^- \psi_{\mathcal{P}}^\ell(u, b) \leq 0, \quad i = 1, \ldots, s,$$

so for all $x \in \mathcal{P}(b)$, $L\psi(Cx, u) \leq 0$. Therefore, there exists an implicit variable satisfying $f(x, u) = 0$ and $h(x, u) \leq 0$. □

This is a sufficient condition for the existence of a feasible implicit variable for a given explicit variable. Note that the condition in Equation (2.8) is a convex constraint with respect to both u and b. This region in the explicit variable space will be denoted by $\mathcal{U}_{(0)}^{\text{cvxrs}} \subseteq \mathcal{U}$ where

$$\begin{aligned}
\mathcal{U}_{(0)}^{\text{cvxrs}} = \{u \mid \exists\, b,\ & K^+ g_{\mathcal{P}}^u(u, b) + K^- g_{\mathcal{P}}^\ell(u, b) \leq b, \\
& L^+ \psi_{\mathcal{P}}^u(u, b) + L^- \psi_{\mathcal{P}}^\ell(u, b) \leq 0\}.
\end{aligned}$$

The subscript (0) denotes that $(x^{(0)}, u^{(0)})$ is used as the nominal point for constructing the convex restriction.

Example 2. (Quadratic Equations) Consider a quadratic equation with $x \in \mathbf{R}$ parametrized by $u \in \mathbf{R}^2$ from the introduction,

$$f(x, u) = x^2 + u_1 x + u_2,$$

where there exist real solutions for x if and only if $u_1^2 - 4u_2 \geq 0$. In addition we consider the inequality constraint, $-2 \leq x \leq 2$. Define $z = x$ and the basis function $\psi(z, u) = f(x, u)$. The residual function is then $g(z, u) = \langle z, z - 2z^{(0)} + u_1 - u_1^{(0)} \rangle + u_2$. The bilinear envelope in Appendix A.1.1 can be applied to z and $z - 2z^{(0)} + u_1 - u_1^{(0)}$ with $\rho_1 = \rho_2 = 1$. Let the derivative of the equation with respect to x evaluated at the nominal point be denoted by $J_0 = 2x^{(0)} + u_1^{(0)}$. The convex restriction condition in Equation (2.8) gives the following closed-form expression,

$$
\begin{aligned}
\mathcal{U}_{(0)}^{\text{cvxrs}} = \{u \mid \exists\, (z^u,\, z^\ell),\ z^u \leq 2,\ z^\ell \geq -2,& \\
-|J_0^{-1}| \left(x^{(0)}(u_1 - u_1^{(0)}) - (x^{(0)})^2 - 0.25(u_1 - u_1^{(0)})^2 + u_2 \right) &\leq z^u, \\
|J_0^{-1}| \left(x^{(0)}(u_1 - u_1^{(0)}) - (x^{(0)})^2 + 0.25(2z^u - 2x^{(0)} + u_1 - u_1^{(0)})^2 + u_2 \right) &\leq -z^\ell, \\
|J_0^{-1}| \left(x^{(0)}(u_1 - u_1^{(0)}) - (x^{(0)})^2 + 0.25(2z^\ell - 2x^{(0)} + u_1 - u_1^{(0)})^2 + u_2 \right) &\leq -z^\ell \}.
\end{aligned}
$$

Figure 2-3 shows this region in explicit variable space where both equality and inequality constraints were considered with the nominal point at $(x^{(0)}, u^{(0)}) = (0, [4, 0])$.

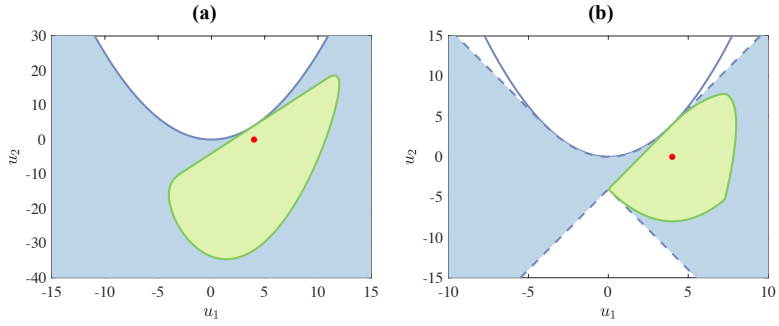

Figure 2-3: The convex restriction of a quadratic equation with (a) the solvability of the equality constraints and (b) the feasibility with the additional inequality constraint, $x \in [-2, 2]$. The blue region shows the true feasible region, and the green region shows the convex restriction. The red dot marks the nominal point.

While the example considers a simple equation, the convex restriction creates a scalable condition for any sparse system of equations where $|\mathcal{I}|$ is finite, independent of the problem size.

Remark 1. (Scalability of Convex Restriction) The number of constraints involved in convex restriction is bounded by $q \cdot 2^{|\mathcal{I}|+2} + 2n + s$.

There are $2n+s$ inequality constraints involved in Equation (2.8), and $\sum_{k=1}^{q} 2^{|\mathcal{I}(k)|}$ inequality constraints involved in g^u, g^ℓ, ψ^u and ψ^ℓ as shown in Equation (2.7). As we saw in Example 1, there exists a representation such that $|\mathcal{I}|$ is independent of the size of the original problem in many applications. Then the number of constraints involved in the convex restriction grows linearly with respect to n and s.

Remark 2. (Retrieval of Implicit Variable) Consider a sequence $\{x_k\}$ generated by $x_k = -(M\Lambda C)^{-1} M g(x_{k-1}, u)$ with $u \in \mathcal{U}^{\text{cvxrs}}$ and the initial condition, $x_0 = x^{(0)}$. If the solution converges to a fixed point, x^*, then $f(x^*, u) = 0$ and $h(x^*, u) = 0$.

Similar to any numerical approach for solving nonlinear equations, the above sequence is not guaranteed to converge. However, the convex restriction condition guarantees that the sequence will not diverge outside of the closed polytope $\mathcal{P}(b)$. Instead of Newton's method, the above iteration can be an alternative method to retrieve the implicit variables more efficiently without requiring the inversion of any matrix.

Lemma 5. (Non-emptiness of Convex Restriction) The convex restriction is non-empty and contains the nominal point. Moreover, if there exists $b \in \mathbf{R}^{2q}$ such that

$$\begin{aligned} K^+ g^u_{\mathcal{P}}(u, b) + K^- g^\ell_{\mathcal{P}}(u, b) &< b \\ L^+ \psi^u_{\mathcal{P}}(u, b) + L^- \psi^\ell_{\mathcal{P}}(u, b) &< 0, \end{aligned} \tag{2.9}$$

the convex restriction contains an open non-empty neighborhood around the nominal point. That is $\forall\, v \in \mathbf{R}^m,\ \exists\, \varepsilon > 0$ such that $u^{(0)} + \varepsilon v \in \mathcal{U}^{\mathbf{cvxrs}}_{(0)}$.

Proof. Let $b^{(0)} = Ax^{(0)}$, then $\mathcal{P}(b) = \{x^{(0)}\}$ since $\mathcal{P}(b)$ is closed. Then,

$$\begin{aligned} K^+ g^u_{\mathcal{P}}(u^{(0)}, b^{(0)}) + K^- g^\ell_{\mathcal{P}}(u^{(0)}, b^{(0)}) &= K g(x^{(0)}, u^{(0)}) = b^{(0)} \\ L^+ \psi^u_{\mathcal{P}}(u^{(0)}, b^{(0)}) + L^- \psi^\ell_{\mathcal{P}}(u^{(0)}, b^{(0)}) &= L \psi(x^{(0)}, u^{(0)}) = 0, \end{aligned}$$

from Condition 3, so $(u^{(0)}, b^{(0)})$ is always feasible to the constraints in Equation (2.8), and thus the convex restriction is always non-empty. Since $g^u_{\mathcal{P}}$ and $g^\ell_{\mathcal{P}}$ are convex and concave respectively, they are continuous functions with respect to b and u. Then for

all $v \in \mathbf{R}^m$, there exists $\varepsilon > 0$ such that

$$K^+ g^u_{\mathcal{P}}(u + \varepsilon v, b) + K^- g^\ell_{\mathcal{P}}(u + \varepsilon v, b) \leq b$$
$$L^+ \psi^u_{\mathcal{P}}(u + \varepsilon v, b) + L^- \psi^\ell_{\mathcal{P}}(u + \varepsilon v, b) \leq 0.$$

Therefore, $u + \varepsilon v \in \mathcal{U}^{\text{cvxrs}}$ from Theorem 4, and the convex restriction contains an open non-empty neighborhood around its nominal point. □

Moreover, the condition in Theorem 4 is an equivalent condition to the original feasibility constraints if the original constraints are convex constraints.

Corollary 1. (Equivalence for Convex Constraints) Suppose that the constraints are convex constraints: $f(x, u)$ is linear and $h(x, u)$ is convex with respect to x and u. Then $u \in \mathcal{U}$ if and only if there exists $b \in \mathbf{R}^{2q}$ that satisfies Equation (2.8).

Proof. Consider the decomposed representation of the constraints using the basis function $\psi(z, u) = \begin{bmatrix} f(z,u)^T & h(z,u)^T \end{bmatrix}^T$ with $z = x$, and $h^u(x, u) = h(x, u)$ since h is already a convex function. Following the convex restriction procedure, the resulting Condition (2.8) can be written as

$$z^\ell \leq -J_f^{-1} f(0, u) \leq z^u \quad \text{and} \quad h_k(z, u) \leq 0, \ \forall z \in \{z \mid z_i \in \{z_i^\ell, z_i^u\}, \ i \in \mathcal{I}_k\}, \quad (2.10)$$

for $k = 1, ..., s$. From Theorem 4, $f(x, u) = 0$ and $h(x, u) \leq 0$. To prove that this is a necessary condition, suppose x and u satisfy $f(x, u) = 0$ and $h(x, u) \leq 0$. Choose $z^u = z^\ell = x$, then it satisfies Equation (2.10), and thus is feasible to Equation (2.8). □

Corollary 1 shows that the convex restriction can retrieve the original feasibility set if the original set is convex. If the feasibility set is non-convex, the convex restriction fundamentally cannot be equivalent to the feasibility set. Note that the condition in Lemma 3 was a necessary and sufficient condition for feasibility, and there were two main steps that introduced conservatism of the convex restriction relative to $\mathcal{U}$. First is the tightness of the concave envelope. This is an unavoidable limitation where the nonlinear functions have to be bounded by concave envelopes. Second is the

decomposition of the basis functions, and the use of the fact that the maximum of the sum is always less than the sum of the maximum,

$$\max_{x\in\mathcal{P}(b)} K_i^+ g^u(Cx,u) \le K_i^+ \max_{x\in\mathcal{P}(b)} g^u(Cx,u).$$

The more variables each combination of g_i and g_j share, the less conservative the convex restriction will be, but the complexity of the restriction will increase as it increases the degree of the sparsity $|\mathcal{I}|$. The next example shows this relationship more explicitly.

Example 3. (Conservatism v.s. Complexity Trade-off) Consider the following system of polynomial equations,

$$\begin{aligned} x_1x_2 + ... + x_1x_n + u_1 &= 0 \\ x_i + u_i &= 0, \quad i = 2, ..., n \\ x_1x_2 + ... + x_1x_n &\le 10. \end{aligned}$$

For a given k, let us select the basis function to be

$$\psi^{(k)}(z,u) = \left[\sum_{i=2}^k x_1x_i, \quad x_1x_{k+1}, \quad ... \quad x_1x_n, \quad x^T, \quad u^T\right]^T,$$

with $z = x$. Decreasing k decomposes the representation further and leads to a more sparse representation. Figure 2-4 shows the trade-off between the conservatism and the complexity as k varies. The conservatism was quantified by solving $\min_{u\in\mathcal{U}_{(0)}^{\text{cvxrs},(k)}} u_1 - u_1^*$ where $\mathcal{U}_{(0)}^{\text{cvxrs},(k)}$ is the convex restriction constructed with the basis function $\psi^{(k)}$ and $u_1^* = -10$ is the global optimal value. The complexity was quantified by the number of constraints involved in the convex restriction, which is proportional to 2^k for a naive implementation without vertex pruning. The degree of sparsity for $\psi_1^{(k)} = \langle x_1, \sum_{i=2}^k x_i\rangle$ is $\mathcal{I}_1 = k$, and the vertex tracking require all combinations of $x_i \in \{x_i^u, x_i^\ell\}$ for $i = 1, ..., k$. However, this is a special case where the vertex pruning drastically reduces the number of constraints regardless of k. The maximum of $\psi_1^{(k)}$ occurs at $(x_1^u, \sum_{i=2}^k x_i^u)$ or $(x_1^\ell, \sum_{i=2}^k x_i^\ell)$ and only 2 vertices need to

be tracked instead of 2^k vertices, and the restriction can scale without sacrificing the performance in this example.

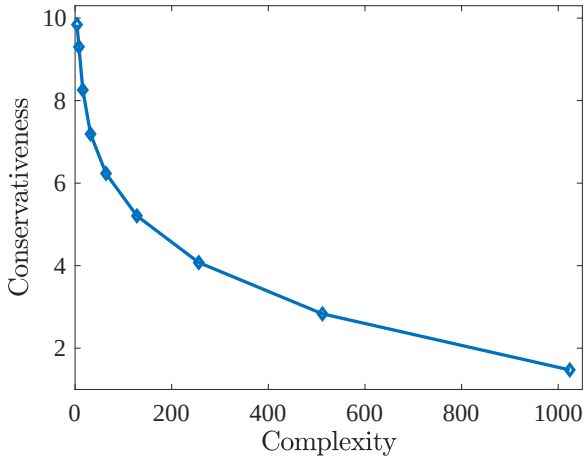

Figure 2-4: Illustration of the trade-off between the complexity and the conservatism. The complexity is quantified by the number of constraints involved, and the conservatism is quantified by the optimality gap.

2.4 Sequential Convex Restriction

In this section, we provide the analysis of the algorithm for solving the optimization problem,

$$\underset{u,x}{\text{minimize}} \quad f_0(u), \quad \text{subject to} \quad f(x,u) = 0,\ h(x,u) \leq 0. \tag{2.11}$$

Sequential convex restriction (SCRS) for nominal constraints belongs to the family of Sequential Convex Optimization, which is a local search method that iteratively solves convex approximations of the original problem. In particular, the related classical algorithms are the Sequential Quadratic Programming (SQP) and trust-region methods [17, 32, 47, 74]. While these methods showed success in practice for solving a large optimization with equality constraints, some of the possible shortcomings were (i) the linearized constraints may be inconsistent, (ii) the solution may be infeasible, and (iii) the iteration may diverge. These shortcomings could be overcome by using extended methods such as Inexact SQP [33, 22, 21]. Sequential convex restriction provides potentially a more elegant way to handle the shortcomings of SQP. An al-

ternative view of SCRS is that the self-mapping set $\mathcal{P}(b)$ can be interpreted as a trust region, and the lifted formulation allows us to co-optimize the decision variables and the trust region cast as a single convex optimization problem.

The problem can be solved by iterating between (a) solving the optimization with convex restriction, and (b) setting the solution as the new nominal point for constructing the convex restriction. The algorithm described here is named sequential convex restriction, and the procedure is described in Algorithm 1 with some termination thresholds $\varepsilon_1, \varepsilon_2, \varepsilon_3 > 0$.

Algorithm 1 Sequential Convex Restriction

Initialization: $u^{(0)}$, $x^{(0)}$, and $k = 0$
while $\|u^{(k+1)} - u^{(k)}\|_2 > \varepsilon_1$ or $\|f_0(u^{(k+1)}) - f_0(u^{(k)})\|_2 > \varepsilon_2$ **do**
  $K = \begin{bmatrix} -I & I \end{bmatrix}^T C(M\Lambda C)^{-1} M$
  $u^{(k+1)} = \arg\min_{u \in \mathcal{U}^{\text{cvxrs}}_{(k)}} f_0(u)$
  $x^{(k+1)} = x^{(k)}$
  while $\|f(x^{(k+1)}, u^{(k+1)}s)\|_2 > \varepsilon_3$ **do**
    $x^{(k+1)} = -(M\Lambda C)^{-1} M g(x^{(k+1)}, u^{(k+1)})$
  end while
  $k := k + 1$
end while

There are three computationally notable steps, which are computing the inverse of the Jacobian to compute K, solving the convex optimization problem with convex restriction, and retrieving the nominal implicit variable. The retrieval of the implicit variable leverages Remark 2 in the proposed algorithm, but this step can be replaced by other procedures such as Newton's method or the Gauss-Seidel method.

2.4.1 Analysis on the Subproblems

Sequential Convex Restriction in Algorithm 1 solves the following convex optimization problem as the subproblems of the algorithm,

$$\begin{aligned} \underset{u,b}{\text{minimize}} \quad & f_0(u) \\ \text{subject to} \quad & K^+ g^u_{\mathcal{P}}(u,b) + K^- g^\ell_{\mathcal{P}}(u,b) \leq b \\ & L^+ \psi^u_{\mathcal{P}}(u,b) + L^- \psi^\ell_{\mathcal{P}}(u,b) \leq 0. \end{aligned} \tag{2.12}$$

The key feature of the convex restriction is that the non-convex constraint can be replaced by a convex approximation that guarantees a feasible solution. Moreover, the containment of the nominal point from Lemma 5 ensures that the optimal value is improved at every iteration.

Corollary 2. (Bounds on the Optimal Cost) Suppose that $u^{(k+1)}$ denotes the solution of the problem in Equation (2.12):

$$u^{(k+1)} = \underset{u \in \mathcal{U}_{(k)}^{\text{cvxrs}}}{\arg\min} f_0(u). \tag{2.13}$$

The optimal value of the problem is bounded by

$$f_0(u^{\text{opt}}) \leq f_0(u^{(k+1)}) \leq f_0(u^{(k)}), \tag{2.14}$$

where u^{opt} is the global optimal solution of the problem in Equation (2.1).

Proof. The lower bound comes from the definition of the global optimal value. From Lemma 5, the convex restriction always contains the nominal point, $u^{(k)} \in \mathcal{U}_{\mathcal{W},(k)}^{\text{cvxrs}}$. Therefore, $\min_{u \in \mathcal{U}_{\mathcal{W},(k)}^{\text{cvxrs}}} f_0(u) \leq f_0(u^{(k)})$. □

2.4.2 Analysis on the Outer-loop of the Algorithm

We show the convergence result for the algorithm, which states that the converged point will satisfy the KKT condition. This is a necessary condition for optimality for non-convex problems.

Corollary 3. (Convergence of SCRS) Suppose the explicit variable u^* is the output of Algorithm 1 such that

$$u^* = \lim_{k \to \infty} \underset{u^{(k+1)} \in \mathcal{U}_{\mathcal{W},(k)}^{\text{cvxrs}}}{\arg\min} f_0(u). \tag{2.15}$$

Then, there exists a corresponding implicit variable x^* such that (x^*, u^*) is feasible and

- $\nabla_x f(x^*, u^*) \mid_{x=x^*}$ is singular, or

- (x^*, u^*) satisfies the KKT condition of the original problem in Equation (2.11).

Proof. The algorithm yields a sequence of explicit variables $\{u^{(k)}\}$ that satisfies $f_0(u^{(k+1)}) \leq f_0(u^{(k)})$ from Corollary 2. Moreover, since the sequence is bounded below by the global optimal solution f_0^*, the sequence converges to a finite value from the Monotone Convergence Theorem. Suppose the converged solution is denoted by (x^*, u^*), which satisfies

$$u^* = \underset{u \in \mathcal{U}_*^{\text{cvxrs}}}{\arg\min} f_0(u), \tag{2.16}$$

where $\mathcal{U}_*^{\text{cvxrs}}$ is the convex restriction with (x^*, u^*) as the nominal point. Without loss of generality, $b^* = \begin{bmatrix} (Cx^*)^T & -(Cx^*)^T \end{bmatrix}^T$ is always a feasible solution for $\mathcal{U}_*^{\text{cvxrs}}$ and is an optimal solution for the above problem. Suppose $\nabla_x f(x^*, u^*) \mid_{x=x^*}$ is non-singular, then $M\Lambda C$ is invertible. Let $\Gamma = -C(M\Lambda C)^{-1}M$, then the following KKT condition is a necessary and sufficient condition for optimality of the problem Equation (2.16),

$$\begin{aligned}
\Gamma^+ g_{\mathcal{P}}^u(u^*, b^*) + \Gamma^- g_{\mathcal{P}}^\ell(u^*, b^*) &\leq z^*, \\
-\Gamma^- g_{\mathcal{P}}^u(u^*, b^*) - \Gamma^+ g_{\mathcal{P}}^\ell(u^*, b^*) &\leq -z^*, \\
L^+ \psi_{\mathcal{P}}^u(u^*, b^*) + L^- \psi_{\mathcal{P}}^\ell(u^*, b^*) &\leq 0, \\
\lambda_1^* \geq 0,\ \lambda_2^* \geq 0,\ \lambda_3^* &\geq 0, \\
\lambda_{1,i}^* \Gamma_i^+ g_{\mathcal{P}}^u(u^*, b^*) + \lambda_{1,i}^* \Gamma_i^- g_{\mathcal{P}}^\ell(u^*, b^*) &= \lambda_{1,i}^* z_i^*,\ i = 1, ..., q, \\
-\lambda_{2,i}^* \Gamma_i^- g_{\mathcal{P}}^u(u^*, b^*) - \lambda_{2,i}^* \Gamma_i^+ g_{\mathcal{P}}^\ell(u^*, b^*) &= -\lambda_{2,i}^* z_i^*,\ i = 1, ..., q, \\
\lambda_{3,i}^* L_i^+ \psi_{\mathcal{P}}^u(u^*, b^*) + \lambda_{3,i}^* L_i^- \psi_{\mathcal{P}}^\ell(u^*, b^*) &= 0,\ i = 1, ..., s, \\
\nabla f_0(u^*) + \sum_{i=1}^q \lambda_{1,i}^* \left\{ \Gamma_i^+ \nabla g_{\mathcal{P}}^u(u^*, b^*) + \Gamma_i^- \nabla g_{\mathcal{P}}^\ell(u^*, b^*) - \nabla z_i(z^*) \right\} & \\
+ \sum_{i=1}^q \lambda_{2,i}^* \left\{ -\Gamma_i^- \nabla g_{\mathcal{P}}^u(u^*, b^*) - \Gamma_i^+ \nabla g_{\mathcal{P}}^\ell(u^*, b^*) + \nabla z_i(z^*) \right\} & \\
+ \sum_{i=1}^q \lambda_{3,i}^* \left\{ L_i^+ \nabla \psi_{\mathcal{P}}^u(u^*, b^*) + L_i^- \nabla \psi_{\mathcal{P}}^\ell(u^*, b^*) \right\} = 0 &
\end{aligned}$$

Since (x^*, u^*) is the nominal point and satisfies Condition 3,

$$g^{\ell}_{\mathcal{P}}(u^*, b^*) = g(z^*, u^*) = g^{u}_{\mathcal{P}}(u^*, b^*),$$
$$\nabla g^{\ell}_{\mathcal{P}}(u^*, b^*) = \nabla g(u^*, b^*) = \nabla g^{u}_{\mathcal{P}}(u^*, b^*).$$

Substitute the above equation and $\nu_i = \sum_{j=1}^{q}(\lambda^*_{2,j} - \lambda^*_{1,j})C_{ji}$ for $i = 1, ..., n$ to the KKT condition of the problem in Equation (2.16), then

$$-(M\Lambda C)^{-1}Mg(x^*, u^*) = x^*,\ L\psi(x^*, u^*) \leq 0,$$
$$\lambda^*_3 \geq 0,\ \lambda^*_{3,i}L_i\psi(x^*, u^*) = 0,\ i = 1, ..., s,$$
$$\nabla f_0(u^*) + \sum_{i=1}^{n}\nu^*_i\left\{[(M\Lambda C)^{-1}]_i M\nabla g(z^*, u^*) + \nabla x_i(x^*)\right\} + \sum_{i=1}^{q}\lambda^*_{3,i}L_i\nabla\psi(z^*, u^*) = 0$$

which is the KKT condition of the nominal problem in Equation (2.11) where the equality constraint is replaced by its fixed point representation. □

Next, we show an example of a polynomial optimization problem that includes nonlinear equality constraints.

Example 4. (Polynomial Optimization) In this example, a polynomial optimization problem adapted from an example in [76] is considered,

$$\begin{aligned}
\underset{u,x}{\text{minimize}} \quad & u_3 \\
\text{subject to} \quad & x_1^2 + x_2^2 + x_3^2 - 1 = 0 \\
& u_1 - x_1^2 = 0 \\
& u_2 - x_2x_3 = 0 \\
& x_1u_1 - 2x_1u_2 + x_2 \leq u_3.
\end{aligned}$$

The robust optimization will be considered later in Example 6. Figure 2-5 shows the convergence of the sequential convex restriction described in Algorithm 1 with four different initial conditions. The triangular-shaped feasible region is created by the solvability condition, and the convergence of the algorithm depends on the initialization. The global optimal point is achieved with the initial condition in (a) in

this example. The initial conditions in (a) and (b) arrive at a local optimal point satisfying the KKT conditions. The initial condition in (c) arrives at the boundary of the constraints where $\nabla_x f(x, u^*) \mid_{x=x^*}$ becomes singular.

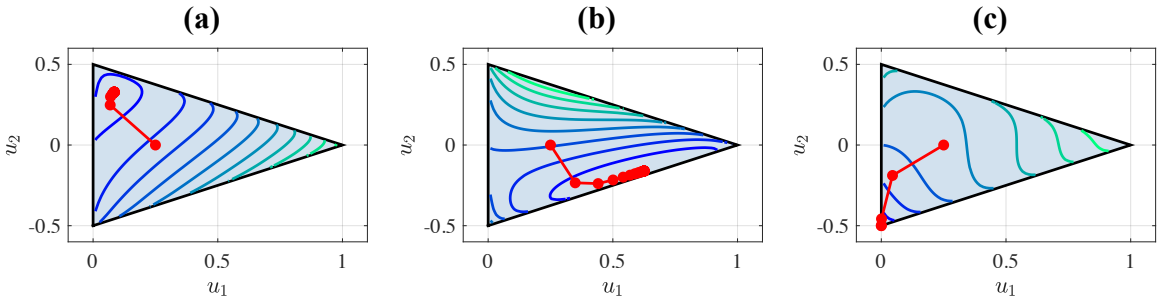

Figure 2-5: The blue region represents the feasible region and the contour line shows the objective function where the darker contour lines have the lower objective value. The initial condition for the explicit variable was set to $u^{(0)} = [0.25,\ 0,\ 2]$. The initial condition for the implicit variable was set to (a) $[0.5,\ -0.866,\ 0]$, (b) $[-0.5,\ -0.866,\ 0]$, and (c) $[0.5,\ 0,\ 0.866]$.

A larger example for solving the Optimal Power Flow problem using the sequential convex restriction was considered in [63] as an extension of [61] for a power systems application. Chapter 3 will discuss its applications in more detail.

While Corollary 3 gives some convergence guarantees, the sequential convex restriction is subject to the Maratos effect similar to SQP, and therefore the fast convergence may not be guaranteed near the optimal point [74]. We see this effect in Figure 2-5 (c) as the nominal point progresses to the local optimal point at a slow rate. Nevertheless, the main motivation for using SCRS is that the optimization problem can include uncertain variables in the presence of nonlinear equality constraints. We discuss its applications to robust optimization in the next chapter.

2.5 Concluding Remarks

In this chapter, we presented a convex sufficient condition for solving a system of nonlinear equations under parametric changes and propose a sequential convex optimization method for solving robust optimization problems with nonlinear equality constraints. By bounding the nonlinearity with concave envelopes and using Brouwer's

fixed point theorem, the sufficient condition is expressed in terms of closed-form convex inequality constraints. Using these conditions, a non-convex optimization problem can be solved as a sequence of convex optimization problems, with a feasibility guarantee.

Chapter 3

Robust Optimization with Equality Constraints

3.1 Convex Restriction under Uncertainty

In this chapter, we extend the convex restriction to include uncertain variables that are bounded by a given uncertainty set $\mathcal{W} \subseteq \mathbf{R}^r$. The nominal optimization problem is similar to Chapter 2, but it now includes uncertain variables:

$$\begin{aligned} \underset{u,x}{\text{minimize}} \quad & f_0(u) \\ \text{subject to} \quad & f(x,u,w) = 0, \\ & h(x,u,w) \leq 0, \quad \forall w \in \mathcal{W}, \end{aligned} \tag{3.1}$$

where $f : (\mathbf{R}^n, \mathbf{R}^m, \mathbf{R}^r) \to \mathbf{R}^n$ and $h : (\mathbf{R}^n, \mathbf{R}^m, \mathbf{R}^r) \to \mathbf{R}^s$ are vectors of continuous nonlinear functions. The decision variables are divided into $x \in \mathbf{R}^n$, referred to as implicit (decision) variables, and $u \in \mathbf{R}^m$, referred to as explicit (decision) variables. Explicit variables are a subset of decision variables that are independent of the uncertain variables, and implicit variables are a subset of decision variables that adapt to the uncertain variables according to the equality constraints. Note that the number of equality constraints and the number of implicit variables are the same, so the implicit variables can be solved by the system of equations if explicit variables are

appropriately chosen. Uncertain variables are denoted by $w \in \mathbf{R}^r$ and are restricted to the uncertainty set, $\mathcal{W}$. This is a semi-infinite optimization problem, where the constraints need to be satisfied for all realizations of the uncertainty set.

We will assume that there is some known nominal value of the uncertain variable, which will be denoted by $w^{(0)}$. The set of robust feasible explicit variables is denoted by

$$\mathcal{U}_{\mathcal{W}} = \{u \mid \forall w \in \mathcal{W},\, \exists\, x,\ f(x,u,w) = 0,\ h(x,u,w) \leq 0\}.$$

3.1.1 General Nonlinear Constraints

The idea remains the same as Chapter 2, and the only modification is that the concave envelopes need to capture the uncertainty set. Similar to the previous section, the nonlinear functions are expressed by a linear combination of basis functions,

$$f(x,u,w) = M\psi(z,u,w) \tag{3.2a}$$

$$h(x,u,w) = L\psi(z,u,w). \tag{3.2b}$$

Equation (3.2a) can be written in the fixed point form,

$$x = -(M\Lambda C)^{-1} M g(z,u,w),$$

where $g(z,u,w) = \psi(z,u,w) - \Lambda z$. The matrix Λ is chosen in the same way as Section 2.3.1, which is $\Lambda = \nabla_z \psi(z, u^{(0)}, w^{(0)}) \mid_{z=z^{(0)}}$ for differentiable f. Let the nonlinear residual be bounded by

$$g^{\ell}_{\mathcal{W},k}(z,u) \leq g_k(z,u,w) \leq g^{u}_{\mathcal{W},k}(z,u),\ \forall w \in \mathcal{W}, \tag{3.3}$$

where $g^u_{\mathcal{W}}$ is a convex over-estimator and $g^{\ell}_{\mathcal{W}}$ is a concave under-estimator of g over the uncertainty set $\mathcal{W}$. Note that when we introduce uncertainty, we cannot satisfy Condition 3 (ii) and (iii) for the basis functions that are dependent on the uncertain variable. Then the bounds over $\mathcal{P}$ and $\mathcal{W}$ can be expressed as

$$g^u_{\mathcal{PW},k}(u,b) \geq g^u_{\mathcal{W},k}(z,u) \quad \forall z \in \{z \mid z_i \in \{z^\ell_i, z^u_i\}, \forall i \in \mathcal{I}_k\}$$
$$g^\ell_{\mathcal{PW},k}(u,b) \leq g^\ell_{\mathcal{W},k}(z,u) \quad \forall z \in \{z \mid z_i \in \{z^\ell_i, z^u_i\}, \forall i \in \mathcal{I}_k\},$$

where the subscript $\mathcal{PW}$ indicates that it is a valid bound over the self-mapping polytope and the uncertainty set. Given these definitions, the following theorem provides a robust feasibility condition.

Theorem 5. (Robust Feasibility under General Uncertainty) For a given explicit variable u, there exists an implicit variable x that satisfies $f(x,u,w) = 0$ and $h(x,u,w) \leq 0$ for all $w \in \mathcal{W}$ if there exists $b \in \mathbf{R}^{2q}$ such that

$$K^+ g^u_{\mathcal{PW}}(u,b) + K^- g^\ell_{\mathcal{PW}}(u,b) \leq b \tag{3.4a}$$
$$L^+ \psi^u_{\mathcal{PW}}(u,b) + L^- \psi^\ell_{\mathcal{PW}}(u,b) \leq 0. \tag{3.4b}$$

Proof. The proof remains mostly similar to Theorem 4. The condition (3.4) ensures that

$$\begin{aligned}\sup_{w\in\mathcal{W}} \max_{x\in\mathcal{P}(b)} K_i g(x,u,w) &\leq K_i^+ \max_{x\in\mathcal{P}(b)} g^u_{\mathcal{W}}(x,u) + K_i^- \min_{x\in\mathcal{P}(b)} g^\ell_{\mathcal{W}}(x,u) \\ &\leq K_i^+ g^u_{\mathcal{PW}}(u,b) + K_i^- g^\ell_{\mathcal{PW}}(u,b) \leq b_i.\end{aligned}$$

From Lemma 3, there exists an implicit variable $x \in \mathcal{P}(b)$ for all $w \in \mathcal{W}$. Similarly,

$$\sup_{w\in\mathcal{W}} \max_{x\in\mathcal{P}(b)} L_i \psi(x,u) \leq L_i^+ \psi^u_{\mathcal{PW}}(u,b) + L_i^- \psi^\ell_{\mathcal{PW}}(u,b) \leq 0, \quad i = 1,\ldots,s,$$

so for all $x \in \mathcal{P}(b)$ and $w \in \mathcal{W}$, $L\psi(Cx,u,w) \leq 0$. Therefore, there exists an implicit variable satisfying $f(x,u,w) = 0$ and $h(x,u,w) \leq 0$ for all $w \in \mathcal{W}$. □

The convex restriction under uncertainty will be denoted by $\mathcal{U}^{\text{cvxrs}}_{\mathcal{W},(0)} \subseteq \mathcal{U}_{\mathcal{W}}$ where

$$\begin{aligned}\mathcal{U}^{\text{cvxrs}}_{\mathcal{W},(0)} = \{u \mid \exists\, b,\ & K^+ g^u_{\mathcal{PW}}(u,b) + K^- g^\ell_{\mathcal{PW}}(u,b) \leq b, \\ & L^+ \psi^u_{\mathcal{PW}}(u,b) + L^- \psi^\ell_{\mathcal{PW}}(u,b) \leq 0\}.\end{aligned}$$

The subscript (0) again indicates that the nominal point is $(x^{(0)}, u^{(0)}, w^{(0)})$.

When the explicit variables are given and the uncertainties are introduced, there will be generally a set of implicit variables defined through the realizations of the uncertain variable and the nonlinear equality constraints. The following remark shows the motivation and the role of the self-mapping polytope, which provides a bound on the set of implicit variables.

Remark 3. Given u and b satisfying the condition (3.4), the self-mapping polytope, $\mathcal{P}(b)$, is an outer-approximation of all possible solutions for implicit variables under the uncertainty set $\mathcal{W}$.

This gives an intuitive reason behind the convex restriction condition in the lifted domain with the parameter b, representing the bound on the implicit variables. The following is an example of the envelopes that capture the uncertain variables.

Example 5. (Nonlinear Network Flow Problem under Uncertainty) Consider a special case of Example 1 where the nonlinear flow models are subject to uncertainty,

$$\sigma(x_i - x_j) = w \sin(x_i - x_j),$$

where the line parameter is subject to the uncertain variable w, bounded by $\mathcal{W} = \{w \mid w \in [w^\ell, w^u]\}$. Given that the basis functions are the same as Example 1, the residual function is

$$g_i(z_i, w) = w \sin z - w^{(0)} \cos(z^{(0)}) z,$$

for $i = 1, \ldots, p$. The concave envelope under uncertainty is then

$$\begin{aligned} g^u_{\mathcal{W},k}(z,u) &\geq \tilde{w} \sin z_i^{(0)} + \tilde{w} \cos z_i^{(0)}(z_i - z_i^{(0)}) + \frac{\tilde{w}}{2}(z_i - z_i^{(0)})^2 - w^{(0)} \cos(z_i^{(0)}) z_i \\ g^\ell_{\mathcal{W},k}(z,u) &\leq \tilde{w} \sin z_i^{(0)} + \tilde{w} \cos z_i^{(0)}(z_i - z_i^{(0)}) - \frac{\tilde{w}}{2}(z_i - z_i^{(0)})^2 - w^{(0)} \cos(z_i^{(0)}) z_i, \end{aligned}$$

for $\tilde{w} \in \{w^u, w^\ell\}$. The convex restriction with the uncertain variable can be derived by Theorem 5 using the envelope above.

Although this procedure is able to capture general nonlinearity and uncertainty sets, finding the upper-convex lower-concave envelope in Equation (3.3) could be

difficult for some of the applications. The next section discusses a special class of constraints where the robustness can be incorporated systematically.

3.1.2 State-Uncertainty Separable Constraints

In this section, we study a special case where the basis functions can be expressed by a sum of two nonlinear functions where implicit variables, x, and uncertain variables, w, are separable. Consider

$$\begin{aligned} f(x,u,w) &= M[\psi(x,u) + \alpha(u,w)] \\ h(x,u,w) &= L[\psi(x,u) + \beta(u,w)], \end{aligned} \tag{3.5}$$

where $\alpha : (\mathbf{R}^m, \mathbf{R}^r) \to \mathbf{R}^p$ and $\beta : (\mathbf{R}^m, \mathbf{R}^r) \to \mathbf{R}^p$ are vectors of continuous functions. The functions α_i are linear with respect to w, and $L_j\beta$ are concave with respect to w for all $u \in \mathbf{R}^m$. The uncertainty set $\mathcal{W}$ is a given non-empty, convex and compact set. The derivation here closely follows [10], which provides a systematic way to construct the robust counterpart for nonlinear uncertain inequality constraints. Let us denote the convex conjugate of some function φ as

$$\varphi^*(v) = \sup_{w \in \mathbf{dom}(\varphi)} \{v^T w - \varphi(w)\},$$

and the concave conjugate of φ as

$$\varphi_*(v) = \inf_{w \in \mathbf{dom}(\varphi)} \{v^T w - \varphi(w)\}.$$

The indicator function of the set $\mathcal{W}$ is

$$\delta(w \mid \mathcal{W}) = \begin{cases} 0 & \text{if } w \in \mathcal{W} \\ \infty & \text{otherwise.} \end{cases}$$

The support function of $\mathcal{W}$ is the conjugate of the indicator function,

$$\delta^*(v \mid \mathcal{W}) = \sup_{w \in \mathbf{R}^r} \{v^T w - \delta(w \mid \mathcal{W})\} = \sup_{w \in \mathcal{W}} v^T w. \tag{3.6}$$

When the implicit variables and the uncertain variables are separable, there is a systematic way to derive the robust feasible condition using the support function and the conjugate function.

Theorem 6. (Robust Feasibility for State-Uncertainty Separable Constraints) For a given explicit variable u, there exists an implicit variable x that satisfies constraints $f(x, u, w) = 0$ and $h(x, u, w) \leq 0$ for all $w \in \mathcal{W}$ if there exists $b \in \mathbf{R}^{2q}$, $v \in \mathbf{R}^r$, and $y \in \mathbf{R}^r$ such that

$$K^+ g^u_{\mathcal{P}}(u, b) + K^- g^\ell_{\mathcal{P}}(u, b) + \xi(u, v) \leq b \tag{3.7a}$$

$$L^+ \psi^u_{\mathcal{P}}(u, b) + L^- \psi^\ell_{\mathcal{P}}(u, b) + \zeta(u, y) \leq 0, \tag{3.7b}$$

where $\xi : (\mathbf{R}^m, \mathbf{R}^r) \to \mathbf{R}^{2q}$ and $\zeta : (\mathbf{R}^m, \mathbf{R}^r) \to \mathbf{R}^s$ are given by

$$\begin{aligned} \xi_i(u, v) &= \delta^*(v \mid \mathcal{W}) - [K_i \alpha]_*(u, v) \\ \zeta_j(u, y) &= \delta^*(y \mid \mathcal{W}) - [L_j \beta]_*(u, y). \end{aligned} \tag{3.8}$$

Proof. From the definition of indicator functions and using the Fenchel duality [13],

$$\begin{aligned} \max_{w \in \mathcal{W}} K_i \alpha(u, w) &= \max_{w \in \mathbf{R}^r} \{K_i \alpha(u, w) - \delta(w \mid \mathcal{W})\} \\ &= \min_{v \in \mathbf{R}^r} \{\delta^*(v \mid \mathcal{W}) - [K_i \alpha]_*(u, v)\}. \end{aligned}$$

Then using the expression above,

$$\begin{aligned} \max_{w \in \mathcal{W}} \max_{x \in \mathcal{P}(b)} [K_i g(Cx, u) + K_i \alpha(u, w)] &\leq \max_{x \in \mathcal{P}(b)} K_i g(Cx, u) + \max_{w \in \mathcal{W}} K_i \alpha(u, w) \\ &\leq K_i^+ g^u_{\mathcal{P}}(u, b) + K_i^- g^\ell_{\mathcal{P}}(u, b) + \xi_i(v, u) \leq b_i, \end{aligned}$$

for some $v \in \mathbf{R}^r$. Therefore, the existence of $v \in \mathbf{R}^r$ guarantees the existence of an

implicit variable under all realizations of $w \in \mathcal{W}$. Similarly, for $j = 1, \ldots, s$,

$$\sup_{w \in \mathcal{W}} \max_{x \in \mathcal{P}(b)} [L_j \psi(Cx, u) + L_j \beta(Cx, u)] \leq L_j^+ \psi_{\mathcal{P}}^u(u, b) + L_j^- \psi_{\mathcal{P}}^\ell(u, b) + \zeta_j(u, y) \leq 0,$$

therefore, there exists an implicit variable satisfying $f(x, u, w) = 0$ and $h(x, u, w) \leq 0$ for all $w \in \mathcal{W}$. □

There is a table of closed-form expressions for ξ and ζ in Equation (3.8) depending on the function and the uncertainty set. We refer readers to [10] for those cases, and we will show only one special case where those functions are linear with respect to w.

3.1.3 Additive Uncertainty Constraints

We consider again a special case of state-uncertainty separable constraints in Equation (3.5) where α and β are linear functions of w such that

$$\begin{aligned} f(x, u, w) &= M[\psi(x, u) + Bw] \\ h(x, u, w) &= L[\psi(x, u) + Dw], \end{aligned} \tag{3.9}$$

where $B \in \mathbf{R}^{n \times r}$ and $D \in \mathbf{R}^{s \times r}$ are constant matrices. In addition, the uncertainty sets considered here are norm-bounded uncertainty sets,

$$\begin{aligned} \mathcal{W}^Q(\gamma) &= \left\{ w \mid \|w - w^{(0)}\|_2 \leq \gamma \right\} \\ \mathcal{W}^B(\gamma) &= \left\{ w \mid \|w - w^{(0)}\|_\infty \leq \gamma \right\}, \end{aligned} \tag{3.10}$$

where $\gamma \in \mathbf{R}$ represents the margin. As $\gamma \to 0$, the uncertainty set vanishes, and the analysis on the nominal constraints applies. Moreover, there is the following manipulation to convert any general nonlinear uncertainty into additive uncertainty.

Remark 4. Any nonlinear constraint, $f(x, u, w) = 0$ and $h(x, u, w) \leq 0$, can be replaced with the additive uncertainty representation, $\tilde{f}(\tilde{x}, u, w) = 0$ and $\tilde{h}(\tilde{x}, u, w) \leq$

0. The functions $\tilde{f} : (\mathbf{R}^{n+r}, \mathbf{R}^m, \mathbf{R}^r) \to \mathbf{R}^{n+r}$ and $\tilde{h} : (\mathbf{R}^{n+r}, \mathbf{R}^m, \mathbf{R}^r) \to \mathbf{R}^s$ are

$$\tilde{f}(\tilde{x}, u, w) = \begin{bmatrix} f(x, u, x_w) \\ x_w - w \end{bmatrix}, \ \tilde{h}(\tilde{x}, u, w) = h(x, u, x_w) \tag{3.11}$$

where $x_w \in \mathbf{R}^r$ and $\tilde{x} = \begin{bmatrix} x^T & x_w^T \end{bmatrix}^T$. The replaced condition is equivalent to the original constraint, and the uncertainty w enters the nonlinear equation as an additive term.

When the system of nonlinear equations can be represented with the additive uncertainty, the following theorem provides a sufficient condition for robust feasibility.

Corollary 4. (Robust Feasibility for Additive Uncertainty) Suppose that the uncertainty set is given by a norm-bounded set, $\mathcal{W}(\gamma) = \{w \mid \|w\| \leq \gamma\}$. For a given explicit variable u, there exists an implicit variable x that satisfies $f(x, u, w) = 0$ and $h(x, u, w) \leq 0$ for all $w \in \mathcal{W}(\gamma)$ if there exists $b \in \mathbf{R}^{2q}$ such that

$$K^+ g^u_{\mathcal{P}}(u, b) + K^- g^\ell_{\mathcal{P}}(u, b) + \xi(\gamma) \leq b \tag{3.12a}$$

$$L^+ \psi^u_{\mathcal{P}}(u, b) + L^- \psi^\ell_{\mathcal{P}}(u, b) + \zeta(\gamma) \leq 0, \tag{3.12b}$$

where for $i = 1, \ldots, n$ and $j = 1, \ldots, s$, ξ_i and ζ_j are given by the following table depending on the type of uncertainty set.

Table 3.1: Required robustness margin for ellipsoidal and interval uncertainty sets

	$\mathcal{W}^Q(\gamma)$	$\mathcal{W}^B(\gamma)$
$\xi_i(\gamma)$	$K_i B w^{(0)} + \gamma \|K_i B\|_2$	$K_i B w^{(0)} + \gamma \|K_i B\|_\infty$
$\zeta_j(\gamma)$	$L_j D w^{(0)} + \gamma \|L_j D\|_2$	$L_j D w^{(0)} + \gamma \|L_j D\|_\infty$

Proof. This is a special case of Theorem 6 with $\alpha(u, w) = Bw$ and $\beta(u, w) = Bw$, so Equation (3.8) can be used to compute ξ and ζ. Since α and β are linear functions with respect to w, their concave conjugate functions are $[K_i \alpha]_*(u, v) = 0$ with $v = (K_i B)^T$,

and $[L_j\beta]_*(u, y) = 0$ with $y = (L_j D)^T$. Substituting v and y to the support function,

$$\xi_i(\gamma) = \delta^*(v \mid \mathcal{W}^Q(\gamma)) \mid_{v=(K_iB)^T} = K_iBw^{(0)} + \gamma\|K_iB\|_2$$
$$\zeta_j(\gamma) = \delta^*(y \mid \mathcal{W}^Q(\gamma)) \mid_{y=(L_jD)^T} = L_jDw^{(0)} + \gamma\|L_jD\|_2.$$

Similarly, the margins ξ and ζ can be derived for the uncertainty set $\mathcal{W}^B(\gamma)$. □

Here the size of the uncertainty set is parametrized by γ where the larger the γ, the more robust the system is against the uncertain variable. The robustness of a solution $(x^{(0)}, u^{(0)})$ is often defined as how much uncertainty a solution can tolerate without violating the constraints. With convex restriction and additive uncertainty constraints, the lower bound on the margin can be computed by solving a convex optimization problem.

Corollary 5. (Robustness Margin) Suppose that $\gamma \in \mathbf{R}$ is given by solving the following optimization problem,

$$\begin{aligned} \underset{\gamma,b}{\text{maximize}} \quad & \gamma \\ \text{subject to} \quad & K^+ g^u_{\mathcal{P}}(u^{(0)}, b) + K^- g^\ell_{\mathcal{P}}(u^{(0)}, b) + \xi(\gamma) \leq b \\ & L^+ \psi^u_{\mathcal{P}}(u^{(0)}, b) + L^- \psi^\ell_{\mathcal{P}}(u^{(0)}, b) + \zeta(\gamma) \leq 0, \end{aligned} \tag{3.13}$$

where ξ and ζ are linear functions of γ given in Corollary 4. Then the explicit variable $u^{(0)}$ has a corresponding implicit variable x satisfying $f(x, u, w) = 0$ and $h(x, u, w) \leq 0$ for all realizations of the uncertainty set $\mathcal{W}(\gamma) = \{w \mid \|w - w^{(0)}\| \leq \gamma\}$.

In addition to finding the robustness margin of a solution, the explicit variable $u^{(0)}$ can be iteratively updated to find the optimal solution given the nonlinear equality and inequality constraints.

3.2 Robust Optimization

In this section, we extend the sequential convex restriction to solve the robust optimization problems with nonlinear equality constraints in Equation (3.1).

Many classes of robust optimization problems are known to have counterparts that can be solved with a finite and explicit optimization problem, however, those results are limited to nonlinear inequality constraints [9, 15, 12, 3, 11, 14, 16, 44]. The equality constraints were mostly assumed to be linear and studied under a special context [41, 23]. The equality constraint was considered in [93], but it relies on the first-order approximation around its neighborhood and does not provide a rigorous guarantee.

3.2.1 Sequential Convex Restriction for Robust Optimization

In this section, we develop the algorithm to solve the robust optimization in Equation (3.1),

$$\begin{aligned} \underset{u}{\text{minimize}} \quad & f_0(u) \\ \text{subject to} \quad & \forall w \in \mathcal{W},\ \exists\, x \in \mathbf{R}^n,\ f(x,u,w) = 0,\ h(x,u,w) \leq 0. \end{aligned}$$

The non-convex constraints in this problem can be restricted to convex constraints by the conditions provided in Theorem 4 for the nominal constraints and Theorem 5 for constraints including uncertainty. Special cases such as state-uncertainty separable constraints or additive uncertainty constraints can use the convex restrictions in Theorem 6 and Corollary 4, respectively. Similar to nominal optimization problem, we iterate between (a) solving the optimization with convex restriction, and (b) setting the solution as the new nominal point for constructing the convex restriction. Algorithm 2 provides the full algorithm with termination thresholds $\varepsilon_1, \varepsilon_2, \varepsilon_3 > 0$.

3.2.2 Analysis on the Optimality Gap

On the other hand, sequential convex restriction described in Algorithm 2 gives a guarantee for robustness against the given uncertainty set. Moreover, we discussed a number of results for the convex restriction of the nominal constraints, and these results imply that SCRS for robust optimization problems will yield a good approximate solution. One thing to note is that while SCRS guarantees robustness, optimality is

Algorithm 2 Sequential Convex Restriction for Robust Optimization Problem

Initialization: $u^{(0)}$, $x^{(0)}$, and $k = 0$
while $\|u^{(k+1)} - u^{(k)}\|_2 > \varepsilon_1$ or $\|f_0(u^{(k+1)}) - f_0(u^{(k)})\|_2 > \varepsilon_2$ **do**
  $K = \begin{bmatrix} -I & I \end{bmatrix}^T C(M\Lambda C)^{-1}M$
  $u^{(k+1)} = \arg\min_{u \in \mathcal{U}^{\text{cvxrs}}_{\mathcal{W},(k)}} f_0(u)$
  $x^{(k+1)} = x^{(k)}$
  while $\|f(x^{(k+1)}, u^{(k+1)}, w^{(0)})\|_2 > \varepsilon_3$ **do**
    $x^{(k+1)} = -(M\Lambda C)^{-1}Mg(x^{(k+1)}, u^{(k+1)}, w^{(0)})$
  end while
  $k := k + 1$
end while

not necessarily guaranteed. The following remark provides a practical way to quantify the optimality gap.

Corollary 6. (Optimality Gap for Robust Optimization Problem) Suppose that u^* denotes the converged solution of Algorithm 2. The optimality gap can be bounded by

$$f_0(u^*) - f_0(u^{\text{robust-opt}}) \leq f_0(u^*) - f_0(u^{\text{nominal-opt}}), \tag{3.14}$$

where $u^{\text{robust-opt}}$ is the globally optimal solution for the robust optimization problem in Equation (3.1), and $u^{\text{nominal-opt}}$ is the globally optimal solution of the nominal problem in Equation (2.11).

Proof. Since the nominal uncertainty is a special case in the uncertainty set, $w^{(0)} \in \mathcal{W}$, it follows that $f_0(u^{\text{nominal-opt}}) \leq f_0(u^{\text{robust-opt}})$. A simple rearrangement leads to the condition in Equation (3.14). □

Next, we show an example in polynomial optimization subject to additive uncertainties.

Example 6. **(Polynomial Optimization)** Consider the robust optimization problem

in Example 4 where the uncertainty set is $\mathcal{W} = \{w \mid \|w\|_2 \leq \gamma\}$ with $\gamma > 0$:

$$\begin{aligned} \underset{u,x}{\text{minimize}} \quad & u_3 \\ \text{subject to} \quad & x_1^2 + x_2^2 + x_3^2 - 1 = 0 \\ & u_1 - x_1^2 + w_1 = 0 \\ & u_2 - x_2 x_3 + w_2 = 0 \\ & x_1 u_1 - 2 x_1 u_2 + x_2 \leq u_3, \ \forall w \in \mathcal{W}^{\mathcal{Q}}(\gamma). \end{aligned}$$

In this example, the uncertainty is additive to the nonlinear equation, and the condition from Corollary 4 was used to guarantee robustness. Figure 3-1 shows the illustration of the results for various sizes of the uncertainty set and initial conditions.

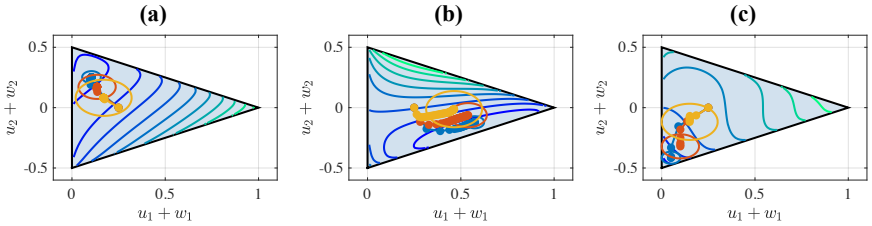

Figure 3-1: The convergence of sequential convex restriction with $\gamma = 0.05$ (blue), $\gamma = 0.1$ (red), and $\gamma = 0.15$ (yellow).

3.3 Concluding Remarks

In this chapter, we have developed the sequential convex restriction for solving a robust optimization problem with nonlinear equality and inequality constraints. We expand the convex restriction of nominal constraints and develop sufficient conditions for robust feasibility against the given uncertainty set. The algorithm guarantees the robust feasibility of the solution at every iteration by leveraging the conditions from convex restriction.

Chapter 4

Applications of Convex Restriction

In this chapter, we present several applications of convex restriction for systems with equality constraints. These applications are some of the standard problems in various fields of study. We first study Model Predictive Control (MPC) problem where the system is governed by nonlinear dynamics. The second application solves the Optimal Power Flow (OPF) problem to deal with nonlinear AC power flow equations in electric power grids. The third application deals with neural network robustness verification problems where nonlinear activation functions enter as nonlinear equality constraints. The last application considers robot kinematics and shows a path planning algorithm based on convex restriction.

4.1 Model Predictive Control (MPC)

Model Predictive Control (MPC) has remained a popular control strategy due to its ability to incorporate complex dynamical systems and safety constraints. One of MPC's advantages is its elegant formulation for considering safety constraints in safety-critical applications such as navigation, robotics, power systems, and chemical plant regulation. Advances in sensing and computation provide new opportunities for MPC formulation to tackle a broader range of systems, where mathematical models can be readily estimated using data. However, uncertainties in models or sensors can cause the system to deviate from the planned trajectory, and there is a need to

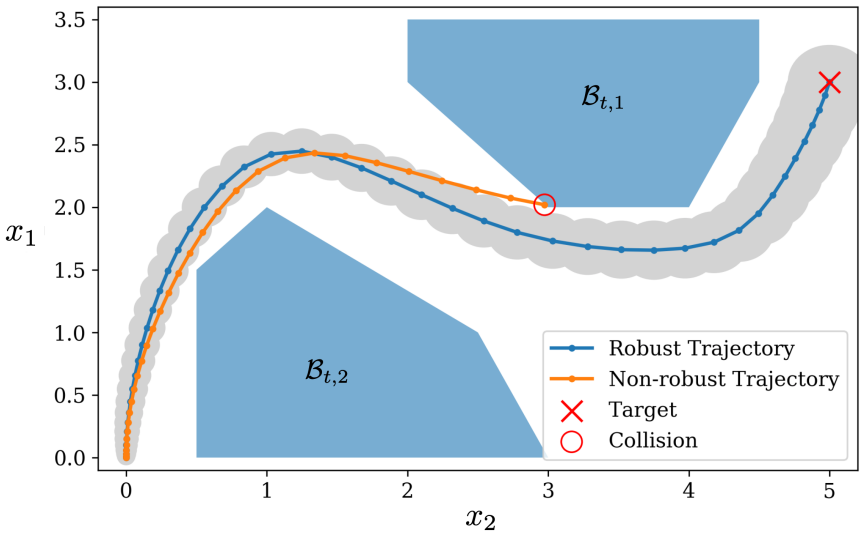

Figure 4-1: Examples of a non-robust and a robust trajectory are shown. Two blocks, $\mathcal{B}_{t,1}$ and $\mathcal{B}_{t,2}$, are the obstacles that the agent needs to avoid. The non-robust trajectory collides at the red circle while the robust trajectory is able to reach the target point without collision.

consider robustness in safety-critical applications.

One of the natural ways to guarantee robustness is to construct a tube or a funnel around a nominal trajectory that contains all possible realizations of the state trajectory under disturbances [24, 55, 81, 7]. An example is shown in Figure 4-1, where the grey tube around the robust trajectory represents the bound on possible realizations of trajectories under uncertainty. If the performance specifications are met within the tube, the controller is verified to be robust against a range of model variations and noise.

4.1.1 Constrained Robust Model Predictive Control Problem

In this section, we provide an overview of the MPC problem with safety and robustness constraints. We consider both the explicit and implicit time-discretization.

1. Explicit time-discretization (Forward Euler): The explicit scheme approximates the differential equation by

$$x_{t+1} = x_t + h \cdot f(x_t, u_{t+1}, w_{t+1}), \tag{4.1}$$

where x_{t+1} can be computed explicitly given x_t.

2. Implicit time-discretization (Backward Euler): The implicit scheme approximates the diffential equation by

$$x_{t+1} = x_t + h \cdot f(x_{t+1}, u_{t+1}, w_{t+1}), \tag{4.2}$$

where x_{t+1} can be obtained by solving a system of nonlinear equations given x_t. Implicit time-discretization schemes admit a more accurate solution compared to the explicit scheme and may use a larger step size h to predict a longer horizon.

The robust MPC problem solves the following optimization problem over a finite horizon of N time steps:

$$\begin{aligned}
\underset{u,x}{\text{minimize}} \quad & c(x,u) \\
\text{subject to} \quad & \forall w_t \in \mathcal{W}_t,\ \forall w_{\text{init}} \in \mathcal{W}_{\text{init}}, \\
& x_0 = w_{\text{init}}, \\
& \text{for} \ \ t = 0, ..., N-1, \\
& \qquad x_{t+1} \in \mathcal{X}_{t+1},\ u_t \in \mathcal{U}_t, \\
\text{(if explicit)} \quad & x_{t+1} = x_t + h \cdot (f(x_t, u_t) + w_t), \\
\text{(if implicit)} \quad & x_{t+1} = x_t + h \cdot (f(x_{t+1}, u_t) + w_t).
\end{aligned} \tag{4.3}$$

The objective function considers the worst-case cost under uncertainty, defined by

$$c(x,u) = \max_{w_t \in \mathcal{W}_t} \left(\sum_{t=0}^{N-1} [c_{x,t}(x_t) + c_{u,t}(u_t)] + c_{x,N}(x_N) \right), \tag{4.4}$$

where $c_{x,t} : \mathbf{R}^n \to \mathbf{R}$ and $c_{u,t} : \mathbf{R}^m \to \mathbf{R}$ for $t = 1, \ldots, N$ are convex cost functions for states and control actions, respectively. The implementation of MPC follows the receding horizon fashion where the first control action of the solution from (4.3) is applied to the plant, and the remaining computed control actions are discarded. This process is repeated with the new system state set to the initial condition.

Modeling Safety Constraints

The state of the system is constrained by safety constraints, which forms a general nonconvex set denoted by $\mathcal{X}_t$. As an example, these constraints could include physical obstacles that the navigating agent must avoid and safety limits that the system and controller need to respect. We represent the safety constraints in the form of avoiding s convex obstacles at time t. The state is declared feasible or safe if $x_t \in \mathcal{X}_t$ or equivalently,

$$x_t \notin \mathcal{B}_{t,(i)}, \quad i = 1, \ldots, s, \tag{4.5}$$

where $\mathcal{B}_{t,(i)} \subseteq \mathbf{R}^n$, $i = 1, \ldots, s$ are convex sets representing the obstacles. The subscript t denotes that the obstacle may be time-dependent to represent moving obstacles. The subscript (i) denotes the index of the obstacle. The safety constraint can be represented as an intersection of the complement of convex obstacles such that

$$\mathcal{X}_t = \left(\bigcup_{i=1}^{s} \mathcal{B}_{t,(i)} \right)^C = \bigcap_{i=1}^{s} \mathcal{B}_{t,(i)}^C, \tag{4.6}$$

where $\mathcal{B}_{t,(i)}^C$ denotes the complement of the set $\mathcal{B}_{t,(i)}$. The safety constraints are assumed to be represented with a finite number of obstacles. This representation includes the majority of practically relevant applications such as the ground vehicle navigation problem.

Modeling Uncertainty Sets

We provide two types of uncertainty sets as examples:

$$\begin{aligned} \mathcal{W}^Q(\gamma) &= \{w \mid (w - w^{(0)})^T \Sigma^{-1} (w - w^{(0)}) \leq \gamma^2\}, \\ \mathcal{W}^I(\gamma) &= \{w \mid |w_i - w_i^{(0)}| \leq \gamma_i,\ i = 1, \ldots, r\}, \end{aligned} \tag{4.7}$$

where the superscripts Q and I denote ellipsoidal and interval uncertainty sets, respectively. The ellipsoidal uncertainty set, $\mathcal{W}^Q(\gamma)$, has its center at the nominal value, $w^{(0)} \in \mathbf{R}^r$, with variance and radius of $\Sigma \in \mathbf{R}^{r \times r}$ and $\gamma \in \mathbf{R}$, respectively. The interval uncertainty set, $\mathcal{W}^I(\gamma)$, is upper and lower bounded by $w_i^{(0)} + \gamma_i$ and $w_i^{(0)} - \gamma_i$

for each element of w_i.

4.1.2 Dynamics as a System of Nonlinear Equations

We consider the *system trajectories* as a collection of system variables over the prediction horizon N. The state, control and uncertainty trajectories will be denoted by $\mathbf{x} \in \mathbf{R}^{(n+1)\cdot N}$, $\mathbf{u} \in \mathbf{R}^{m\cdot N}$, and $\mathbf{w} \in \mathbf{R}^{n+r\cdot N}$ where

$$\mathbf{x} = \begin{bmatrix} x_0 \\ \vdots \\ x_N \end{bmatrix}, \quad \mathbf{u} = \begin{bmatrix} u_1 \\ \vdots \\ u_N \end{bmatrix}, \quad \mathbf{w} = \begin{bmatrix} w_{\text{init}} \\ w_1 \\ \vdots \\ w_N \end{bmatrix}.$$

The uncertain variable, $\mathbf{w}$, includes both the uncertain initial condition, w_{init}, and the uncertain dynamics $w_0, \ldots, w_{N-1}$. We will write that $\mathbf{w} \in \mathcal{W}(\gamma)$ if $w_{\text{init}} \in \mathcal{W}_{\text{init}}(\gamma)$ and $w_t \in \mathcal{W}_t(\gamma)$ for $t = 1, \ldots, N$. The cardinality of $\mathbf{x}$ will be denoted by $|\mathbf{x}|$ so that $\mathbf{x} \in \mathbf{R}^{|\mathbf{x}|}$.

The dynamic equations of N time steps can be cast as a system of nonlinear equations by concatenating the equality constraints in (4.3). This formulation converts the dynamic equation in (5.1) to finding a zero of a set of algebraic equations $F(\mathbf{x}, \mathbf{u}, \mathbf{w}) = 0$ where $F : (\mathbf{R}^{|\mathbf{x}|}, \mathbf{R}^{|\mathbf{u}|}, \mathbf{R}^{|\mathbf{w}|}) \to \mathbf{R}^{|\mathbf{x}|}$ defines the dynamics of the system. For example, the dynamic equation in (4.1) can be rearranged to $x_t + h \cdot f(x_t, u_{t+1}, w_{t+1}) - x_{t+1} = 0$, and the initial can be written as $w_{\text{init}} - x_0 = 0$. Then, the set of equations for explicit time-discretization scheme is given by

$$F_{\text{explicit}}(\mathbf{x}, \mathbf{u}, \mathbf{w}) = \begin{bmatrix} w_{\text{init}} - x_0 \\ x_0 + h \cdot f(x_0, u_1, w_1) - x_1 \\ \vdots \\ x_{N-1} + h \cdot f(x_{N-1}, u_N, w_N) - x_N \end{bmatrix}, \tag{4.8}$$

and the equations for implicit scheme is given by

$$F_{\text{Implicit}}(\mathbf{x}, \mathbf{u}, \mathbf{w}) = \begin{bmatrix} w_{\text{init}} - x_0 \\ x_0 + h \cdot f(x_1, u_1, w_1) - x_1 \\ \vdots \\ x_{N-1} + h \cdot f(x_N, u_N, w_N) - x_N \end{bmatrix}. \tag{4.9}$$

The number of equations in $F(\mathbf{x}, \mathbf{u}, \mathbf{w})$ is the same as the number of unknown variables in $\mathbf{x}$, which is the state trajectory given the control and uncertain variables.

Fixed-Point Analysis of Discrete-time Dynamical Systems

Consider the nonlinear equation $F(\mathbf{x}, \mathbf{u}, \mathbf{w}) = 0$ defined in (4.8) or (4.9) depending on the choice of time-discretization scheme. Let $\frac{\partial F}{\partial \mathbf{x}} \Big|_{(0)} = \frac{\partial F}{\partial \mathbf{x}} \Big|_{\mathbf{x}=\mathbf{x}^{(0)}, \mathbf{u}=\mathbf{u}^{(0)}, \mathbf{w}=\mathbf{w}^{(0)}}$ denote the Jacobian of F with respect to $\mathbf{x}$ evaluated at the nominal system trajectory. Note that the variables $\mathbf{x}^{(0)}$, $\mathbf{u}^{(0)}$, and $\mathbf{w}^{(0)}$ denote the nominal trajectories. The dynamic equation, $F(\mathbf{x}, \mathbf{u}, \mathbf{w}) = 0$, can be written as the following fixed-point equation:

$$\mathbf{x} = -\left(\frac{\partial F}{\partial \mathbf{x}} \Big|_{(0)}^{-1} \right) \boldsymbol{g}(\mathbf{x}, \mathbf{u}, \mathbf{w}) - \left(\frac{\partial F}{\partial \mathbf{x}} \Big|_{(0)}^{-1} \cdot \frac{\partial F}{\partial \mathbf{w}} \Big|_{(0)} \right) \mathbf{w}, \tag{4.10}$$

where $\boldsymbol{g} : (\mathbf{R}^{|\mathbf{x}|}, \mathbf{R}^{|\mathbf{u}|}, \mathbf{R}^{|\mathbf{w}|}) \to \mathbf{R}^{|\mathbf{x}|}$ is the residual function:

$$\boldsymbol{g}(\mathbf{x}, \mathbf{u}, \mathbf{w}) = F(\mathbf{x}, \mathbf{u}, \mathbf{w}) - \left(\frac{\partial F}{\partial \mathbf{x}} \Big|_{(0)} \right) \mathbf{x} - \left(\frac{\partial F}{\partial \mathbf{w}} \Big|_{(0)} \right) \mathbf{w}. \tag{4.11}$$

Closed-form expressions for the Jacobian and the residual function are provided in Appendix A.3.1 and A.3.2.

Lemma 6. The inverse of the Jacobian, $\frac{\partial F}{\partial \mathbf{x}} \Big|_{(0)}^{-1}$, exists for both explicit and implicit time-discretization schemes if the step size, h, is sufficiently small. Then, the set of dynamic equations, $F(\mathbf{x}, \mathbf{u}, \mathbf{w}) = 0$, is satisfied if and only if (4.10) is satisfied.

Proof. A closed-form representation of the Jacobian inverse is provided in Lemma 15

and 16 in Appendix A.3.1. Substituting the residual function in Equation (4.11) to (4.10), $0 = -\frac{\partial F}{\partial \mathbf{x}} \Big|_{(0)}^{-1} F(\mathbf{x}, \mathbf{u}, \mathbf{w})$. Since the Jacobian is invertible, $F(\mathbf{x}, \mathbf{u}, \mathbf{w}) = 0$. $\square$

Convex Restriction of Control Actions

Using envelopes and the fixed-point equation, we present the convex sufficient condition that guarantees that the self-mapping polytope is indeed the outer approximation of possible state trajectories. Let the matrices $K \in \mathbf{R}^{|\mathbf{x}| \times |\mathbf{x}|}$ and $R \in \mathbf{R}^{|\mathbf{x}| \times |\mathbf{w}|}$ be defined by

$$K = -\frac{\partial F}{\partial \mathbf{x}} \Big|_{(0)}^{-1}, \qquad R = -\frac{\partial F}{\partial \mathbf{x}} \Big|_{(0)}^{-1} \cdot \frac{\partial F}{\partial \mathbf{w}} \Big|_{(0)}. \tag{4.12}$$

Let the constant matrices K^+, $K^- \in \mathbf{R}^{|\mathbf{x}| \times |\mathbf{x}|}$ denote $K_{ij}^+ = \max\{K_{ij}, 0\}$ and $K_{ij}^- = \min\{K_{ij}, 0\}$ for each element of K. The following theorem provides a convex inner-approximation of the control action and an interval outer-approximation of the state trajectory against the uncertainty with a given robustness margin γ.

Theorem 7. Suppose that for a control trajectory $\mathbf{u}$, there exist variables $\mathbf{x}^u,\ \mathbf{x}^\ell \in \mathbf{R}^{|\mathbf{x}|}$ and $\boldsymbol{g}_{\mathcal{P}}^u,\ \boldsymbol{g}_{\mathcal{P}}^\ell \in \mathbf{R}^{|\mathbf{x}|}$ that satisfies convex inequality constraints in (2.7) and

$$\begin{aligned} K^+ \boldsymbol{g}_{\mathcal{P}}^u + K^- \boldsymbol{g}_{\mathcal{P}}^\ell + \xi^u(\gamma) &\leq \mathbf{x}^u, \\ K^+ \boldsymbol{g}_{\mathcal{P}}^\ell + K^- \boldsymbol{g}_{\mathcal{P}}^u + \xi^\ell(\gamma) &\geq \mathbf{x}^\ell, \end{aligned} \tag{4.13}$$

and for $i = 1, \ldots, |\mathbf{x}|$,

$$\begin{aligned} \xi_i^u(\gamma) &= \max_{\mathbf{w} \in \mathcal{W}(\gamma)} R_i \mathbf{w}, \\ \xi_i^\ell(\gamma) &= \min_{\mathbf{w} \in \mathcal{W}(\gamma)} R_i \mathbf{w}. \end{aligned} \tag{4.14}$$

Then, for every $\mathbf{w} \in \mathcal{W}(\gamma)$, there exists a state trajectory $\mathbf{x}$ such that $\mathbf{x} \in \mathcal{P}(\mathbf{x}^u, \mathbf{x}^\ell)$.

Convex Restriction of Safety Constraints

In this section, we propose a procedure for deriving the convex restriction of the safety constraints. The objective is to find a convex subset of $\mathcal{X}_t$ around $x_t^{(0)}$ for $t = 1, \ldots, N$. The restricted convex set will be used to certify that the trajectories lie

inside the safety constraints. The procedure relies on the projection of nominal state to obstacles at each time step,

$$P_{\mathcal{B}_{t,i}}[x_t^{(0)}] = \underset{x \in \mathcal{B}_{t,i}}{\arg\min} \|x - x_t^{(0)}\|_2^2, \tag{4.15}$$

where $\mathcal{B}_{t,i},\ i = 1, \ldots, s$ are obstacles. The following lemma provides the convex restriction of the safety constraints using the projections.

Lemma 7. The state at time step t satisfies the safety constraints, $x_t \in \mathcal{X}_t$, if x_t satisfies

$$L_t x_t + d_t < 0, \tag{4.16}$$

where the constants $L_t \in \mathbf{R}^{s \times n}$ and $d_t \in \mathbf{R}^s$ are

$$L_t = \begin{bmatrix} (P_{\mathcal{B}_{t,1}}[x_t^{(0)}] - x_t^{(0)})^T \\ \vdots \\ (P_{\mathcal{B}_{t,s}}[x_t^{(0)}] - x_t^{(0)})^T \end{bmatrix},\ d_t = -L_t \begin{bmatrix} P_{\mathcal{B}_{t,1}}[x_t^{(0)}] \\ \vdots \\ P_{\mathcal{B}_{t,s}}[x_t^{(0)}] \end{bmatrix}.$$

A formal proof is presented in Appendix A.3.3, and Figure 4-2 illustrates the underlying idea. Since the obstacles $\mathcal{B}_{t,i}$ are assumed to be convex, the supporting hyperplane at the projection provides a half-space where an obstacle cannot exist. By intersecting these half-spaces, we can derive a convex restriction of safety constraints at each state at time t. Next, we provide a sufficient condition for the robust feasible control action by ensuring that the self-mapping tube $\mathcal{P}(\mathbf{x}^u, \mathbf{x}^\ell)$ lies inside the convex restriction of safety constraints.

Theorem 8. The control trajectory $\mathbf{u}$ is a robust feasible control action if there exist variables $\mathbf{x}^u,\ \mathbf{x}^\ell,\ \boldsymbol{g}_{\mathcal{P}}^u,\ \boldsymbol{g}_{\mathcal{P}}^\ell \in \mathbf{R}^{|\mathbf{x}|}$ that satisfies convex inequality constraints in (2.7), (4.13), and

$$L_t^+ x_t^u + L_t^- x_t^\ell + d_t < 0, \quad \forall t = 1, \ldots, N. \tag{4.17}$$

Proof. Conditions (2.7) and (4.13) ensure that there exists a state trajectory $\mathbf{x} \in \mathcal{P}(\tilde{\mathbf{z}})$

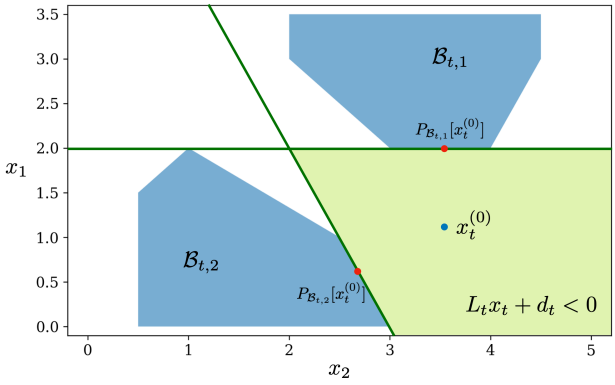

Figure 4-2: Illustration of convex restriction of safety constraints. The blue dot shows the current nominal state $x_t^{(0)}$, and the red dots show their projection to the obstacles. The supporting hyperplanes at the projected point provide half-spaces that are guaranteed to avoid obstacles. By finding the intersection of half-spaces, convex restrictions of safety constraints are shown in the green region.

from Theorem 7. Inequality condition in (4.17) ensures that

$$L_t x_t + d_t \leq L_t^+ x_t^u + L_t^- x_t^\ell + d_t < 0,$$

for $t = 1, \ldots, N$. From Lemma 7, for all $\mathbf{x} \in \mathcal{P}(\mathbf{x}^\ell, \mathbf{x}^u)$, $x_t \in \mathcal{X}_t$, and thus there exists state trajectories satisfying the safety constraints for all $\mathbf{w} \in \mathcal{W}$. □

4.1.3 Numerical Results

This section presents a numerical example that is illustrated on a ground vehicle navigation model. This example contains nonconvex safety constraints, which are obstacles in the context of navigation problems. The numerical experiments were done on 3.3 GHz Intel Core i7 with 16 GB Memory, and the convex optimization problems were implemented with Python with CVXPY with ECOS as the solver [39]. The MOSEK solver was used to solve the convex Quadratically Constrained Quadratic Programming problems generated by convex restriction.

Ground Vehicle Model

The dynamics of the ground vehicle is given by

$$\frac{d}{dt}\begin{bmatrix} x_1 \\ x_2 \\ v \\ \theta \end{bmatrix} = \begin{bmatrix} v\cos\theta + w_1 \\ v\sin\theta + w_2 \\ u_1 + w_3 \\ v\tan u_2 + w_4 \end{bmatrix} \tag{4.18}$$

where $(x_1, x_2) \in \mathbf{R}^2$ and θ are the vehicle's position and direction. The variable v is the speed, and u_1 and u_2 are acceleration and steering velocity. Euler's forward method was used for time discretization with the step size $h = 0.05$. The degree of sparsity in this system is $|\mathcal{I}|$=2 since the terms $v\cos\theta$ and $v\sin\theta$ involve v and θ as the dependent variables. The safety constraints considered two time-invariant obstacles, which are expressed by a polytope of the form $\mathcal{B}_{(i)}$, $i = 1, 2$. These obstacles are shown in blue in Figure 4-4. The control actions were subject to the limits, $u_{t,1} \in [-1,\ 1]$ and $u_{t,2} \in [-0.785,\ 0.785]$, and the vehicle speed is limited by $x_{t,3} \in [-5.55,\ 15.28]$.

The uncertainty in initial condition is set to $\mathcal{W}_{\text{init}}(\gamma_{\text{init}}) = \{(x_1, x_2, v, \theta) \mid x_1^2 + x_2^2 \leq \gamma_{\text{init},x}^2,\ |v| \leq \gamma_{\text{init},v},\ |\theta| \leq \gamma_{\text{init},\theta}\}$ where $\gamma_{\text{init},x} = 0.05$, $\gamma_{\text{init},v} = 0.05$, and $\gamma_{\text{init},\theta} = 0.005$. The uncertainty set in dynamics is set to $\mathcal{W}_t(\gamma_{\text{dyn}}) = \{w \mid w_1^2 + w_2^2 \leq \gamma_{\text{dyn},x}^2,\ |w_3| \leq \gamma_{\text{dyn},v},\ |w_4| \leq \gamma_{\text{dyn},\theta}\}$ where $\gamma_{\text{dyn},x} = 0.05$, $\gamma_{\text{dyn},v} = 0.005$, and $\gamma_{\text{dyn},\theta} = 0.005$. The cost function for the robust MPC problem was set to $c_{u,t}(u_t) = 0.01u_{t,1}^2 + 0.001u_{t,2}^2$ and $c_{x,t}(x_t) = (x - x_{\text{target}})^T Q(x - x_{\text{target}})$ where $x_{\text{target}} = (3, 5, 0, 0)$ and $Q = \text{diag}([1, 1, 0.5, 0.0001])$.

Constrained Robust Model Predictive Control

The constrained robust MPC was solved using sequential convex restriction. The subproblems were solved with SCR described in Algorithm 1.

Figure 4-3 shows the convergence plot for both nominal and worst-case costs. The average solver time per iteration was 0.733 seconds, and it took five iterations to converge. The figure provides some insight into the conservatism of our approach. The

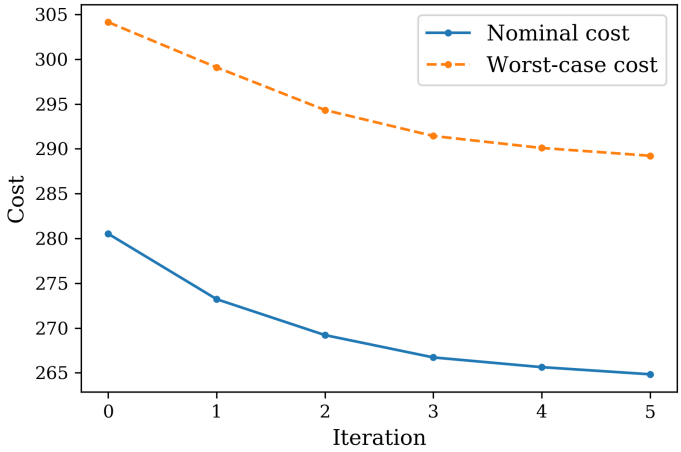

Figure 4-3: The convergence of sequential convex restriction is shown. The blue plot shows the nominal cost as a function of number of iterations, and the orange plot shows the bound on worst-case cost.

worst-case cost provides the upper bound, and the nominal cost provides the lower bound on the control cost for all realizations of the uncertainty set. This corresponds to an uncertainty of 8.44 % with respect to the worst-case cost.

The following experiments show the result where the initial trajectory was provided by path-following feedback control. The trajectory was optimized again using SCR with $N = 50$.

Figure 4-4 shows the nominal state trajectories of the solution to the algorithm as well as the set of possible state trajectories under uncertainty and the self-mapping tube. The set of possible state trajectories under uncertainty grows with time due to the propagation of uncertain variables in dynamics. The self-mapping tube is guaranteed to contain the possible state trajectory and satisfies the safety constraints. The circles represent the inner approximation of possible state realization. Any point inside the circle can be realized by some uncertainty trajectory within the specified uncertainty set.

Figure 4-5 shows the state and control trajectories of the solution from sequential convex restriction. The position of the vehicle safely arrives at the target point. The trajectories of the vehicle's velocity and angle are tight to the self-mapping tube since the associated dynamics are linear and are not affected by the uncertain variables.

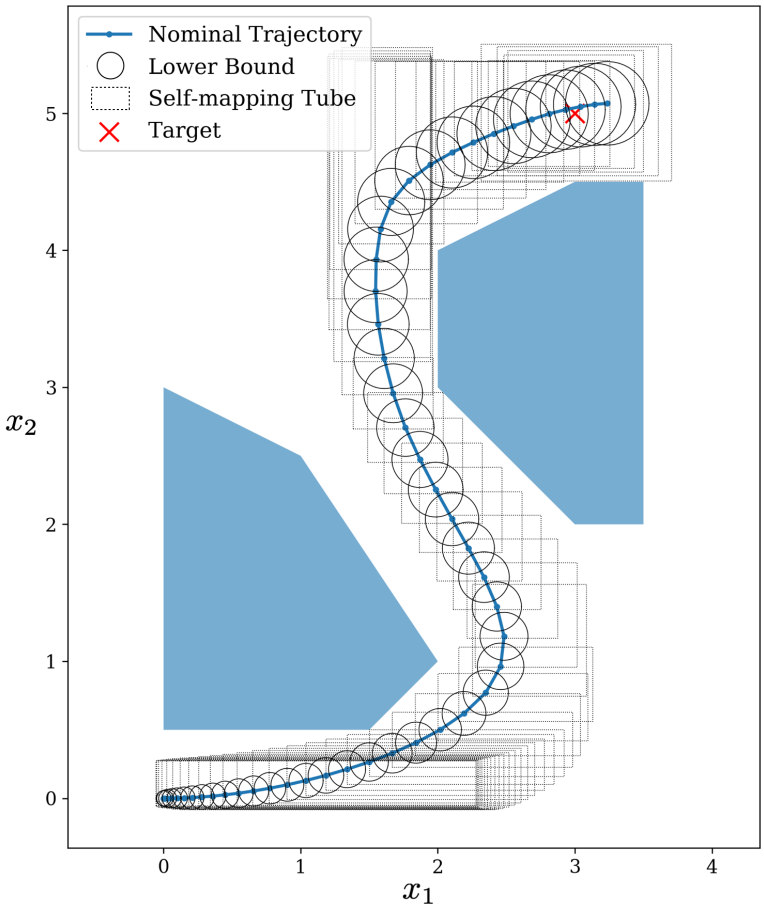

Figure 4-4: The nominal state trajectory obtained by the sequential convex restriction is shown in the blue line. The obstacles are shown in two blue regions, and the uncertainty set is shown with black circles. The grey rectangular boxes show the solution for the self-mapping tube $\mathcal{P}(\tilde{\mathbf{z}})$, which provides the outer approximation of the possible state trajectories.

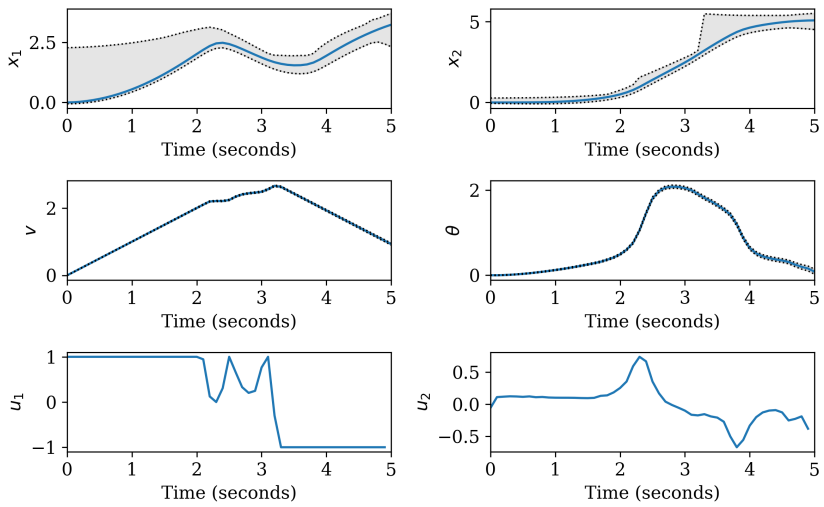

Figure 4-5: The state trajectories for the obtained control action is shown with the self-mapping tube obtained by the convex restriction. The control action obtained by the convex restriction is shown. The limits of the control inputs are $u_1 \in [-100, 20]$ and $u_2 \in [-1.5, 1.5]$.

One unconventional feature in convex restriction that distinguishes itself from conventional approaches is that it does not rely on propagating the uncertainty set in the time domain. The outer approximation in Figure 4-4 is verified via the fixed-point theorem, and the tube does not become overly conservative over time. The outer approximation's tightness is enforced only on the bottom and left faces of the rectangles where the worst-case cost occurs since it is the furthest point away from the target point. This feature allows us to obtain the tube that satisfies the safety constraint while not overly approximating the worst-case realization of the state trajectories.

4.2 Optimal Power Flow (OPF)

The operation of the power grid requires the system operator to determine a dispatch point to the generators such that the grid supplies electricity to consumers securely and reliably. In order to determine the dispatch point with minimum generation cost, the optimal power flow (OPF) problems are solved with the physical models of the grid, such as the AC power flow equation, and operational constraints such as voltage magnitude, line flow, and generator limits.

Notation

The scalars n_{b}, n_{g}, n_{pv}, n_{pq}, n_{l}, and n_{d} denote the number of buses, generators, PV, PQ buses, lines, and loads, respectively. The variables $p_{\mathrm{g}} \in \mathbf{R}^{n_{\mathrm{g}}}$ and $q_{\mathrm{g}} \in \mathbf{R}^{n_{\mathrm{g}}}$ represent the generators' active and reactive power outputs. Uncontrollable active and reactive power injections are denoted by $p_{\mathrm{d}} \in \mathbf{R}^{n_{\mathrm{d}}}$ and $q_{\mathrm{d}} \in \mathbf{R}^{n_{\mathrm{d}}}$ where positive values indicate stochastic loads and negative values indicate uncertain generation such as renewables. The voltage magnitudes and phase angles are $v \in \mathbf{R}^{n_{\mathrm{b}}}$ and $\theta \in \mathbf{R}^{n_{\mathrm{b}}}$. The *from* and *to* buses for the lines are denoted by "f" and "t". The non-reference, PV, and PQ elements of a vector are denoted with subscripts "ns", "pv", and "pq". Let $E \in \mathbf{R}^{n_{\mathrm{b}} \times n_{\mathrm{l}}}$ be the incidence matrix of the grid. The connection matrices for generator buses and load buses are denoted by $C_{\mathrm{g}} \in \mathbf{R}^{n_{\mathrm{b}} \times n_{\mathrm{g}}}$ and $C_{\mathrm{d}} \in \mathbf{R}^{n_{\mathrm{b}} \times n_{\mathrm{d}}}$, respectively. The matrices I and $\mathbf{0}$ denote identity and zero matrices of appropriate size. The vertical concatenation of vectors a and b is denoted by (a, b).

AC Optimal Power Flow Problem Formulation

For notational convenience, we denote the angle differences between the terminals of the transmission lines as φ:

$$\varphi_l = \theta_l^{\mathrm{f}} - \theta_l^{\mathrm{t}}, \qquad l = 1, \ldots, n_{\mathrm{l}}, \tag{4.19}$$

where θ_i^{f} and θ_i^{t} are the phase angles of the *from* bus and *to* bus of line l. The AC OPF problem is:

$$\underset{x, u, \overline{s}^{\mathrm{f}}, \overline{s}^{\mathrm{t}}}{\text{minimize}} \quad c(p_{\mathrm{g}}) = \sum_{i=1}^{n_{\mathrm{g}}} c_i(p_{\mathrm{g},i}) \tag{4.20}$$

subject to: for $k = 1, \ldots, n_{\mathrm{b}}$,

$$p_k^{\mathrm{inj}} = \sum_{l=1}^{n_{\mathrm{l}}} v_l^{\mathrm{f}} v_l^{\mathrm{t}} \left(G_{kl}^{\mathrm{c}} \cos \varphi_l + B_{kl}^{\mathrm{s}} \sin \varphi_l\right) + G_{kk}^{\mathrm{d}} v_k^2, \tag{4.21a}$$

$$q_k^{\mathrm{inj}} = \sum_{l=1}^{n_{\mathrm{l}}} v_l^{\mathrm{f}} v_l^{\mathrm{t}} \left(G_{kl}^{\mathrm{s}} \sin \varphi_l - B_{kl}^{\mathrm{c}} \cos \varphi_l\right) - B_{kk}^{\mathrm{d}} v_k^2, \tag{4.21b}$$

$$p_{\mathrm{g},i}^{\min} \leq p_{\mathrm{g},i} \leq p_{\mathrm{g},i}^{\max}, \qquad i = 1, \ldots, n_{\mathrm{g}}, \tag{4.22a}$$

$$q_{\mathrm{g},i}^{\min} \leq q_{\mathrm{g},i} \leq q_{\mathrm{g},i}^{\max}, \qquad i = 1, \ldots, n_{\mathrm{g}}, \tag{4.22b}$$

$$v_i^{\min} \leq v_i \leq v_i^{\max}, \qquad i = 1, \ldots, n_{\mathrm{b}} \tag{4.22c}$$

$$\varphi_l^{\min} \leq \varphi_l \leq \varphi_l^{\max}, \qquad l = 1, \ldots, n_{\mathrm{l}}, \tag{4.22d}$$

$$(s_{\mathrm{p},l}^{\mathrm{f}})^2 + (s_{\mathrm{q},l}^{\mathrm{f}})^2 \leq (s_l^{\max})^2, \qquad l = 1, \ldots, n_{\mathrm{l}}, \tag{4.22e}$$

$$(s_{\mathrm{p},l}^{\mathrm{t}})^2 + (s_{\mathrm{q},l}^{\mathrm{t}})^2 \leq (s_l^{\max})^2, \qquad l = 1, \ldots, n_{\mathrm{l}}. \tag{4.22f}$$

where the matrices $G^{\mathrm{c}},\ G^{\mathrm{s}},\ B^{\mathrm{c}},\ B^{\mathrm{s}} \in \mathbf{R}^{n_{\mathrm{b}} \times n_{\mathrm{l}}}$ and $G^{\mathrm{d}},\ B^{\mathrm{d}} \in \mathbf{R}^{n_{\mathrm{b}} \times n_{\mathrm{b}}}$ are transformed admittance matrices for the respective conductance and susceptance terms. The exact definitions of the transformed matrices are available in [63]. The objective $c : \mathbf{R}^{n_g} \to \mathbf{R}$ is a monotonically increasing function of the active power generation. The active and reactive power injections are $p^{\mathrm{inj}} = C_{\mathrm{g}} p_{\mathrm{g}} - C_{\mathrm{d}} p_{\mathrm{d}}$ and $q^{\mathrm{inj}} = C_{\mathrm{g}} q_{\mathrm{g}} - C_{\mathrm{d}} q_{\mathrm{d}}$. Superscripts max and min denote the maximum and minimum limits of the associated quantity. Constraints (4.22a) and (4.22b) impose the generators' active and reactive power output limits. Constraints (4.22c) and (4.22d) limit the voltage magnitudes and the angle differences. Constraints (4.22e) and (4.22f) impose line flow limits where $s_{\mathrm{p},l}^{\mathrm{f/t}}$ and $s_{\mathrm{q},l}^{\mathrm{f/t}}$ are the active and reactive power flowing into the line l at the *from* and *to* buses, respectively.

Power Injection Uncertainty Modelling

The variable $w = (p_d,\, q_d) \in \mathbf{R}^{2n_d}$ consists of uncertain active and reactive power injections $p_{\mathrm{d}} \in \mathbf{R}^{n_d}$ and $q_{\mathrm{d}} \in \mathbf{R}^{n_d}$. The nominal value of the uncertain variable is $w^{(0)}$. We consider a bounded uncertainty set $\mathcal{W}$ modeled with a *confidence ellipsoid* containing all power injections within a ball of radius γ centered on the nominal power injections:

$$\mathcal{W}(\gamma) = \{w \mid (w - w^{(0)})^T \Sigma^{-1} (w - w^{(0)}) \leq \gamma^2\}. \tag{4.23}$$

The power injection covariance matrix $\Sigma \in \mathbf{R}^{2n_d \times 2n_d}$ and the radius $\gamma \in \mathbf{R}$ determine the shape and size, respectively, of the uncertainty set. The covariance matrix Σ

captures the correlations between power injections. By choosing an appropriate value for γ, the confidence ellipsoid can be designed such that the probability of containing the uncertainty realization is greater than the desired threshold. For example, if the uncertainty is drawn from a univariate normal distribution, we can ensure that 95% of the uncertainty realizations are within the confidence ellipsoid by setting γ to be twice the variance.

Basis Function Formulation of the Power Flow Equations

In this section, we rewrite the AC power flow equations in terms of basis functions that serve as building blocks for the power flow nonlinearities. The vector of nonlinear functions, $\psi : (\mathbf{R}^{n_\mathrm{b}+n_\mathrm{pq}}, \mathbf{R}^{2n_\mathrm{g}}) \to \mathbf{R}^{n_\mathrm{g}+2n_\mathrm{l}+n_\mathrm{b}}$, denotes the basis function, $\psi(x,u) = (\psi^\mathrm{p}, \psi^\mathrm{cos}, \psi^\mathrm{sin}, \psi^\mathrm{quad})$, where

$$\psi_i^\mathrm{p}(x,u) = p_{\mathrm{g,ref},i} + \alpha_i \Delta, \qquad i = 1,\ldots,n_\mathrm{g}, \tag{4.24a}$$

$$\psi_l^\mathrm{cos}(x,u) = v_l^\mathrm{f} v_l^\mathrm{t} \cos(\varphi_l), \qquad l = 1,\ldots,n_\mathrm{l}, \tag{4.24b}$$

$$\psi_l^\mathrm{sin}(x,u) = v_l^\mathrm{f} v_l^\mathrm{t} \sin(\varphi_l), \qquad l = 1,\ldots,n_\mathrm{l}, \tag{4.24c}$$

$$\psi_k^\mathrm{quad}(x,u) = v_k^2, \qquad k = 1,\ldots,n_\mathrm{b}. \tag{4.24d}$$

The AC power flow equations in (4.21) can be written in terms of the basis functions and the uncertain variables as

$$M\psi(x,u) + Rw = 0, \tag{4.25}$$

where $M \in \mathbf{R}^{(n_\mathrm{b}+n_\mathrm{pq})\times(n_\mathrm{g}+2n_\mathrm{l}+n_\mathrm{b})}$ and $R \in \mathbf{R}^{(n_\mathrm{b}+n_\mathrm{pq})\times 2n_\mathrm{d}}$ are constant matrices defined as

$$M = \begin{bmatrix} C_\mathrm{g} & -G^\mathrm{c} & -B^\mathrm{s} & -G^\mathrm{d} \\ \mathbf{0} & B^\mathrm{c}_\mathrm{pq} & -G^\mathrm{s}_\mathrm{pq} & B^\mathrm{d}_\mathrm{pq} \end{bmatrix}, \quad R = -\begin{bmatrix} C_\mathrm{d} & \mathbf{0} \\ \mathbf{0} & C_\mathrm{d,pq} \end{bmatrix}. \tag{4.26}$$

The matrix $B^\mathrm{c}_\mathrm{pq} \in \mathbf{R}^{n_\mathrm{pq}\times n_\mathrm{l}}$ is a submatrix of $B^\mathrm{c} \in \mathbf{R}^{n_\mathrm{b}\times n_\mathrm{l}}$ containing the rows corresponding to the PQ buses. Matrices G^s_pq, B^d_pq, $C_\mathrm{g,pq}$, and $C_\mathrm{d,pq}$ are defined

similarly.

Convex Restriction of OPF constraints

Direct application of Theorem 6 provides the following result for robust feasibility of AC OPF constraints.

Theorem 9. (Robust Feasibility Condition for AC Optimal Power Flow) The dispatch point $u = (p_{g,\mathrm{ref}},\, v_{\mathrm{g}})$ is robustly feasible with respect to the uncertainty set $\mathcal{W}(\gamma)$ if there exist bounds on the internal states $z^u = (\varphi^u,\, v^u_{\mathrm{pq}},\, \Delta^u)$, $z^\ell = (\varphi^\ell,\, v^\ell_{\mathrm{pq}}, \Delta^\ell)$, $g^u_{\mathcal{P}}$, $g^\ell_{\mathcal{P}}$, $\psi^u_{\mathcal{P}}$, and $\psi^\ell_{\mathcal{P}}$ that satisfy (2.7), (2.8), and the following set of operational constraints:

$$
\begin{aligned}
p^{\min}_{\mathrm{g},i} \leq & p_{\mathrm{g,ref},i} + \alpha\Delta^\ell, && i = 1,\dots,n_{\mathrm{g}}, && \text{(4.27a)}\\
& p_{\mathrm{g,ref},i} + \alpha\Delta^u \leq p^{\max}_{\mathrm{g},i}, && i = 1,\dots,n_{\mathrm{g}}, && \text{(4.27b)}\\
q^{\min}_{\mathrm{g},i} \leq & q^\ell_{\mathrm{g},i}, \quad q^u_{\mathrm{g},i} \leq q^{\max}_{\mathrm{g},i}, && i = 1,\dots,n_{\mathrm{g}}, && \text{(4.27c)}\\
v^{\min}_{\mathrm{pq},i} \leq & v^\ell_{\mathrm{pq},i}, \;\; v^u_{\mathrm{pq},i} \leq v^{\max}_{\mathrm{pq},i}, && i = 1,\dots,n_{\mathrm{pq}} && \text{(4.27d)}\\
v^{\min}_{\mathrm{g},i} \leq & v_{\mathrm{g},i} \leq v^{\max}_{\mathrm{g},i}, && i = 1,\dots,n_{\mathrm{g}} && \text{(4.27e)}\\
\varphi^{\min}_l \leq & \varphi^\ell_l, \qquad \varphi^u_l \leq \varphi^{\max}_l, && l = 1,\dots,n_{\mathrm{l}}, && \text{(4.27f)}\\
(s^{\mathrm{f},u}_{\mathrm{p},l})^2 + & (s^{\mathrm{f},u}_{\mathrm{q},l})^2 \leq (s^{\max}_l)^2, && l = 1,\dots,n_{\mathrm{l}}, && \text{(4.27g)}\\
(s^{\mathrm{t},u}_{\mathrm{p},l})^2 + & (s^{\mathrm{t},u}_{\mathrm{q},l})^2 \leq (s^{\max}_l)^2, && l = 1,\dots,n_{\mathrm{l}}. && \text{(4.27h)}
\end{aligned}
$$

The reactive power generation bounds q^ℓ_{g} and q^u_{g} satisfy

$$
\begin{aligned}
L^+_{\mathrm{q}}\psi^u_{\mathcal{P}} + L^-_{\mathrm{q}}\psi^\ell_{\mathcal{P}} + \zeta^u(\gamma) &\leq C_{\mathrm{g,pv}}\, q^u_g,\\
L^-_{\mathrm{q}}\psi^u_{\mathcal{P}} + L^+_{\mathrm{q}}\psi^\ell_{\mathcal{P}} + \zeta^\ell(\gamma) &\geq C_{\mathrm{g,pv}}\, q^\ell_g,
\end{aligned}
\qquad (4.28)
$$

$$
\begin{aligned}
\zeta^u_i(\gamma) &= C_{\mathrm{d,pv},i}\Sigma^{1/2}_{\mathrm{q}} w^{(0)} + \gamma \left\| C_{\mathrm{d,pv},i}\Sigma^{1/2}_{\mathrm{q}} \right\|_2,\\
\zeta^\ell_i(\gamma) &= C_{\mathrm{d,pv},i}\Sigma^{1/2}_{\mathrm{q}} w^{(0)} - \gamma \left\| C_{\mathrm{d,pv},i}\Sigma^{1/2}_{\mathrm{q}} \right\|_2,
\end{aligned}
\qquad (4.29)
$$

and the line flow bounds $s_{\mathrm{p}}^{\mathrm{t},u}$, $s_{\mathrm{q}}^{\mathrm{f},u}$, and $s_{\mathrm{q}}^{\mathrm{t},u}$ satisfy

$$\begin{aligned} L_{\mathrm{j,\ line}}^{\mathrm{k},+}\psi_{\mathcal{P}}^{u} + L_{\mathrm{j,line}}^{\mathrm{k},-}\psi_{\mathcal{P}}^{\ell} &\leq s_{\mathrm{j}}^{\mathrm{k},u}, \\ -L_{\mathrm{j,line}}^{\mathrm{k},-}\psi_{\mathcal{P}}^{u} - L_{\mathrm{j,line}}^{\mathrm{k},+}\psi_{\mathcal{P}}^{\ell} &\leq s_{\mathrm{j}}^{\mathrm{k},u}. \end{aligned} \tag{4.30}$$

for $\mathrm{k} \in \{\mathrm{f}, \mathrm{t}\}$ and $\mathrm{j} \in \{\mathrm{p}, \mathrm{q}\}$. The decision variables $\psi_{\mathcal{P}}^{u}$ and $\psi_{\mathcal{P}}^{\ell}$ are the basis function bounds over $\mathcal{P}(z^u, z^\ell)$, and they are constrained by (2.7) by replacing the function g by ψ.

4.2.1 Illustrative Example using a 9-Bus System

We begin by considering the 9-bus system from [28] with uncertain loads at buses 5 and 7. This 9-bus system is operating in a normal condition with positive active and reactive power load demands. The participation factors are set to 1 for the generator at bus 1 and 0 for the other generators, which corresponds to the single slack bus formulation.

Comparison of nominal and robust solution

We first consider normally distributed loads with a mean equal to the nominal load $w^{(0)}$ and standard deviation equal to 10% of $w^{(0)}$ without correlation between loads. For our robust AC OPF algorithm, we use an uncertainty set $\mathcal{W}(\gamma_{\mathrm{req}})$ that encloses two standard deviations of the considered load uncertainty by setting $\Sigma = \mathbf{diag}(p_{\mathrm{d}}^2)$ and $\gamma_{\mathrm{req}} = 0.2$. To assess the quality of our solutions from the probabilistic aspect, we compute the probability of constraint violations using 10,000 samples of the random loads.

Fig. 4-6 shows the uncertainty set and the convex restriction for the loads at buses 5 and 7. The nominal loads and the confidence ellipsoid are intrinsic to the uncertainty model and do not change with the dispatch point. Changes in the dispatch point adjust the set of feasible demands, and thus the feasible sets are shown in Figs. 4-6(a) and (b) are different while the nominal load stays at the same location. Specifically, the robust dispatch solution changes the feasible set of loading conditions

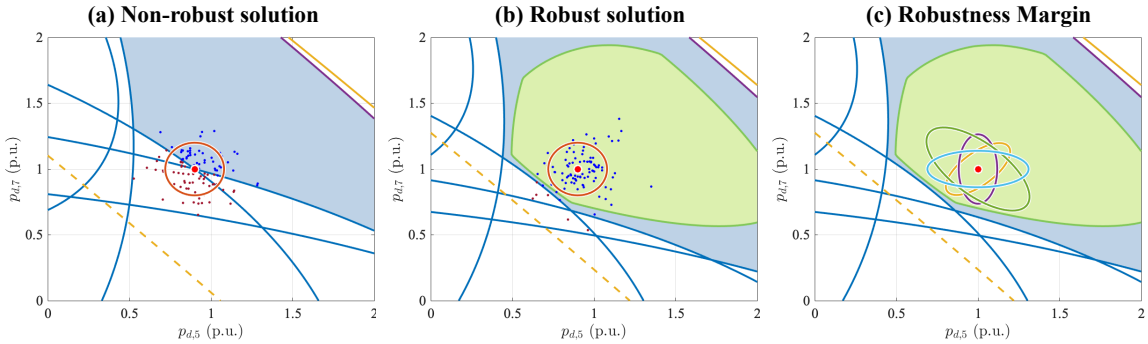

Figure 4-6: Figure (a) shows the vulnerability of non-robust optimal solution for electric gird where more than half of the operating point fails to meet the operational constraints. Figure (b) and (c) shows a robust optimal solution obtained by convex restriction.

such that it inscribes the confidence ellipsoid. The quality of our solution is evident by examining the distance between the boundaries of the feasible region, convex restriction, and uncertainty set. For the nominal (non-robust) OPF solution in Fig. 4-6(a), the operational cost is 5296.69 \$/hr and constraint violations occur in 55.18% of the samples. The most common violations are the maximum voltage magnitude limits at buses 6 and 8. For the robust OPF solution in Fig. 4-6(b), we observe that all uncertainty realizations within the considered uncertainty set (red circle) are feasible, as guaranteed by our algorithm. The generation cost for the robust dispatch point (5342.99 \$/hr) is 0.87% greater than the cost for the nominal dispatch point, but only 0.13% of the samples result in constraint violations.

Robustness Margin Maximization

We next examine a scenario where the system operators want to determine the operating point with the largest robustness margin. First, we let the dispatch point u be a decision variable and maximize the robustness margin. The resulting robustness margin γ was 0.380, which is 90% greater than what was required ($\gamma_{\text{req}} = 0.2$) in the robust OPF solution above. This achieves robustness against $\pm 38\%$ fluctuations in loads at every bus while the generation cost (5383.96 \$/hr) only increased by 0.77% relative to the robust OPF solution.

Second, we examine a scenario where the dispatch point is given by $u = u^{(0)}$ and

introduce correlation between loads. We define the dispatch point $u^{(0)}$ as the solution in Fig. 4-6(b), and maximize the robustness margin with the additional constraint $u = u^{(0)}$. We solve this problem several times for different correlation matrices Σ. The legend of Fig. 4-6(c) gives the robustness margins γ obtained for different correlation matrices Σ, with the corresponding uncertainty sets shown by the ellipses.

Computation Time

Since the robustness condition is convex, these problems can be solved efficiently. For the 9-bus system, the robust AC OPF algorithm converged in two iterations, each taking an average of 0.0497 seconds to compute. The number of iterations indicates how many times the sub-optimization problem was solved. The average computation time for obtaining the robustness margins is 0.0585 seconds.

4.2.2 Robustness vs. Cost Trade-Off for the IEEE 118-Bus System

We next study the trade-off between operating cost and the probability of constraint violations by solving the robust AC OPF problem for the IEEE 118-bus system [50]. Load uncertainty is modeled via a Gaussian distribution with variance equal to 1% of the nominal load. The results are plotted in Fig. 4-7 with the enforced robustness margin γ_{req} on the x-axis. The left y-axis (in blue) shows the empirically determined join violation probability, i.e., the probability that a sample from the considered uncertainty distribution violates one or more constraints. The right y-axis (in orange) shows both the nominal ($c^{(0)}$) and worst-case (c^u) generation costs.

We observe that increasing the robustness margin results in lower violation probability and higher generation cost. By examining this trade-off, operators can balance generation cost and robustness based on the assessed level of power injection uncertainty. For example, we can avoid constraint violations with 99% probability against random samples from the Gaussian distribution by setting $\gamma_{\text{req}} = 0.03$, which increases the cost relative to the nominal solution by 0.24%.

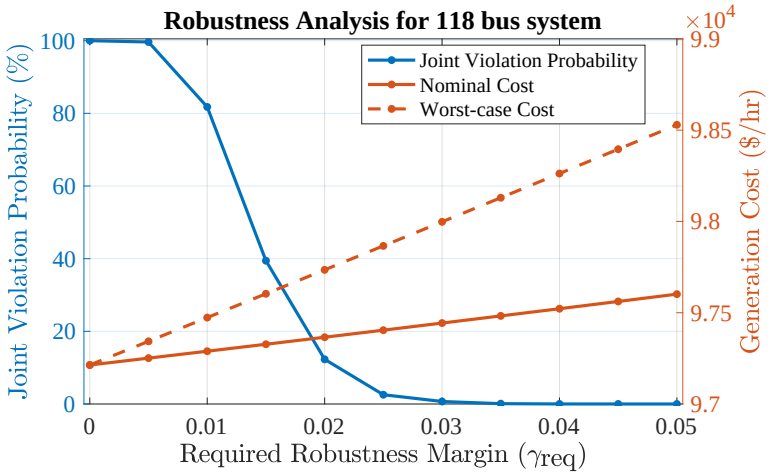

Figure 4-7: The trade-off between generation cost and robustness for the IEEE 118-bus system. The x-axis shows the required robustness margin, γ_{req}. The solid and dashed red lines show the nominal and worst-case generation costs, $c^{(0)}$ and c^u, respectively. The blue lines show the joint probability of constraint violations with stochastic uncertainty.

4.2.3 Numerical Studies using the PGLib Test Cases

Finally, we show the effectiveness of our robust AC OPF algorithm using the PGLib test cases [50] with sizes up to 179 buses. Each generator's participation factor is proportional to the generator's capacity, i.e., $\alpha_i = (p_{\text{g},i}^{\max} - p_{\text{g},i}^{\min}) / \sum_{i=1}^{n_g} (p_{\text{g},i}^{\max} - p_{\text{g},i}^{\min})$. The uncertainty set for the robust OPF problem was modeled by 1% demand fluctuations at every load bus (i.e., $\Sigma = \mathbf{diag}(p_{\text{d}}^2)$ and $\gamma_{\text{req}} = 0.01$).

Table 4.1 compares the generation cost of the nominal (non-robust) solution obtained using PowerModels.jl [31] with our robust dispatch point in the second and fifth columns, respectively. The bound on the optimality gap in Corollary 6 is shown in the tenth column, which is computed by taking the difference in generation costs between the nominal and robust OPF solution. The optimality gap is approximately less than 1%, indicating that only a marginal trade-off in generation cost is necessary to achieve this level of robustness. The robustness against stochastic uncertainty was evaluated by checking the feasibility of 10,000 samples from Gaussian and uniform distributions. Columns 3 and 6 in Table 4.1 used samples from a uniform distribution within the uncertainty set. Since our robust OPF solution guarantees robust

Table 4.1: Violation Probability and Cost Comparison for Selected PGLib Test Cases

	Nominal OPF Solution			Robust OPF Solution					Optimality
		Violation Prob. (%)			Violation Prob. (%)		Solve	Num.	Gap (%)
Test Case	Cost ($/h)	(Uniform)	(Gaussian)	Cost ($/h)	(Unif.)	(Gauss.)	time (sec)	iter.	Local
Typical Operating Conditions (TYP)									
case3_lmbd	5812.64	49.88	49.47	5829.93	0	0.20	0.04	4	0.30
case5_pjm	17551.89	100.00	100.00	17631.82	0	5.18	0.07	3	0.46
case14_ieee	2178.08	91.30	91.44	2180.96	0	2.10	0.12	2	0.13
case24_ieee_rts	63352.20	99.40	99.66	63566.97	0	5.62	0.71	3	0.34
case30_as	803.13	49.07	50.10	803.13	0	1.94	0.26	2	0.00
case30_fsr	575.77	69.12	71.99	580.01	0	0.03	0.38	2	0.74
case30_ieee	8208.52	68.74	80.84	8232.81	0	2.70	0.38	3	0.30
case39_epri	138415.56	99.96	99.94	138643.93	0	5.60	0.51	4	0.16
case57_ieee	37589.34	96.91	98.04	37602.58	0	5.34	0.95	3	0.04
case73_ieee_rts	189764.08	100.00	100.00	190139.37	0	9.86	1.74	3	0.20
case118_ieee	97213.61	100.00	100.00	97261.57	0	12.89	6.32	3	0.05

feasibility, there was no violated case for uniform distribution. Columns 4 and 7 used a Gaussian distribution with its mean set to the nominal loads and variance set to 0.5% of the nominal loads. The results show that while the nominal OPF solution is very sensitive to fluctuation, the robust solution makes the grid significantly more robust against stochastic uncertainty. Columns 8 and 9 show the solver time and the number of iterations, respectively. All of the studied test cases required fewer than five iterations. Columns 10 and 11 show bounds on the optimality gaps computed by the right-hand side of (3.14) in Corollary 6. The optimality gap in column 10 is calculated using the generation cost from a local search method (IPOPT [90]), and column 11 uses the lower bound on the generation cost from the quadratic convex (QC) relaxation [30]. We note that the optimality gap from the QC relaxation in column 11 includes both the relaxation gap and the gap from the robust convex restriction.

4.3 Analysis of Neural Networks

Neural networks are increasingly integrated as a critical component in safety-critical systems by learning underlying models from data and making predictions and decisions. While the multi-layer, nonlinear structure of the neural network gives the ability to represent functions with high complexity, making decisions and analyzing predictions is difficult due to its non-convex and nonlinear nature. The problems in decision and prediction are often cast as an optimization where a trained neural network approximates the objective function or constraints.

For example, trained neural networks are embedded to learn and estimate the model [80, 6, 73, 29] or the cost-to-go function in reinforcement learning [71, 82] such that the decisions are made by optimizing over the trained models. Analyzing a trained neural network also involves an optimization problem. The robustness verification problem can be cast as a feasibility problem where the output label does not change within the permissible perturbation [40, 42, 56, 84, 85, 88, 92]. Another example is finding an adversarial example, which searches for a minimum distortion

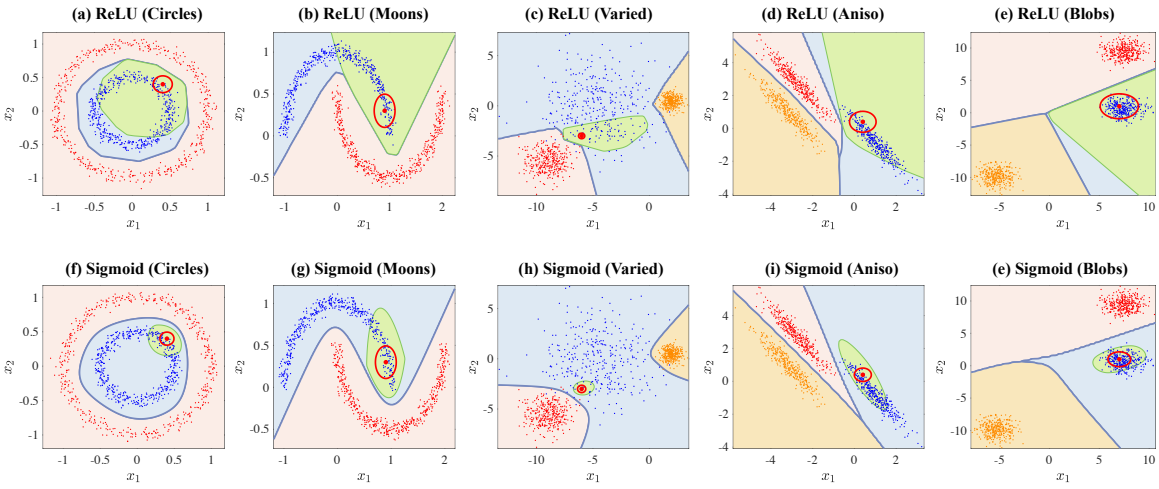

Figure 4-8: Convex restriction of neural networks trained for two-dimensional classification problems. The convex restriction (green region) provides an inner approximation of a class identified by the neural network (blue region). The scattered dots are data used to train the neural network, and the red dot is the nominal input data where the convex restriction is constructed around.

to an image that causes incorrect prediction of a neural network [46, 57, 72, 25, 45].

In this section, we propose a convex sufficient condition over the input to the neural network such that the output satisfies upper and lower bound constraints. An example is shown in Figure 4-8 where a neural network was trained for a classification task, and the decision margins are plotted with different colors for each class.

4.3.1 Problem Formulation

We consider a trained L-layer feedforward neural network with nonlinear activation functions. The input dimension is denoted by d_0, and the number of hidden units at layer k is denoted by d_k. Let $x \in \mathbb{R}^{d_0}$ be the input data to the neural network, and $z_k \in \mathbb{R}^{d_k}$ be the output variable at layer k. The weights between layers $k-1$ and k are denoted by $W_k \in \mathbb{R}^{d_k \times d_{k-1}}$, and the bias at layer k is denoted by $b_k \in \mathbb{R}^{d_k}$ for $k = 1, \ldots, L$. The neural network can be written as the algebraic equations,

$$\begin{aligned} z_0 &= x, \\ z_k &= \sigma_k(W_k z_{k-1} + b_k), \quad k = 1, \ldots, L, \end{aligned} \tag{4.31}$$

where $\sigma_k : \mathbb{R}^{d_k} \to \mathbb{R}^{d_k}$ is a vector of activation functions at k-th layer. The activation functions are arbitrary nonlinear functions that are continuous, including ReLU, sigmoid, pooling functions, and the convolutional layer. The analysis is carried out on a *trained* neural network where the weights are fixed. Both classification and regression problems are considered with the following setup.

Classification problems label each data point to a class $k \in \{1, \ldots, d_L\}$, where the input data is predicted by $k = \arg\max_i z_{L,i}$. The constraint for fixing the label in classification can be set by $z_{L,k} \geq z_{L,i}$ for $i = 1, \ldots, d_L$ where k is the desired output class. *Regression* problems have a predictor $y \in \mathbb{R}^{d_L}$ given by the output layer of the neural network, $y = z_L$. Constraints on the output of the neural network can be directly imposed on z_L.

Neural Constrained Optimization Problems

We consider the following canonical optimization problem involving a neural network,

$$\underset{x,z}{\text{minimize}} \quad c(z,\, x) \quad \text{subject to} \quad f(z,\, x) = 0, \quad h(z,\, x) \leq 0. \tag{4.32}$$

where $z = \begin{bmatrix} z_0^T & \ldots & z_L^T \end{bmatrix}^T \in \mathbb{R}^n$ with $n = \sum_{k=0}^{L} d_k$, and $f : (\mathbb{R}^n, \mathbb{R}^{d_0}) \to \mathbb{R}^n$ is defined as

$$f(z, x) = \begin{bmatrix} x - z_0 \\ \sigma_1(W_1 z_0 + b_1) - z_1 \\ \vdots \\ \sigma_L(W_L z_{L-1} + b_L) - z_L \end{bmatrix}. \tag{4.33}$$

The equality constraint can be viewed as a square system with n unknown variables ($z \in \mathbb{R}^n$) and n equations parametrized by $x \in \mathbb{R}^{d_0}$. The choice of the cost function $c : (\mathbb{R}^n, \mathbb{R}^{d_0}) \to \mathbb{R}$ and inequality constraints $h : (\mathbb{R}^n, \mathbb{R}^{d_0}) \to \mathbb{R}^m$ depend on the problem formulation. If the neural network outputs a scalar that represents the objective function, then it can be simply set to $c(z, x) = z_N$. If the neural network models the constraint, then it can be added as a constraint $h(z, x) = z_N - b \leq 0$ where b is some constant. For classification problems, the inequality constraint can

be set to $h_i(z, x) = z_{L,i} - z_{L,k} \leq 0$ for $i = 1, \ldots, d_L$ where k is the target label.

Robustness Margin of Neural Networks: The robustness margin for the neural network can be defined as how much norm-bounded perturbation can be added to the input data without changing the output label. Such a problem can be cast as an optimization problem in (3.1).

Adversarial Example: Finding an adversarial example is minimizing some distance metric subject to the neural network in (4.31). This problem can be also cast as an optimization problem in (3.1).

Optimization over Neural Networks In general, convex restriction provides a way to optimize with the neural network as a constraint. For example, we may want to minimize the input data with respect to some objective function. This problem could be solved by a sequence of convex optimization by replacing the neural network with convex restriction.

Convex restriction of neural networks

In this section, we present the convex sufficient condition for the equality and inequality constraints imposed by the neural network in (4.32). By applying envelopes for activation functions to the fixed-point representation of the neural network, the following theorem states our main result.

Theorem 10. (Convex Restriction of Neural Networks) Given the input data $x \in \mathbb{R}^{d_0}$ with some perturbation within a ball $\mathcal{B}_\gamma(x^{(0)})$, the output of the neural network in (4.31) is bounded by $z^\ell \leq z \leq z^u$ if there exists z^u, $z^\ell \in \mathbb{R}^n$ and $g^u_{\mathcal{P}}$, $g^\ell_{\mathcal{P}} \in \mathbb{R}^n$ such that

$$
\begin{aligned}
&K^+ g^u_{\mathcal{P}} + K^- g^\ell_{\mathcal{P}} + \xi = z^u, \\
&K^- g^u_{\mathcal{P}} + K^+ g^\ell_{\mathcal{P}} - \xi = z^\ell, \\
&\xi_i = \gamma \|K_{i,1:d_0}\|_2, \;\; i = 1, \ldots, n \\
&g^u_{\mathcal{P},0} \geq x, \;\; g^u_{\mathcal{P},k} \geq g^u_k(z^u_{k-1}), \;\; g^u_{\mathcal{P},k} \geq g^u_k(z^\ell_{k-1}), \;\; k = 1, \ldots, L, \\
&g^\ell_{\mathcal{P},0} \leq x, \;\; g^\ell_{\mathcal{P},k} \leq g^\ell_k(z^u_{k-1}), \;\; g^\ell_{\mathcal{P},k} \leq g^\ell_k(z^\ell_{k-1}), \;\; k = 1, \ldots, L,
\end{aligned}
\tag{4.34}
$$

where $K_{i,1:d_0} \in \mathcal{R}^{1\times d_0}$ is a row vector that corresponds to the i-th row and 1-st to d_0-th columns of the matrix K.

4.3.2 Experiments

We demonstrate our condition using optimization test functions [51] and MNIST dataset of hand-written digits [59]. We note that the focus of this paper is on the analysis of trained neural networks, and our results hold regardless of the training data and training procedure. Pytorch was used to construct and train a neural network [77], and CVXPY [35] with Gurobi [48] as the solvers were used to solve convex optimization problems. The problems were solved on a laptop with 3.3 GHz Intel Core i7 and 16 GB memory. More illustrations and our code are available in the supplement.

Solving an optimization problem with an unknown objective function and constraints

For solving optimization problems with trained neural networks, we sample data from standard optimization test functions and train neural networks to fit the data. We evaluate our approach on a neural network trained to learn an optimization test function. We generated 50000 random points from a uniform distribution and evaluated it using the Rosenbrock function, $v(x) = \sum_{i=1}^{d_0-1}[100(x_{i+1} - x_i^2)^2 + (1 - x_i)^2]$ where d_0 is 1000. We trained a neural network with three hidden layers and 1000 total hidden nodes. Figure 4-9 shows an illustration for $d_0 = 2$ where the scattered data are training data, and the surface plot is the learned function using the neural network. We solve an optimization problem where the objective is to minimize the learned function $\tilde{v}(x)$. We compare the performance of sequential convex restriction with subgradient descent [77] and trust-region method [89]. Figure 4-9 (b) shows the comparisons where mixed-integer linear programming provides a global minimum solution, and convex relaxation provides a lower bound on the objective function. The performance of sequential convex restriction is usually comparable to the trust-region

method.

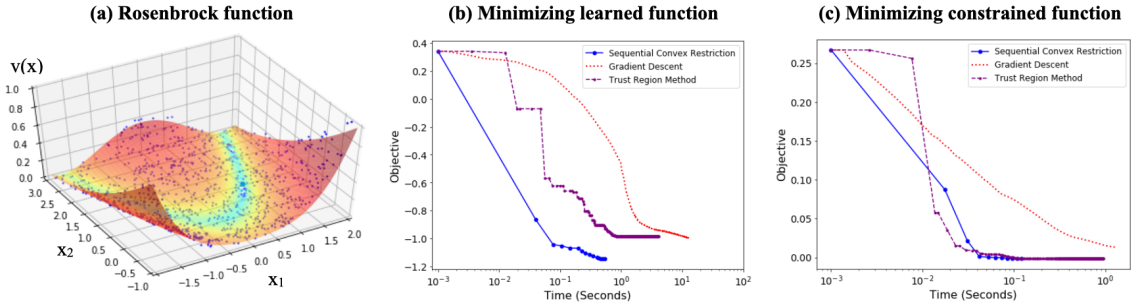

Figure 4-9: Figure (a) shows the trained test optimization function. Figure (b) and (c) show comparisons with other methods.

Finding an adversarial morphing

We consider morphing from an initial input data to a target data without changing the neural network's prediction. We train a 5-layer neural network where the first two layers are convolutional layers with ReLU activation functions, and the next two layers are ReLU layers. There are a total of 9154 hidden nodes in the neural network. Figure 4-10 shows the solutions from sequential convex restriction, which took 36.88 seconds per iteration on average. Since every consecutive solution from sequential convex restriction belongs to a convex set, it follows from the definition of the convex set that

$$\forall\, \alpha \in [0,1], \quad \alpha \cdot x^{(k)} + (1-\alpha) \cdot x^{(k+1)} \in \mathcal{U}^{\text{cvxrs}} \subseteq \mathcal{U}$$

for every iteration k. Therefore, a piece-wise linear transition from the initial input data produces a target label while satisfying the neural network out constraints.

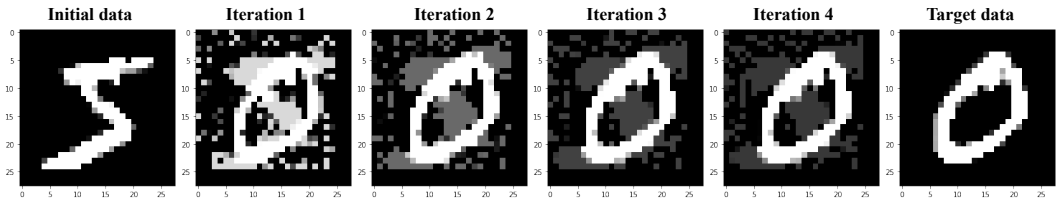

Figure 4-10: Numerical experiment for finding a targeted adversarial example.

4.4 Collision-free Motion Planning in Robotics

In this section, we consider robotic motion planning to generate collision-free trajectories. The problem considers both the nonlinear kinematics of the robot and the nonconvex obstacles, which can be represented as equality and inequality constraints. We search for the configuration of the robot such that it is closest to the targeting end-effector position and provide a collision-free path to go from the initial configuration to the solved configuration.

4.4.1 Problem Formulation

We assume the robot is position controlled with the kinematic equation given by

$$u = f(q) \tag{4.35}$$

where $u \in \mathbb{R}^m$ and $q \in \mathbb{R}^n$ are the end-effector coordinates and the configuration of the robot. Moreover, we add obstacles that the end-effector must avoid. If the end-effector does not collide with the obstacle and has a corresponding configuration, then we declare that the end-effector is safe or feasible. A feasible end-effector is denoted by $u \in \mathcal{U}$.

Problem Statement: Our objective is to find a path such that convex restriction provides a convex sufficient condition that ensures both the satisfaction of kinematic constraints in (4.35) and the safety constraints $u \in \mathcal{U}$.

In particular, we will use a piece-wise linear path in the end-effector space such that the sequence $u^{(0)}, u^{(1)}, \ldots, u^{(N)}$ has the property that a linear transition from a consecutive end-effector will be always feasible (i.e., $\alpha u^{(i)} + (1-\alpha)u^{(i)}$ for $\alpha \in [0,1]$ is feasible). Finding the configuration such that the end-effector is at the desired position can be cast as the following optimization problem,

$$\underset{u,q}{\text{minimize}} \quad f_0(u, u_{\text{ref}}) \quad \text{subject to} \quad u = f(q),\ u \in \mathcal{U}, \tag{4.36}$$

where $f_0(u, u_{\text{ref}})$ denotes the distance metric between the target and planned end-effector, and $\mathcal{U}$ denotes the safety constraints of the robot.

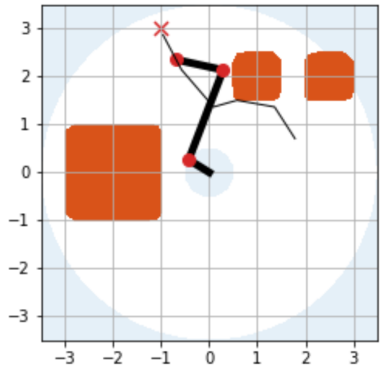

Figure 4-11: An illustration of the problem set up with three-armed robot.

We use a simple 3-armed robot illustrated in Figure 4-11. The end-effector of the system was defined as

$$u = [x,\ y,\ q_1]^T,$$

where x and y are the positions of the end of the arm in cartesian coordinates, and q_1 is one of the joint angles. Since the degree of freedom of the robot arm is 3, we can specify the position of the end-effector as well as the orientation. The kinematic equation of the system is

$$f(q) = \begin{bmatrix} L_1\cos(q_1) + L_2\cos(q_1+q_2) + L_3\cos(q_1+q_2+q_3) \\ L_1\sin(q_1) + L_2\sin(q_1+q_2) + L_3\sin(q_1+q_2+q_3) \\ q_1 \end{bmatrix}, \tag{4.37}$$

where $L_1 = 1$, $L_2 = 2$, and $L_3 = 0.5$. Due to the Kinematic constraints, there is an inherent limitation to the end-effector position. For this particular system, the constraints are such that the position of the end-effector should be within some range from the origin (i.e. $\sqrt{x^2+y^2} \in [L_2 - L_1 - L_3, L_1 + L_2 + L_3]$). An illustration of the experiment is shown in Figure 4-11. The figure shows the robot with black lines showing links and red dots showing joints. The orange squares represent obstacles that the robot needs to avoid. We impose the collision constraints only on the end-effector (the end of the robot arm) and have not considered the collision of any other

parts of the robot. Extensions to consider the entire body of the robot will be a future work of this project. The blue region shows the kinematic constraints that were described. Only the empty space of Figure 4-11 is reachable or manipulable by the robot. The desired end-effector position is marked by the red x mark. An example of a feasible path is shown with a black line.

Using the kinematic equations, the sequential convex restriction was applied with illustration in Figure 4-12. The green contour line shows the convex restriction around the given robot configuration. This case shows a successful case where the robot is able to reach the target position. We note that the collision constraints are applied only at the end-effector, and the body collisions were not considered.

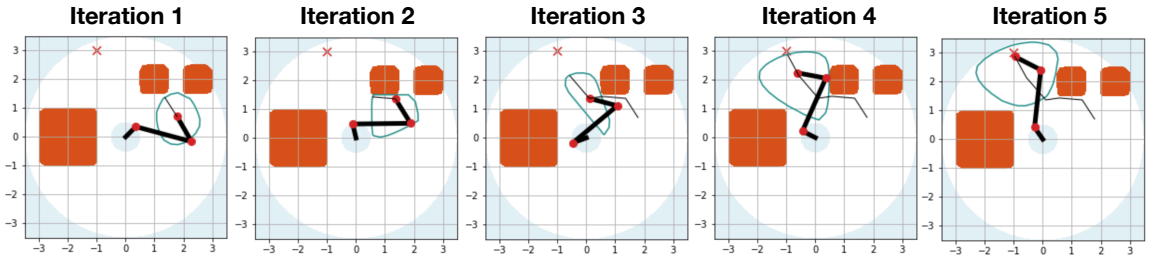

Figure 4-12: The convex restriction is drawn with a green contour line, which represents end-effector positions that the robot arm can maneuver. Convex optimization problems can be solved sequentially to move the robot arm from some initial condition to the desired position.

4.4.2 Simulation Results

In this section, we show some of the successful test cases where the sequential convex restriction. Figures (a), (b), and (d) show the trajectory where the robot avoids the obstacles that are between the initial and desired points. Figures (b) and (e) demonstrate cases where sequential convex restriction can go through a narrow passage.

In addition, we conduct additional experiments by randomly sampling the obstacles with various locations and sizes, the initial configuration of the robot, and the target point. These were drawn from a uniform distribution. The success rate of reaching the target point was about 63 percent with an average computation time per iteration of 0.0488 seconds. The number of samples for this experiment was 1000.

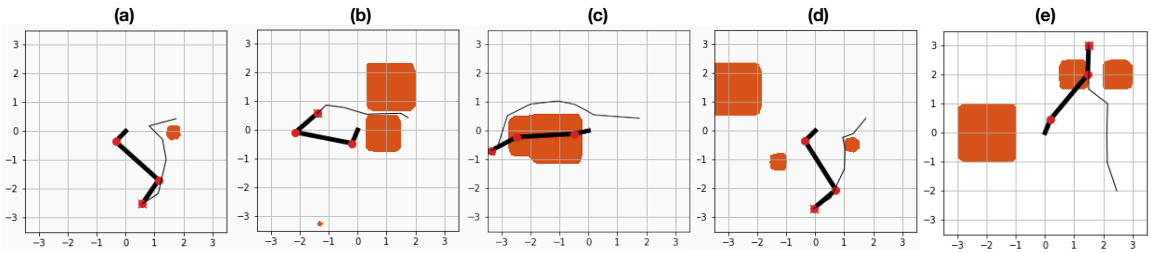

Figure 4-13: Successful test cases of Sequential Convex Restriction.

Failure Modes

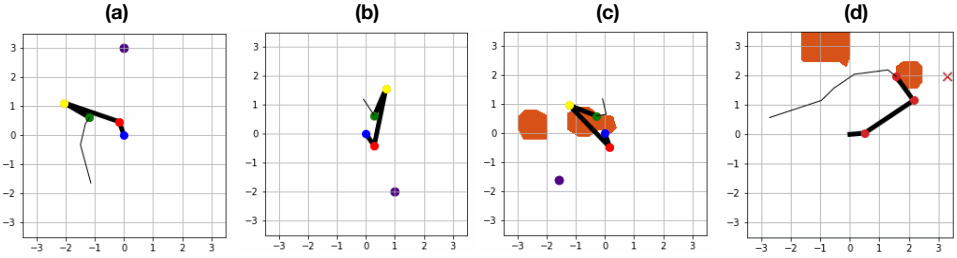

Figure 4-14: Failed test cases of Sequential Convex Restriction.

While the previous section showed cases where the end-effector arrived at the desired solution, there were cases where the algorithm failed due to the kinematic constraints. There are two main failure modes to the algorithm.

1. Since we specify the end-effector position of the robot, the manipulation becomes prohibitive when the robot is at a configuration where the Kinematic Jacobian is singular (e.g., the robot arm is at a straight-up position where $q_1 = q_2 = q_3 = 0$). Figure 4-14 (a) and (b) show the algorithm being stuck at the end-effector where the kinematic Jacobian becomes singular.

2. Similar to the potential fields method and TrajOpt [83], the sequential convex restriction is a local search method and may experience local solutions for the end-effector that is not the desired end-effector. Figure 4-14 (c) and (d) show the cases where the robot is stuck at a local solution.

4.5 Concluding Remarks

This chapter presented a number of applications for sequential convex restriction. The problems considered in this chapter were considered challenging due to the nonlinearity introduced by the system model. Convex restriction enables the use of rich theory and efficient algorithms for convex optimization, which provides a potential for tractable analysis of its applications. We showed that the coefficient involved in the MPC problem and neural network verification problem can be computed efficiently by exploiting their sequential structure. We showed extensive numerical studies for the OPF problem to demonstrate the effectiveness of the proposed approach.

Chapter 5

Reachability Analysis with Contraction Metric

5.1 Introduction

Safety and reliability became one of the most important questions in recent control applications such as autonomous driving and renewable integration in electrical power grids. There is a growing need for a set of tools that can measure reliability in safety-critical applications. These applications have various sets of safety constraints that need to be satisfied. The problem becomes challenging for nonlinear dynamical systems subject to uncertainty.

In this section, we develop a theory and algorithm for reachability analysis and combine the results with contraction analysis in order to bring a powerful set of tools for verification problems in control. Reachability analysis provides a verification procedure for nonlinear dynamical systems such that the agent avoids any obstacles and remains in a safe set.

One of the precedent work regarding the idea of bounding trajectory started with interval analysis, which was developed for bounding rounding and measurement errors [52]. More recently, the generalization of intervals to other shapes such as polytopes or ellipsoids showed more promising results for studying dynamical systems [8, 34, 58]. This approach provides a rigorous enclosure of trajectories to model equations by

building a "funnel" of possible outcomes and had success in applications such as robotics and motion planning [86] and power systems [78, 27].

More recently, a similar type of analysis based on polytope with the assistance of optimization has been proposed in [8, 34] for polynomial systems. The algorithm in the paper is scalable only to relatively low-order polynomial systems, and it needs to be scalable to larger systems. Existing methods based on linear sensitivity analysis or approximated order estimates are not rigorous and do not guarantee stability. On the other hand, the interval analysis approach gives a rigorous bound on the possible trajectories and determines the effect of uncertainties.

However, the convergence of the bounded states in interval analysis has not been possible because it is usually conservative. The intervals form a box that typically does not converge in under-damped systems. To alleviate this major limitation, we introduce a novel approach that constructs the bounding template using a polytope, which incorporates the geometrical characterization of system dynamics.

5.2 Preliminaries

5.2.1 System Model

We consider an autonomous nonlinaer system of the form,

$$x_{t+1} = f_t(x_t,\, w_t), \quad x_0 \in \mathcal{X}_0 \tag{5.1}$$

where $x \in \mathbf{R}^n$ is the state, $w \in \mathbf{R}^r$ is the uncertain parameters and $f_t(x, w) : (\mathbf{R}^n, \mathbf{R}^r) \to \mathbf{R}^n$ is a vector of nonlinear functions at time t. The system in (5.1) includes feedback controlled system $x_{t+1} = \tilde{f}_t(x_t,\, u_t,\, w_t)$ with control policy $u_t = \pi_t(x_t)$. Defining $f_t(x_t,\, w_t) := \tilde{f}_t(x_t,\, \pi_t(x_t),\, w_t)$, Equation (5.1) can model feedback systems without the loss of generality.

5.2.2 Reachability Analysis

Finite-time forward reachability analysis is widely used for applications in safety and robustness verification. Reachability analysis aims to find a set $\mathcal{P}_t$ for some $t > 0$ such that

$$x_0 \in \mathcal{X}_0 \quad \Rightarrow \quad x_t \in \mathcal{P}_t. \tag{5.2}$$

The forward reachability analysis aims to find the smallest region $\mathcal{P}_t$ such that (5.2) is satisfied. We consider the following applications for reachability analysis for safety verification.

Finite-time Reach Verification

The nonlinear system in Equation (5.1) is said to achieve finite-time arrival with respect to $(\mathcal{X}_0, \mathcal{S})$ if

$$x \in \mathcal{X}_0 \quad \Rightarrow \quad x_T \in \mathcal{G}, \tag{5.3}$$

where $\mathcal{X}_0$ is a set of initial conditions and $\mathcal{S} \subseteq \mathbf{R}^n$ is a set of acceptable target states. The finite-time arrival can be directly implied from the definition of reachability analysis. By ensuring that the result of the reachability analysis satisfies $\mathcal{P}_T \subseteq \mathcal{G}$, the finite stability can be verified for the given nonlinear system. In contrast to Lyapunov stability, the definition in (5.3) uses pre-specified initial state-bound $\mathcal{X}_0$ and the target state bounds $\mathcal{G}$ and is not concerned with intermediate time steps. Finite-time stability can be useful for guaranteeing that for any initial condition starting within the set $\mathcal{X}_0$, the system is able to achieve the target state at the final time step.

Finite-time Avoid Verification

The nonlinear system in Equation (5.1) is said to achieve reach-avoidance if

$$x \in \mathcal{X}_0 \quad \Rightarrow \quad x_t \notin \mathcal{B}_t, \tag{5.4}$$

where $\mathcal{X}_0$ is a set of initial conditions and $\mathcal{B}_t \subseteq \mathbf{R}^n$ is a set of unsafe states at time t.

5.2.3 Contraction Analysis

Contraction theory studies the differential analysis of neighboring trajectories [67]. Consider a discrete-time autonomous system $x_{t+1} = f(x_t)$. Consider an infinitesimal displacement between two neighboring trajectories denoted by δx. We denote the change in coordinate with

$$\delta z = \Theta(x)\delta x, \tag{5.5}$$

where $\Theta(x, t)$ is a square matrix, which transforms the state, and its corresponding virtual dynamics:

$$\delta x_{t+1} = \frac{\partial f}{\partial x}(x_t)\delta x_t. \tag{5.6}$$

5.3 Reachability Analysis with Convex Relaxation

In this section, we consider the reachable set represented by polytopes and present an optimization-based method for computing those sets.

Computing Reachable Set with Polytopes

We consider the following poloytope as a candidate for reachability verifications,

$$\mathcal{P}_t(z_t^u, z_t^\ell) = \{x_t \mid z_t^\ell \leq A_t x_t \leq z_t^u\}, \tag{5.7}$$

where z_t^ℓ, $z_t^u \in \mathbf{R}^p$ are parameters that defines the set, and $A_t \in \mathbf{R}^{p\times n}$ is a matrix with $\ker(A_t) = 0$. We assume that the polytope is represented as an intersection of half-spaces (H-polytope) where the number of hyper planes is finite. The reachability analysis can be performed by computing the reachable set in the consecutive the consecutive time step (i.e., $x_t \in \mathcal{P}_t(z_t^u, z_t^\ell) \Rightarrow x_{t+1} \in \mathcal{P}_{t+1}(z_t^u, z_t^\ell)$.)

Lemma 8. Suppose that the variables $z^u \in \mathbf{R}^m$ and $z^\ell \in \mathbf{R}^m$ are given by

$$
\begin{aligned}
z^u_{k,t+1} = \max_{x_t, x_{t+1}, w_t} \quad & A_{k,t+1} x_{t+1} \\
\text{subject to} \quad & x_{t+1} = f(x_t) \\
& x_t \in \mathcal{P}_t(z^u_t,\, z^\ell_t),
\end{aligned}
\tag{5.8}
$$

Then, for every $x_t \in \mathcal{P}_t(z^u_t, z^\ell_t)$, the next state satisfies $x_{t+1} \in \mathcal{P}_{t+1}(z^u_{t+1}, z^\ell_{t+1})$.

Proof. By definition, $z^\ell_{t+1} \leq A_{t+1} x_{t+1} \leq z^u_{t+1}$, and therefore, $x^{(t+1)} \in \mathcal{P}_{t+1}$ □

The problem in (5.8) are non-convex problems, and is NP-hard to solve in general.

Convex Relaxation

Given knowledge about nonlinearity, we can use known upper-concave lower-convex envelopes to relax the nonlinear equality constraints.

Corollary 7. (Upper-Concave Lower-Convex Envelopes) Suppose that the function f_k is known to be bounded by some analytical functions f^u_k and f^ℓ_k such that

$$
f^\ell_{k,\mathcal{D}}(x) \leq f_k(x) \leq f^u_{k,\mathcal{D}}(x), \quad x \in \mathcal{D}, \tag{5.9}
$$

where $f^\ell_{k,\mathcal{D}}$ is concave and $f^u_{k,\mathcal{D}}$ is convex function of x in the domain $\mathcal{D}$.

The subscript $\mathcal{D}$ in the envelope denotes that the domain for the envelope is $\mathcal{D}$. Having smaller $\mathcal{D}$ allows more accurate estimators.

Lemma 9. (Convex Relaxation) Suppose that function f^u and f^ℓ Suppose that the variables z^u and z^ℓ are given by

$$
\begin{aligned}
z^u_{k,t+1} = \max_{z} \quad & A_{k,t+1} x_{t+1} \\
\text{subject to} \quad & f^\ell(x_t) \leq x_{t+1} \leq f^u(x_t) \\
& x_t \in \mathcal{P}_t(z^u_t,\, z^\ell_t),
\end{aligned}
\tag{5.10}
$$

Then, for every $x_{t+1} \in \mathcal{P}_{t+1}(z^u_{t+1}, z^\ell_{t+1})$.

Algorithm for computing reachable sets

Algorithm 3 Reachability Analysis

1: *Initialize*: Compute nominal trajectory
2: **for** $t = 1, \ldots, T$ **do**
3: **for** $k = 1, \ldots, n$ **do**
4: Update z^u and z^ℓ in Equation (5.10):

$$\begin{aligned} z^u_{k,t+1} = \max_{z} \quad & A_{k,t+1} x_{t+1} \\ \text{subject to} \quad & f^\ell(x_t) \leq x_{t+1} \leq f^u(x_t) \\ & x_t \in \mathcal{P}_t(z^u_t,\, z^\ell_t), \end{aligned} \tag{5.11}$$

5: **end for**
6: **end for**
7: **return** $\mathcal{P}(z^u,\, z^\ell)$.

5.4 Obtaining Reachable Set Templates via Contraction Analysis

In this section, we provide a numerical method for computing contraction metrics in discrete-time dynamical systems.

5.4.1 Global Contraction metric

Lemma 10. Suppose that there exists a contraction metric Θ such that for every $x \in \mathcal{D}$,

$$\Theta\left(f(x)\right) \frac{\partial f}{\partial x}(x) = \sqrt{\beta}\Theta(x). \tag{5.12}$$

Then, the system is semi-contracting with metric $M = \Theta^T\Theta$ in the domain $\mathcal{D}$.

Proof. Consider the virtual displacement $\delta z^T_{t+1}\delta z_{t+1}$. Equation 5.12 implies that

$$\begin{aligned} &\delta z^T_{t+1}\delta z_{t+1} = \delta x^T_{t+1}\Theta^T_{t+1}\Theta_{t+1}\delta x_{t+1} \\ &= \delta x^T_t \frac{\partial f}{\partial x}^T \Theta^T_{t+1}\Theta_{t+1}\frac{\partial f}{\partial x}\delta x_t = \beta\delta x^T_t\Theta^T_t\Theta_t\delta x_t = \beta\delta z^T_t\delta z_t. \end{aligned}$$

□

Corollary 8. Suppose that the condition in Equation 5.12 holds. Then, $F^T_t F_t = \beta I$ where F_t is the generalized Jacobian.

Proof. Given that the generalized Jacobian is defined as $F_t = \Theta_{t+1}\frac{\partial f}{\partial x}\Theta_t^{-1}$:

$$\begin{aligned} F_t^T F_t &= \left(\Theta_t^T\right)^{-1} \frac{\partial f}{\partial x}^T \Theta_{t+1}^T \Theta_{t+1} \frac{\partial f}{\partial x} \Theta_t^{-1} \\ &= \left(\Theta_t^T\right)^{-1} \left(\beta \Theta_t^T \Theta_t\right) \Theta_t^{-1} = \beta I. \end{aligned}$$

□

5.4.2 Contraction metric for a nominal trajectory

Consider a nominal trajectory $x_1, \ldots, x_N$ that satisfies $x_{t+1} = f(x_t)$.

Lemma 11. Suppose that the metric is computed recursively by solving the equation,

$$\Theta(x_{t+1})\frac{\partial f}{\partial x}(x_t) = \sqrt{\beta}\Theta(x_t) \tag{5.13}$$

Then the metric $M(x) = \Theta(x)^T\Theta(x_t)$ is a valid contraction metric for the dynamical system, $x_{t+1} = f(x_t)$.

This metric can be computed by solving a system of linear equation $\Theta(x_{t+1}) = \left(\frac{\partial f}{\partial x}(x_t)\right)^{-1}\Theta(x_t)$, or more efficiently by propagating the metric backwards in time by $\Theta(x_t) = \Theta(x_{t+1})\frac{\partial f}{\partial x}(x_t)$.

5.4.3 Contraction in Invariant Set

Corollary 9. If the system is linear (i.e., $f(x) = Ax$), then the condition in Lemma 9 is a necessary and sufficient condition.

Lemma 12. Suppose that for every $x \in \mathcal{P}_t(z_t^u, z_t^\ell)$,

$$\frac{\partial f}{\partial x}(x)^T M_{t+1}\frac{\partial f}{\partial x}(x) \leq M_t, \tag{5.14}$$

then the trajectories in $\mathcal{P}_t(z_t^u, z_t^\ell)$ is contracting and converges exponentially to each other.

5.5 Numerical Studies

A transmission line or generator contingency on power systems is a common cause of loss of synchronism. The existence of a feasible solution is insufficient, and the dynamic stability of the system should be studied as well in order to ensure the security of the grid. In this paper, we consider the second-order swing equation with Kron reduction, which is widely used:

$$m_k\ddot{\delta}_k + d_k\dot{\delta}_k + \sum_{j\in\mathcal{N}_k} a_{kj}\sin(\delta_k - \delta_j) = P_{mk} \tag{5.15}$$

where m_k, d_k and P_{mk} are the inertia, damping and mechanical power injection at bus k, respectively. $a_{kj} = B_{kj}V_kV_j$ is the constant as we assume that the voltage is strictly regulated to 1 p.u. We can rewrite the swing equation with the following compact vector notation,

$$\begin{aligned}\dot{\delta} &= \omega \\ \dot{\omega} &= M^{-1}(-D\omega - E^TX^{-1}\sin(E\delta) + P_{inj}).\end{aligned} \tag{5.16}$$

where M, D and X are diagonal matrix with diagonal entries being the inertia and damping of generators and line impedance respectively. P_{inj} is a vector of power injection.

2 bus system

In this section, we present the result on a 2 bus system for illustration of our approach. Figure 5-1 shows the phase portrait of the system as well as the polytope computed at every time step. In this case, every trajectory from the initial operating point set is stabilized to the equilibrium. We note that this approach can survive near the unstable equilibrium point where the system becomes highly nonlinear in 2-dimensional analysis. Figure 5-2 shows the Monte-Carlo simulation as well as the bound computed using the reachability approach. The bound is shown to be very tight to the Monte-Carlo simulation and converges to the equilibrium.

Figure 5-3 shows a case where the initial polytope goes through the unstable equilibrium. While some of the solutions are able to reach back to the equilibrium, the polytope grows due to the trajectories that do not converge to the desired equilibrium.

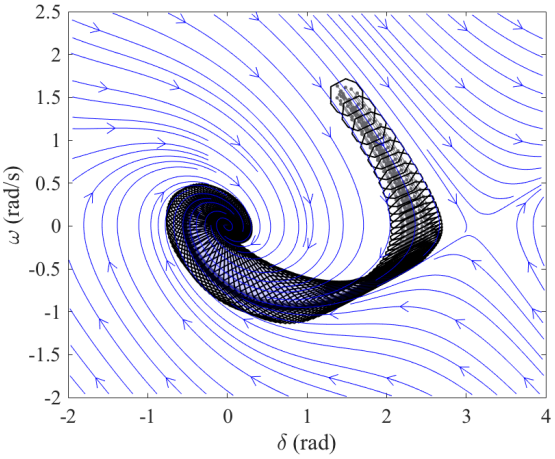

Figure 5-1: The phase portrait of the dynamics as well as the polytopes computed with the reachability analysis is shown for a 2 bus system. In this case all the initial conditions converged to the equilibrium.

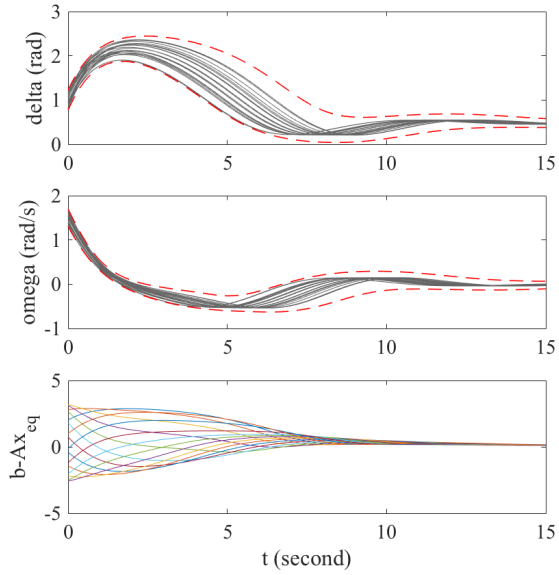

Figure 5-2: The time domain simulation of the system based on the Monte-carlo simulation is shown. The red dashed lines are the bound from the reachability analysis. On the bottom, the distance of each planes from the equilibrium is shown, which converged to zero.

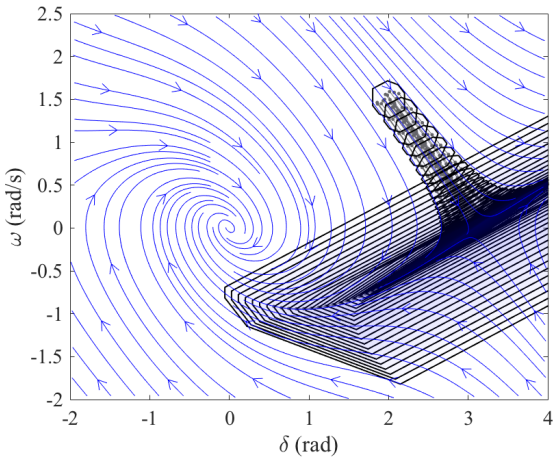

Figure 5-3: Case study for an unstable case in 2 bus system is shown in this figure.

39 bus system

In Figure 5-4, the contraction of the polytope is also shown. It also demonstrates an exponential convergence towards the equilibrium.

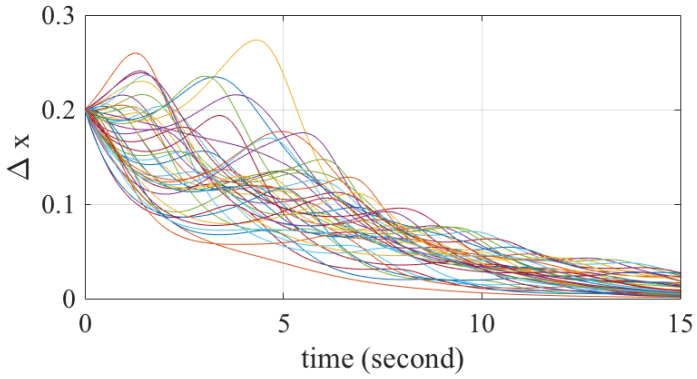

Figure 5-4: Contraction of polytope size on a 39 bus system.

5.6 Concluding Remarks

We present the reachability analysis approach for discrete-time nonlinear systems. We presented an algorithm based on convex relaxation to compute reachable sets. The states are bounded using polytope that is adapted to the natural modal shape of the system dynamics in the neighborhoods of the equilibrium. We demonstrate our

method on IEEE test cases to certify the stability and bound the state trajectories.

Chapter 6

Constrained-Input Constrained-Output Analysis

6.1 Introduction

In the presence of external disturbances to a dynamical system, the behavior of state variables changes constantly. One way to characterize the system is determining the relationship between the input signal and the output signal. Consider a dynamical system with input u and output y,

$$\dot{x} = f(x, u),$$
$$y = h(x, u).$$

The input signal $u : [0, \infty) \to \mathbf{R}^n$, the state $x : [0, \infty) \to \mathbf{R}^s$, and output signal $y : [0, \infty) \to \mathbf{R}^m$ maps the time interval $[0, \infty)$ into Euclidean space, and $f : (\mathbf{R}^s, \mathbf{R}^n) \to \mathbf{R}^n$ and $h : (\mathbf{R}^s, \mathbf{R}^n) \to \mathbf{R}^m$ are vectors of continuous function. We assume that there is a known nominal equilibrium x_{eq} and u_{eq} such that $f(x_{\text{eq}}, u_{\text{eq}}) = 0$, and the initial condition starts at that equilibrium (i.e., $x(0) = x_{\text{eq}}$ and $u(0) = u_{\text{eq}}$). This chapter focuses on finding the relationship between the bound on the peak magnitude of input signal and output signal. Input to output analysis in this chapter aims to follow the following condition:

$$\forall\, i,\ \max_{t\geq 0} |u_i(t)| \leq \bar{u}_i \quad \Rightarrow \quad \forall\, j,\ \max_{t\geq 0} |y_j(t)| \leq \bar{y}_j, \tag{6.1}$$

for some bounds $\bar{u} \in \mathbf{R}^n$ and $\bar{y} \in \mathbf{R}^m$. We want to find the least conservative estimate of $\bar{y}_j$ while guaranteeing condition (6.1) since a trivial bound $\bar{y}_j$ would be infinite. For engineering applications, we are sometimes interested in computing maximum tolerable input disturbance given output constraints (i.e., given $\bar{y}$, compute maximum $\bar{u}$ that satisfies condition (6.1).) Alternatively, computing the worst-case damage to the system when the input disturbance is known can be useful to assess potential damage to the system.

One of the applications of the input-output relationship problems has been the transient stability of power systems under operational (e.g., frequency) constraints. These studies can be divided into three main groups. The first group proposes numerical simulations under stochastic disturbances, where the output trajectory is computed for a given realization of the disturbance [37, 69, 75]. Time-domain simulations yield high fidelity assessments when the disturbance and the operating conditions are known exactly. However, when there is limited information about the disturbance, the assessment may require a large number of simulations. The second group is based on reachability analysis, where the output trajectories are bounded inside the reachable set [26, 27, 62, 1, 94]. While some of these formulations allow differential-algebraic equations to model the power grid dynamics, they rely on the approximation of the dynamics via linearization or Taylor-series expansion [26, 27]. The works in [27, 62] give tight time-dependent bounds on the output, but they require solving an optimization problem at every time step. The third and final group is based on Input-to-State Stability (ISS) [2, 91] analysis. ISS provides a powerful rigorous approach to tackle such a problem, however finding a Lyapunov function that renders this approach non-conservative is in general very difficult.

6.2 Background

6.2.1 Lur'e System Representation

Lur'e system represents a system as an interconnection of a linear dynamical system with a nonlinear static state feedback. The Lur'e system, together with the efficient bounding of the nonlinearity between linear functions, heavily simplifies the analysis of the nonlinear systems. The nominal form of the dynamical systems is given by

$$\dot{x} = Ax + B_v v + B_u u \tag{6.2a}$$

$$v = \psi(z) \tag{6.2b}$$

$$y = C_y x + D_y u \tag{6.2c}$$

$$z = C_z x, \tag{6.2d}$$

where $x(t) \in \mathbf{R}^s$, $u(t) \in \mathbf{R}^n$, and $y(t) \in \mathbf{R}^m$ are system state, input signal, and output signal, respectively. Variables $z(t) \in \mathbf{R}^\ell$ and $v(t) \in \mathbf{R}^q$ are transformed system state, and $A \in \mathbf{R}^{s\times s}$, $B_v \in \mathbf{R}^{s\times q}$, $B_u \in \mathbf{R}^{s\times n}$, $C_y \in \mathbf{R}^{m\times s}$, $D_y \in \mathbf{R}^{m\times n}$, and $C_z \in \mathbf{R}^{\ell\times s}$ are constant matrices defined in the system. The function $\psi : \mathbf{R}^\ell \to \mathbf{R}^\ell$ is a vector of function, and we assume that it is decentralized, i.e., $v_i = \psi_i(z_i)\ \forall i \in \{1, \ldots, \ell\}$.

Transfer Function Matrix

Let the transfer function matrix $G(s)$ represent the linear dynamics in Laplace domain where the linear system is defined by Equations (6.2a), (6.2c), and (6.2d). Then the Lur'e system (6.2) can be graphically represented as in Figure 6-1. Following this representation of the system, the transfer function matrix G can be divided into four blocks:

$$G(s) = \begin{bmatrix} G_{y,u}(s) & G_{y,v}(s) \\ G_{z,u}(s) & G_{z,v}(s) \end{bmatrix} \tag{6.3}$$

where each block of transfer matrix can be computed by $G_{i,j}(s) = C_i(sI - A)^{-1}B_j$, with $i \in \{y, z\}$ and $j \in \{u, v\}$. This representation of the system implies that the initial condition of the system is at the equilibrium (i.e. $x_0 = \mathbf{0}$). Given the system

model described in this section, the problem can be formulated as follows.

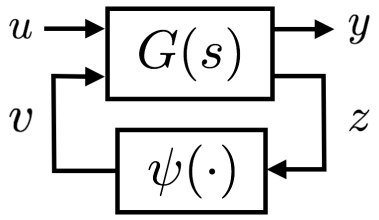

Figure 6-1: Lur'e system representation of the power system dynamics in $G(s)$ and the nonlinear components in $\psi(\cdot)$.

6.2.2 Problem Formulation

Consider the system model (6.2), containing the additive magnitude-bounded disturbance u. This chapter concentrates on finding the maximum bound on the magnitude of the disturbance such that the output signal satisfies safety constraints. In order to quantify the magnitude of the disturbance u, we propose the following element-wise infinity norm.

Definition 2. Let $u(t) \in \mathbf{R}^n$. Its element-wise $\mathcal{L}$-infinity norm, which we denote by $|u|_{\mathcal{L}_\infty^n} \in \mathbf{R}^n$, is defined as

$$\left[|u|_{\mathcal{L}_\infty^n}\right]_i = \sup_{t\geq 0} |u_i(t)| \tag{6.4}$$

where $\left[|u|_{\mathcal{L}_\infty^n}\right]_i$ and u_i are the i-th entries of $|u|_{\mathcal{L}_\infty^n}$ and u, respectively.

Remark 5. The element-wise $\mathcal{L}$-infinity generalizes the standard $\mathcal{L}_\infty$ norm of u, defined as $\|u\|_{\mathcal{L}_\infty} = \max_i(\sup_{t\geq 0} |u_i(t)|)$. The proposed element-wise norm allows us to represent different magnitudes at each component of the vector, rather than bounding them uniformly. This fact will be exploited later, where an optimization problem will be formulated to compute the maximum magnitude of the admissible disturbance. To avoid any confusion, we denoted the element-wise $\mathcal{L}$-infinity norm of an n-dimensional signal by $\mathcal{L}_\infty^n$, where the superscript n should remind the reader that $|\cdot|_{\mathcal{L}_\infty^n}$ is an n-dimensional vector.

Problem Formulation

Consider the system written in the Lur'e form (6.2), with initial condition $x_0 = \mathbf{0}$. The objective of our problem is to find the maximum bound $\bar{u} \in \mathbf{R}^n$ on the disturbance such that if $|u|_{\mathcal{L}_\infty^n} \leq \bar{u}$, then $|y|_{\mathcal{L}_\infty^m} \leq \bar{y}$.

6.2.3 Preliminaries

Definition 3. A mapping $H : \mathcal{L}_e^m \to \mathcal{L}_e^q$ is $\mathcal{L}$ stable if there exists a class $\mathcal{K}$ function

Let $y = Hu$ define an input-output relation, where H is an operator that specifies the output y in terms of the input u. In the following we will introduce three types of input-output relations for the operator H with respect to the element-wise infinity norm $|\cdot|_{\mathcal{L}_\infty}$. The first type is the Bounded Input Bounded Output stability, which is defined as follows.

Definition 4 (**Bounded Input Bounded Output**). The operator H is BIBO stable if for every input constraint $\bar{u}$, if $|u|_{\mathcal{L}_\infty^n} \leq \bar{u}$, then the output $|y|_{\mathcal{L}_\infty^m}$ is bounded.

Notice that it is not always possible to meet such a condition, especially for nonlinear systems. We now define the second type of input-output stability, namely the Constrained Input Bounded Output (CIBO) stability.

Definition 5. **(Constrained Input Bounded Output)** The operator H is CIBO stable if there exists an input constraint $\bar{u}$, such that for every input u with $|u|_{\mathcal{L}_\infty^n} \leq \bar{u}$, the output $|y|_{\mathcal{L}_\infty^m}$ is bounded.

Recall from Section 6.2.2 that we want to find the maximum bound on the magnitude of the disturbance such that the output signal satisfies safety constraints. We formalize this concept into the third and last type of input-output stability, Constrained Input Constrained Output (CICO) stability.

Definition 6. **(Constrained Input Constrained Output)** The operator H is CICO stable if given an output constraint $\bar{y}$, there exists an input constraint $\bar{u}$, such that for every input with u with $|u|_{\mathcal{L}_\infty^n} \leq \bar{u}$, the output satisfies $|y|_{\mathcal{L}_\infty^m} \leq \bar{y}$.

In Section 6.3 we will propose conditions under which the system (6.2) is BIBO, CIBO, and CICO stable.

System Gain

Let $y = Hu$ be a BIBO stable system. If there exists a non-negative constant matrix $\gamma_H \in \mathbf{R}^{m\times n}$ such that

$$|y|_{\mathcal{L}_\infty^m} \leq \gamma_H |u|_{\mathcal{L}_\infty^n}, \tag{6.5}$$

then we refer to γ_H as the gain matrix of the system.

When the input is bounded, i.e., $|u|_{\mathcal{L}_\infty^n} \leq \bar{u}$, we denote the gain matrix by $\gamma_H(\bar{u})$ to remind that it is a function of the domain parametrized by $\bar{u}$.

For a BIBO stable linear system, where the operator H corresponds to the transfer function $G(s)$ in equation (6.3), the gain matrix γ_G can be computed using the following lemma.

Lemma 13. Given a BIBO stable linear system with transfer function $G(s)$, the ij element of the gain matrix γ_G can be computed as

$$\gamma_{G,ij} = \|G_{ij}\|_{\mathcal{L}_1} \tag{6.6}$$

with $\|G_{ij}\|_{\mathcal{L}_1} = \int_{-\infty}^{\infty} |h_{ij}(\tau)| d\tau$, where h_{ij} is the impulse response of G_{ij}.

Proof. For the i-th element of the output vector,

$$|y_i(t)| \leq \sum_j \bar{u}_j \int_{-\infty}^{\infty} |h_{ij}(\tau)| d\tau = \sum_j \|G_{ij}\|_{\mathcal{L}_1} \bar{u}_j.$$

□

The matrix γ_G, can be divided, according to (6.3), into

$$\gamma_G = \begin{bmatrix} \gamma_{y,u} & \gamma_{y,v} \\ \gamma_{z,u} & \gamma_{z,v} \end{bmatrix}, \tag{6.7}$$

where $\gamma_{y,u} \in \mathbf{R}^{m\times n}$, $\gamma_{y,v} \in \mathbf{R}^{m\times \ell}$, $\gamma_{z,u} \in \mathbf{R}^{\ell\times n}$, and $\gamma_{z,v} \in \mathbf{R}^{\ell\times \ell}$ are the gain matrices computed as shown in Lemma 13.

The gain of the nonlinear component, γ_ψ, can be computed by

$$\gamma_{\psi,ij} = \sup_{z_j} \left| \frac{v_i}{z_j} \right|. \tag{6.8}$$

For number of applications, the expression for Equation (6.8) have a closed-form solution. We will present a power grid example later in the simulation section.

6.3 Input-Output Stability Analysis

In this section, we establish the mathematical framework for the analysis and assessment of the system under the additive disturbance u. The proposed framework combines the input-output stability approach with the sector bounds on the nonlinearity v in the Lur'e system to propose a novel small-gain theorem based on the element-wise $\mathcal{L}$-infinity norm $|\cdot|_{\mathcal{L}_\infty}$.

Given the computed gain matrices of the system, the following inequalities hold:

$$|y|_{\mathcal{L}_\infty^m} \leq \gamma_{y,u}|u|_{\mathcal{L}_\infty^n} + \gamma_{y,v}|v|_{\mathcal{L}_\infty^\ell} \tag{6.9a}$$

$$|z|_{\mathcal{L}_\infty^\ell} \leq \gamma_{z,u}|u|_{\mathcal{L}_\infty^n} + \gamma_{w,v}|v|_{\mathcal{L}_\infty^\ell} \tag{6.9b}$$

$$|v|_{\mathcal{L}_\infty^\ell} \leq \gamma_\psi|z|_{\mathcal{L}_\infty^\ell} \tag{6.9c}$$

The gain matrices are non-negative, i.e., $\gamma_{i,j} \geq 0, \forall\, i, j$. Using this property, we state the following lemma, which will be important in the proof of the subsequent results of this section.

Lemma 14. Given the positive matrices $\gamma_{w,v}$ and γ_ψ, the following three conditions are equivalent:

(i) $\rho(\gamma_{z,v}\gamma_\psi) < 1$

(ii) $(I - \gamma_{z,v}\gamma_\psi)^{-1} \geq 0$

(iii) There exists $x \geq 0$ such that $(I - \gamma_{z,v}\gamma_\psi)x > 0$

Proof. The proof is based on the properties of Z and M-matrices. A matrix is a Z-matrix if its off-diagonal elements are non-positive, and it is an M-matrix if it is a Z-matrix and its eigenvalues have non-negative real parts. First the matrix $I - \gamma_{z,v}\gamma_\psi$ is a Z-matrix since the gain matrices are non-negative. Now notice that $\rho(\gamma_{z,v}\gamma_\psi) < 1$ if and only if the eigenvalues of $I - \gamma_{z,v}\gamma_\psi$ have positive real parts, which is the definition of a nonsingular M-matrix. Given that $I - \gamma_{z,v}\gamma_\psi$ is a nonsingular M-matrix, condition (i), (ii), and (iii) are equivalent [79]. □

Remark 6. Since the matrix $\gamma_{z,v}\gamma_\psi$ is nonnegative, it has a real eigenvalue equal to its spectral radius $\rho(\gamma_{z,v}\gamma_\psi)$ [20].

In the next theorem, we present the condition under which the system is BIBO stable.

Theorem 11 (**Small-Gain Theorem**). The system (6.2) is BIBO stable if the gain matrices γ_G and γ_ψ are finite, and $\rho(\gamma_{z,v}\gamma_\psi) < 1$.

Proof. By substituting Equation (6.9b) into Equation (6.9c) and rearranging, we have

$$(I - \gamma_{z,v}\gamma_\psi)|z|_{\mathcal{L}_\infty^\ell} \leq \gamma_{z,u}|u|_{\mathcal{L}_\infty^n}.$$

Since $\rho(\gamma_{z,v}\gamma_\psi) < 1$, Lemma 14 guarantees that $(I - \gamma_{z,v}\gamma_\psi)^{-1} \geq 0$. As such,

$$|z|_{\mathcal{L}_\infty^\ell} \leq (I - \gamma_{z,v}\gamma_\psi)^{-1}\gamma_{z,u}|u|_{\mathcal{L}_\infty^n}.$$

The output can be bounded by

$$\begin{aligned}
|y|_{\mathcal{L}_\infty^m} &\leq \gamma_{y,u}|u|_{\mathcal{L}_\infty^n} + \gamma_{y,v}|v|_{\mathcal{L}_\infty^\ell} \\
&\leq \gamma_{y,u}|u|_{\mathcal{L}_\infty^n} + \gamma_{y,v}\gamma_\psi|z|_{\mathcal{L}_\infty^\ell} \\
&\leq \left[\gamma_{y,u} + \gamma_{y,v}\gamma_\psi(I - \gamma_{z,v}\gamma_\psi)^{-1}\gamma_{z,u}\right]|u|_{\mathcal{L}_\infty^n}.
\end{aligned}$$

Therefore, the system is BIBO stable. □

Remark 7. Theorem 11 ensures more than just BIBO stability. The last inequality in the proof implies that there exists a non-negative constant gain matrix $\gamma_H =$

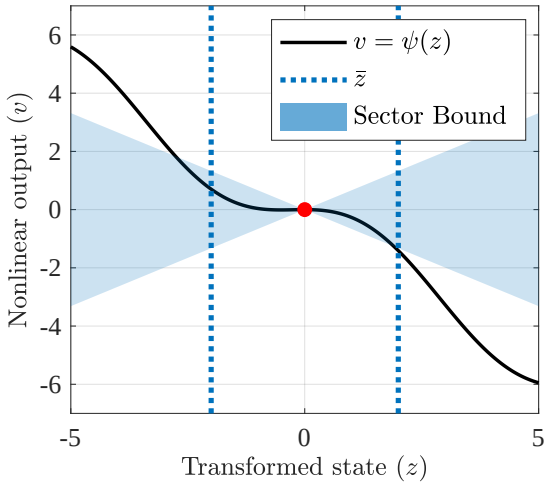

Figure 6-2: Sector bound for $v = \psi(z) = \sin(z + \varphi^*) - \cos(\varphi^*)z$.

$\left[\gamma_{y,u} + \gamma_{y,v}\gamma_\psi(I - \gamma_{z,v}\gamma_\psi)^{-1}\gamma_{z,u}\right]$ such that

$$|y|_{\mathcal{L}_\infty^m} \leq \gamma_H |u|_{\mathcal{L}_\infty^n}, \tag{6.10}$$

and therefore the system is finite gain $\mathcal{L}_\infty^{\cdot}$ stable [54].

Theorem 11 presents a novel small-gain theorem, defined for the element-wise $\mathcal{L}$-infinity norm $|\cdot|_{\mathcal{L}_\infty^{\cdot}}$. The small-gain condition ensures BIBO stability, which guarantees that the output is bounded for any bounded input. For general nonlinear systems, the boundedness of the output cannot be guaranteed for every bounded input. However, if the magnitude of the disturbance is constrained by some appropriate $\bar{u}$, the output could be bounded.

The condition in Theorem 11 is not satisfied for an arbitrary nonlinear gain matrix γ_ψ. Indeed, since $\rho(\gamma_{z,v}\gamma_\psi) < 1$, it results that for fixed linear gain matrix $\gamma_{z,v}$, there exists a limit on the magnitude of γ_ψ such that our system is BIBO stable. This can be deduced from the fact that γ_ψ is a non-negative diagonal matrix, and therefore the spectral radius $\rho(\gamma_{z,v}\gamma_\psi)$ is a strictly increasing function in γ_ψ. Let $\bar{z}$ be some magnitude bound on z, i.e., $|z|_{\mathcal{L}_\infty^\ell} \leq \bar{z}$. Now γ_ψ is function of $\bar{z}$, i.e., $\gamma_\psi = \gamma_\psi(\bar{z})$, and that larger $\bar{z}$ results in larger $\gamma_\psi(\bar{z})$ (see Figure 6-2). As a consequence, the condition in Theorem 11 could be satisfied for some $\bar{z}$.

This observation is exploited in the following theorem, where a sufficient condition

for the CIBO stability of our system is presented.

Theorem 12. Let $\bar{u}$ be a bound on the magnitude of the input, i.e., $|u|_{\mathcal{L}_\infty^n} \leq \bar{u}$. If γ_G and γ_ψ are finite, and if there exist $\bar{u}$ and $\bar{z}$ satisfying

$$\gamma_{z,u}\bar{u} < (I - \gamma_{z,v}\gamma_\psi(\bar{z}))\bar{z} \tag{6.11}$$

then the system (6.2) is CIBO stable and $|z|_{\mathcal{L}_\infty^\ell} \leq \bar{z}$.

Proof. Since the gain matrix is a positive matrix and $\bar{u} \geq 0$, $(I-\gamma_{z,v}\gamma_\psi(\bar{z}))\bar{z} > \gamma_{z,u}\bar{u} \geq 0$ with $\bar{z} \geq 0$. From Lemma 14, $\rho(\gamma_{z,v}\gamma_\psi) < 1$, and by using Theorem 11, the system is BIBO stable for $|u|_{\mathcal{L}_\infty^n} \leq \bar{u}$. Substituting condition (6.11) and Equation (6.9c) into Equation (6.9a), we have

$$\begin{aligned} |z|_{\mathcal{L}_\infty^\ell} &\leq \gamma_{z,u}|u|_{\mathcal{L}_\infty^n} + \gamma_{z,v}|v|_{\mathcal{L}_\infty^\ell} \\ &\leq (I - \gamma_{z,v}\gamma_\psi(\bar{z}))\bar{z} + \gamma_{z,v}\gamma_\psi(\bar{z})|z|_{\mathcal{L}_\infty^\ell}. \end{aligned}$$

By rearranging,

$$(I - \gamma_{z,v}\gamma_\psi(\bar{z}))|z|_{\mathcal{L}_\infty^\ell} \leq (I - \gamma_{z,v}\gamma_\psi(\bar{z}))\bar{z}.$$

Now, $I - \gamma_{z,v}\gamma_\psi(\bar{z})$ is inverse-positive from Lemma 14, so $|z|_{\mathcal{L}_\infty^\ell} \leq \bar{z}$. □

Remark 8. Theorem 12 provides a local small-gain condition over the domain $|z|_{\mathcal{L}_\infty^\ell} \leq \bar{z}$. If the condition (6.11) is satisfied for all $\bar{z}$, then it is equivalent to the small-gain condition from Theorem 11, and the system is BIBO stable.

This remark can be directly observed from Lemma 14. This inequality condition is a different representation of the small-gain condition, but further exploits the fact that γ_ψ can be a function of $\bar{z}$. There is a natural trade-off based on the value of $\bar{z}$. The nonlinear gain γ_ψ increases as $\bar{z}$ increases, which makes it difficult to meet the small-gain condition. On the other hand, small $\bar{z}$ imposes a stricter bound on the phase difference on the transmission lines. This trade-off is represented as the product of $I - \gamma_{z,v}\gamma_\psi(\bar{z})$ and $\bar{z}$, which are monotonically decreasing and linearly increasing functions of $\bar{z}$, respectively.

Now, in order to enforce output constraints, we need to impose an additional condition that will guarantee CICO stability. This is presented in the following theorem.

Theorem 13. Let $\bar{u}$ be a bound on the magnitude of the input, i.e., $|u|_{\mathcal{L}_\infty^n} \leq \bar{u}$. If γ_G and γ_ψ are finite, and if there exist $\bar{u}$ and $\bar{z}$ such that

$$\begin{aligned} \gamma_{z,u}\bar{u} &< (I - \gamma_{z,v}\gamma_\psi(\bar{z}))\bar{z} \\ \gamma_{y,u}\bar{u} + \gamma_{y,v}\gamma_\psi(\bar{z})\bar{z} &\leq \bar{y} \end{aligned} \tag{6.12}$$

then the system (6.2) is CICO stable. Moreover, we have $|z|_{\mathcal{L}_\infty^\ell} \leq \bar{z}$ and $|y|_{\mathcal{L}_\infty^m} \leq \bar{y}$.

Proof. From Theorem 12, the first condition in (6.12) ensures $|z|_{\mathcal{L}_\infty^\ell} \leq \bar{z}$. Moreover, the substitution of the condition in this theorem and Equation (6.9c) into Equation (6.9a) results in

$$|y|_{\mathcal{L}_\infty^m} \leq \gamma_{y,u}|u|_{\mathcal{L}_\infty^n} + \gamma_{y,v}\gamma_\psi|z|_{\mathcal{L}_\infty^\ell} \leq \gamma_{y,u}\bar{u} + \gamma_{y,v}\gamma_\psi\bar{z} \leq \bar{y}.$$

□

The inequalities proposed in Theorem 13 provide a sufficient condition for CICO stability. Condition (6.12) will be used in the next section as a constraint in an optimization problem that computes the maximum admissible disturbance magnitude.

6.4 Computation of the Disturbance Bound

In the following, an optimization problem is formulated to find the bound $\bar{u}$ on the disturbance such that the frequencies of the generators remain inside the operational limits. Given a potential disturbance u, the system operator only needs to check that $|u|_{\mathcal{L}_\infty^n} \leq \bar{u}$ is satisfied to ensure that the safety constraints are not violated. The input-output stability framework developed in Theorem 13 will be used to solve this problem.

The maximum bound on the magnitude of the admissible disturbance can be

computed with the following optimization problem:

$$\begin{aligned} \underset{\bar{z}\geq 0,\ \bar{u}\geq 0,\ \mu}{\text{maximize}} \quad & \mu \\ \text{subject to} \quad & \gamma_{z,u}\bar{u} < (I - \gamma_{z,v}\gamma_{\psi}(\bar{z}))\bar{z} \\ & \gamma_{y,u}\bar{u} + \gamma_{y,v}\gamma_{\psi}(\bar{z})\bar{z} \leq \bar{y} \\ & \mu \leq c^T\bar{u} \end{aligned} \tag{6.13}$$

where $\bar{y}$ is the output peak magnitude limit provided by the system operators. The vector $c \in \mathbf{R}^n$ is used to fix the ratio of the disturbance entering at each component of the vector. This procedure allows us to find the maximum disturbance magnitude at a particular index, or alternatively, at a combination of indices.

The term $\gamma_{\psi}(\bar{z}))\bar{z}$ in Equation (6.13) introduce nonlinearity to the system, and the constraint could be non-convex as a result. In the next section, we present an example where there is an analytical expression for the nonlinear term.

6.4.1 Analytical derivation of nonlinear gain

Consider the following nonlinear function as an example for $v = \psi(z)$:

$$\psi(z) = \sin(\varphi^* + z) - \sin\varphi^* - \text{diag}(\cos\varphi^*)z$$

We derive an explicit expression for the gain of nonlinear component γ_{ψ}. Recall that γ_{ψ} is function of $\bar{z}$:

$$\gamma_{\psi,ii}(\bar{z}_i) = \sup_{|z_i|\leq\bar{z}_i} \left| \frac{\sin(z_i + \varphi_i^*) - \sin(\varphi_i^*)}{z_i} - \cos(\varphi_i^*) \right| \tag{6.14}$$

where $\varphi^* = E^T\delta^*$.

In the following corollary, we derive an analytical expression for the gain of the nonlinear components $\gamma_{\psi,ii}(\bar{z}_i)$, for angle deviation constraints that are of practical interest.

Corollary 10. Let $\bar{z}$ be a bound on the angle difference between generators and $\varphi^* =$

$E^T\delta^*$ be such that $|\varphi_i^*| + \bar{z}_i \leq \pi, |\varphi_i^*| \leq \frac{\pi}{2}\ \forall i$. Then,

$$\gamma_{\psi,ii}(\bar{z}_i) \leq \cos|\varphi_i^*| - \frac{\sin(|\varphi_i^*| + \bar{z}_i) - \sin|\varphi_i^*|}{\bar{z}_i}. \tag{6.15}$$

Proof. From Equation (6.14) and given $|\varphi_i^*| \leq \frac{\pi}{2}$, we have

$$\begin{aligned}
\gamma_{\psi,ii}(\bar{z}_i) &= \sup_{|z_i|\leq\bar{z}_i} \left| \frac{\sin(z_i + \varphi_i^*) - \sin(\varphi_i^*)}{z_i} - \cos(\varphi_i^*) \right| \\
&= \sup_{|z_i|\leq\bar{z}_i} \left| \frac{\sin z_i - z_i}{z_i} \cos\varphi_i^* + \frac{\cos z_i - 1}{z_i} \sin\varphi_i^* \right| \\
&\leq \sup_{|z_i|\leq\bar{z}_i} \frac{|z_i| - \sin|z_i|}{|z_i|} \cos|\varphi_i^*| + \frac{1 - \cos|z_i|}{|z_i|} \sin|\varphi_i^*|
\end{aligned}$$

Moreover, the function inside the supremum is increasing monotonically with respect to z_i for $|\varphi_i^*| + \bar{z}_i \leq \pi$. Therefore, the inequality (6.15) holds true. □

Propostion 1. The optimization problem (6.13) is convex within the region defined by the angle deviation constraints $|\varphi_i^*| + \bar{z}_i \leq \pi, |\varphi_i^*| \leq \frac{\pi}{2}\ \forall i$.

Proof. Using the explicit expression for $\gamma_\psi(\bar{z})$ in the constraint $\gamma_{z,u}\bar{u} \leq (I - \gamma_{z,v}\gamma_\psi(\bar{z}))\bar{z}$, we obtain the following constraint:

$$\begin{aligned}
\gamma_{z,u}\bar{u} \leq (I - \gamma_{z,v}\mathrm{diag}(\cos\varphi^*))\bar{z} \\
- \gamma_{z,v}\sin|\varphi^*| + \gamma_{z,v}\sin(|\varphi^*| + \bar{z}).
\end{aligned} \tag{6.16}$$

The sinusoidal term is concave within the region defined by the bound $0 \leq |\varphi_i^*| + \bar{z}_i \leq \pi$, and therefore the constraint in equation (6.16) forms a convex region. Similarly, the constrained output condition is similarly bounded to a convex region of a sinusoidal function. Therefore, the constraints are convex, and we can conclude that the optimization problem (6.13) is convex. □

6.5 Numerical Simulations

In this section, we numerically validate the theoretical and computational results presented in this paper. For illustration purposes, we first consider a single machine infinite bus system, on which we test and interpret the proposed results. Then, some practically important disturbance scenarios (e.g., simultaneous tripping of generators and loads, as well as the uncertainty from wind generation) will be tested on the standard IEEE 9-bus and 39-bus test cases.

Power Grid

We first discuss the model used in this experiment. Consider the following second-order swing equation for modeling the power system dynamics:

$$\begin{aligned} M\ddot{\delta}_G + D_G\dot{\delta}_G + E_G\Phi\sin(E^T\delta) &= p \\ D_L\dot{\delta}_L + E_L\Phi\sin(E^T\delta) &= P_L + u_L \\ T\dot{p} + p + R^{-1}\dot{\delta}_G &= P_G + u_G. \end{aligned} \tag{6.17}$$

where $u = \begin{bmatrix} u_G^T & u_L^T \end{bmatrix}^T$ is the disturbance vector. This simple formulation of the disturbance could incorporate a rich variety of uncertainty scenarios, such as load shedding, generation tripping, and stochastic fluctuations in the power output from wind turbines.

For $u_L = \mathbf{0}$ and $u_G = \mathbf{0}$, let δ^* and $\dot{\delta} = \mathbf{0}$ represent the equilibrium point of (6.17), with generator power injection p^*. Then, we define the state of the system as $x = \begin{bmatrix} x_1^T & x_2^T & x_3^T & x_4^T \end{bmatrix}^T$, with $x_1 = \delta_G - \delta_G^*$, $x_2 = \dot{\delta}_G$, $x_3 = \delta_L - \delta_L^*$, and $x_4 = p - p^*$.

Now let $z = E^T\delta - E^T\delta^*$ be the phase difference on each transmission line subtracted by its equilibrium, and y be the vector containing the frequencies of the generators $y = \dot{\delta}_G$. Finally, let $\varphi^* = E^T\delta^*$, and $v = \sin(\varphi^* + z) - \sin(\varphi^*) - \mathrm{diag}(\cos(\varphi^*))z$. With these new variables, the system (6.2) can be written in the Lur'e form $\dot{x} =$

$Ax + B_v v + B_u u$ as follows:

$$\dot{x} = \begin{bmatrix} \mathbf{0} & I & \mathbf{0} & \mathbf{0} \\ A_{21} & -M^{-1}D_G & A_{23} & M^{-1} \\ A_{31} & \mathbf{0} & A_{33} & \mathbf{0} \\ \mathbf{0} & -R^{-1}T^{-1} & \mathbf{0} & -T^{-1} \end{bmatrix} x + \begin{bmatrix} \mathbf{0} \\ -M^{-1}E_G\Phi \\ -D_L^{-1}E_L\Phi \\ \mathbf{0} \end{bmatrix} v + \begin{bmatrix} \mathbf{0} & \mathbf{0} \\ \mathbf{0} & \mathbf{0} \\ \mathbf{0} & D_L^{-1} \\ T^{-1} & \mathbf{0} \end{bmatrix} u \tag{6.18}$$

The complete model can be compactly written as

$$\dot{x} = Ax + B_v v + B_u u \tag{6.19a}$$

$$v = \sin(\varphi^* + z) - \sin\varphi^* - \operatorname{diag}(\cos\varphi^*)z \tag{6.19b}$$

$$y = \begin{bmatrix} \mathbf{0} & I & \mathbf{0} & \mathbf{0} \end{bmatrix} x = C_y x \tag{6.19c}$$

$$z = \begin{bmatrix} E_G^T & \mathbf{0} & E_L^T & \mathbf{0} \end{bmatrix} x = C_z x. \tag{6.19d}$$

The matrix A in (6.2) was obtained by linearization of the system (6.19) around the equilibrium point $x = \mathbf{0}$. The vector v represents the static nonlinear feedback of the state x, i.e., $v = \psi(z) = \psi(C_z x)$.

6.5.1 Single Machine Infinite Bus (SMIB)

The procedure and results are illustrated on a system composed of a single machine connected to an infinite bus through a lossless line. The dynamic equation is given by

$$M\ddot{\delta} + D\dot{\delta} + \phi\sin\delta = p + u \tag{6.20}$$

where $M = 1$, $D = 1.2$, $p = 0.2$ and $\phi = 0.8$ are the parameters used in this study. For $u = 0$, its equilibrium is given by $\delta^* = \arcsin(p/\phi)$, $\dot{\delta} = 0$. Let the output be the frequency in Hertz, $y = \dot{\delta}/2\pi$. Substituting $z = \delta - \delta^*$, and $v = \sin(\delta) - \cos(\delta^*)w$, we get

$$M\ddot{x} + D\dot{x} + \phi\cos(\delta^*)x + \phi v = u. \tag{6.21}$$

In frequency domain,

$$\begin{aligned} Z(s) &= \frac{1}{Ms^2 + Ds + \phi\cos(\delta^*)}\big[U(s) - \phi V(s)\big] \\ &= G_{w,u}U(s) + G_{w,v}V(s), \end{aligned} \tag{6.22}$$

and $Y(s) = sZ/2\pi$.

The gains corresponding to the transfer functions $G_{y,u}$, $G_{y,v}$, $G_{z,u}$, and $G_{z,v}$ are $\gamma_{y,u} = 0.178$, $\gamma_{y,v} = 0.142$, $\gamma_{z,u} = 1.434$, and $\gamma_{z,v} = 1.148$, respectively. Following the proposed procedure, the nonlinear gain is a function of the bound on the phase difference. This can be seen in Figure 6-3(a).

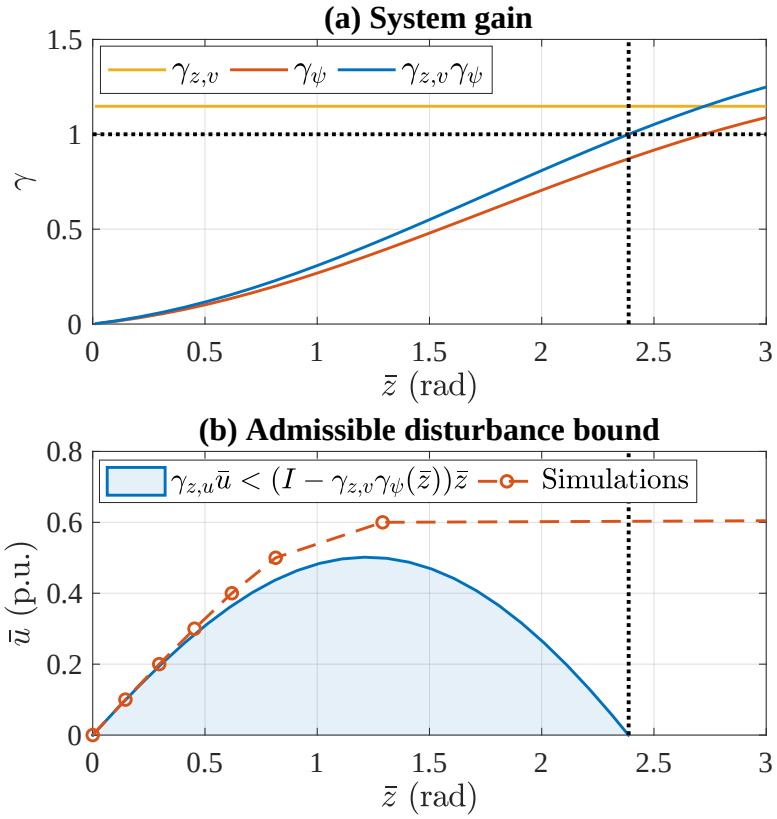

Figure 6-3: Maximum disturbance magnitude allowed as a function of sector bound for a SMIB system.

Since the gain matrices are just scalars, the condition for BIBO stability is simply $\gamma_{z,v}\gamma_{\psi} < 1$. In Figure 6-3(b) we plot with blue the CIBO stability condition presented in Theorem II. The vertical dashed black lines in the Figures 6-3(a) and 6-3(b) show

that the small-gain condition is violated if the CIBO stability condition is not satisfied.

In Figure 6-3(b), the estimation of the upper bound on the disturbance magnitude was computed by time-domain simulations. After applying a step disturbance with magnitude bounded by $\bar{u}$, the maximum phase difference deviation $\bar{z}$ was recorded. All the simulation points are represented with orange, and they are all connected by a dashed orange line. Since every simulation point is only a single realization among all possible disturbances, it only provides an upper-bound on the magnitude of the disturbance.

The approach proposed in this section uses convex optimization to efficiently compute the maximum magnitude for the admissible disturbance. Figure 6-3(b) shows that the gap between the upper-bound and the bound on the magnitude based on our method is very tight. The maximum disturbance magnitude allowed occurs when $\bar{z}$ is about 1.2 rad, which can be computed with the optimization problem (6.13). The small-gain condition in Figure 6-3(a) is violated when the angle deviation is about 2.4 rad. The bound on the disturbance magnitude becomes zero at the same $\bar{z}$, which illustrates the equivalence of conditions (i) and (iii) in Lemma 14. In Figure 6-4, the maximum frequency deviation is computed with the second condition in Theorem 13. Similarly, a lower-bound on the frequency deviation was computed using the same procedure explained for the upper-bound on the magnitude of the disturbance.

6.5.2 9-bus and 39-bus systems

This section presents numerical case studies on the IEEE 9-bus and 39-bus systems. The nonlinear optimization was performed using the interior point method in IPOPT [90] on a PC laptop with an Intel Core I7 3.3 GHz CPU and 16GB of memory. In Figure 6-5, we show a graphical representation of the computed maximum bound on the magnitude of the disturbance that can enter every single bus. The results suggest that the bigger disturbances are allowed to enter the buses with many neighbors to distribute the impact. For the generator nodes, the second-order dynamics together with the governor reduce the damping ratio, and only small disturbances are admissible.

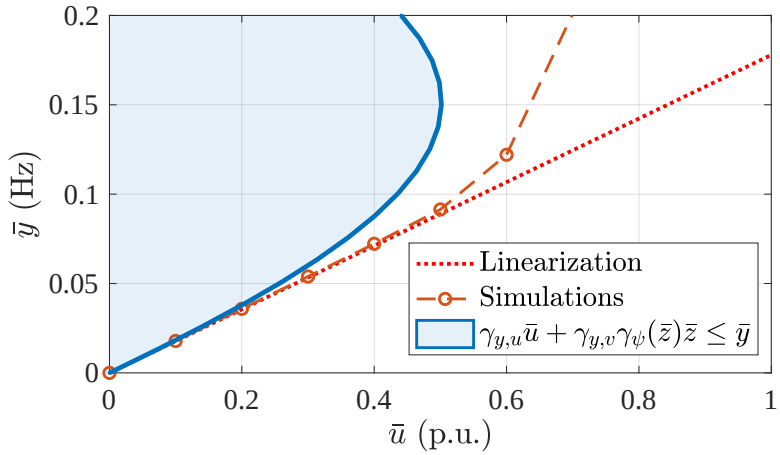

Figure 6-4: Maximum frequency deviation for a SMIB system.

Regarding the computation time, for the 9-bus system, the gain matrix took 1.86 seconds to compute, while the optimization took 0.017 seconds. For the 39-bus system, the computation time for the gain matrix was 166.9 seconds, while the optimization time was 0.148 seconds. Therefore, the most computationally intense step in our method is the computation of the gain matrix of the linear component, which requires simulation of impulse response and numerical integration. However, the computation time of the gain matrix could be improved by estimating only an upper-bound, rather than its exact value [4].

For the 39-bus case study, we consider the following disturbance scenarios: a step disturbance to represent the simultaneous tripping of distributed generators, and continuous disturbances to represent the varying power output from wind generation.

Simultaneous Distributed Generators tripping

In this scenario, we consider the simultaneous tripping of the loads at buses 3, 15, and 27. The active power loads at those buses are 3.22 p.u., 3.2 p.u., and 2.81 p.u., respectively. Under the frequency constraint of 0.5 Hz, the maximum tripped load magnitude needs to be less than 0.939 p.u. Without the frequency constraint, the maximum disturbance magnitude allowed at each load is 2.29 p.u..

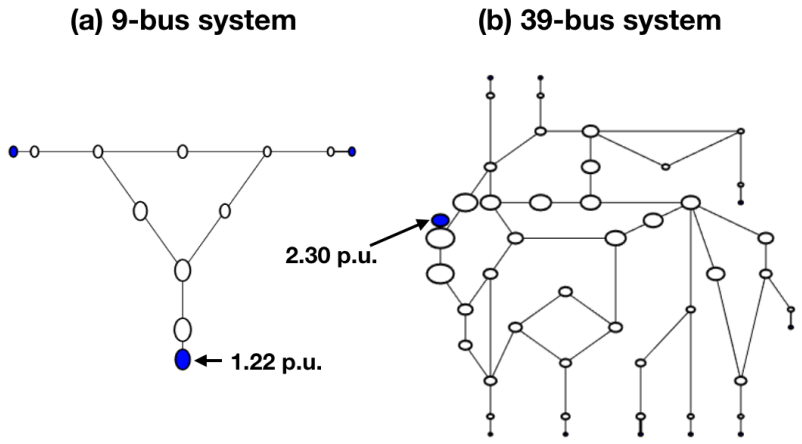

Figure 6-5: Maximum disturbance bound at every bus for the 9-bus and 39-bus systems. A disturbance on every individual node is considered and the resulting maximum bound is represented as the size of circle at that node. For both systems, a reference circle is labeled with its value.

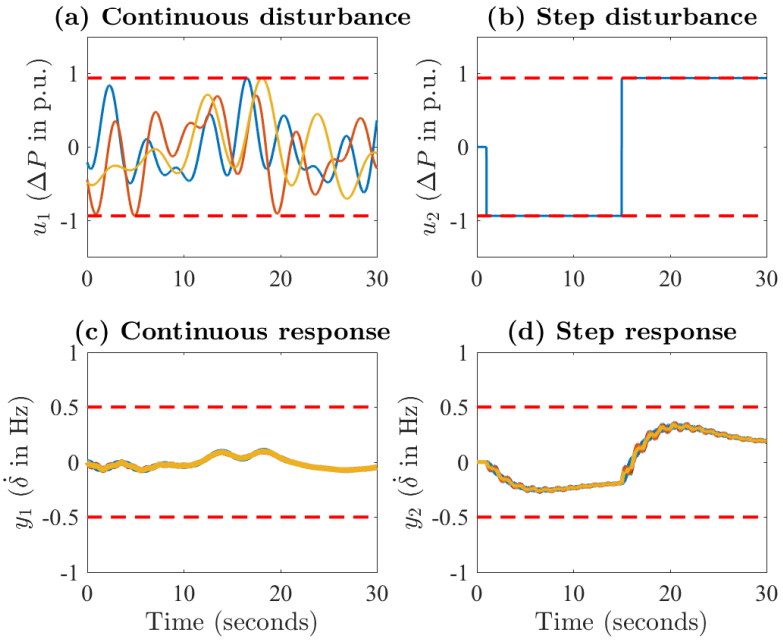

Figure 6-6: Simulation results for (a)varying wind generation, and (b) simultaneous generation tripping, together with their frequency response for the 39-bus system.

Wind generation

In this scenario, we consider the varying power output from wind generation at buses 1, 9, and 16. Under the frequency constraint of 0.5 Hz, the deviation from the nominal generation needs to be less than 1.305 p.u. Without the frequency constraint, a deviation in the active power of 2.02 p.u. is allowed at each wind generator.

6.6 Concluding Remarks

In this section, we proposed a notion of input-output stability in the presence of constraints on inputs and outputs. The applications in the electric power grid showed promising results for mitigating instabilities due to renewable energy. Time-domain simulation-based assessment of the system robustness against uncertain and stochastic disturbances is extremely time-consuming. The proposed method provided an optimization-based method with a robustness guarantee. The derived certificate is efficiently constructed via convex optimization and is shown to be non-conservative for different IEEE test cases.

Chapter 7

Conclusion

This chapter summarizes the contributions of this thesis and discusses potential future work and open problems. We developed a set of algorithms to solve robustness verification and optimization problems in both steady-state and dynamical settings. Our approach focused on providing guarantees for safety by ensuring that we meet a set of constraints. We achieve computational tractability by enforcing convexity using nonlinear envelopes. We summarize chapter-specific contributions below.

7.1 Summary of Contributions

In Chapter 2, we provided a convex sufficient condition that satisfies a set of nonlinear equality and inequality constraints. The benefit of convex restriction is that we can exploit convexity to enjoy computational efficiency and rich theory with a guarantee of feasibility. The technique developed in this chapter can be applied to a general set of nonlinear equations as long as the functions are continuous. We exploited the decomposability of the sparse structure in the problem and showed examples of how the trade-off between conservativeness and tractability can be controlled.

In Chapter 3, convex restriction was extended to consider uncertain variables that are unknown but bounded. The general approach is to ensure that the uncertainty set is inscribed by the convex restriction. Since convex restriction is a set of convex quadratic constraints, the standard robust counterpart of the constraint can be de-

rived. We present a number of cases where there are analytical expressions for the required robustness margin. The expressions are incorporated into convex restriction so that they can be added as a constraint to an optimization problem with the desired objective function.

In Chapter 4, we present a number of applications in robotics, neural network robustness verification, model predictive control, and optimal power flow problems. Its application in robust model predictive control requires the satisfaction of safety constraints under all realizations of uncertainty. Our formulation's main advantage is that it gives a unified treatment to the problem involving nonlinear dynamics, nonconvex safety constraints, and provable robustness against uncertainty. For power grid application, our approach addresses inherent uncertainties in power injections due to the growing quantities of renewable generation. The main advantage of our approach is its theoretical guarantees with respect to both power flow solvability and operational constraint satisfaction for robust AC OPF problems. In neural networks and robotics applications, convex restriction provides a method to find a convex subset of decision boundary and feasible configuration space. We demonstrated its wide applications across many domains.

In Chapter 5, we investigate reach avoid the problem with reachability analysis. We use convex relaxation to bound nonlinearity and the reachable sets could be solved via convex optimization. We explored methods to compute contraction metrics for discrete-time nonlinear systems. We showed that the contraction metrics could be used to construct the templates for reachable sets. In particular, the template from contraction metric yield if and only if condition for linear systems. We demonstrated the proposed method on IEEE power grid test cases.

In Chapter 6, we developed a method to quantify the relationship between the peak magnitudes of input and output of nonlinear dynamical systems. The method gives us the ability to compute the peak magnitude bounds on the input such that we satisfy constraints on peak magnitude bounds on the output. This is useful for engineering applications where there are safety constraints on the output, and the system operator needs to determine how much uncertainty the system can tolerate before violating

the safety constraints. We formulate the system as a Lur'e problem and use upper-convex lower-concave envelopes to bound the nonlinearity. The proposed condition is a convex sufficient condition with peak magnitudes on the input and output as decision variables. The condition can be used as a constraint in optimization to determine the worst-case bound on the input that is tolerable by the system without violating output constraints. We have demonstrated our approach in IEEE test cases for electric power grids.

7.2 Future Directions

The work presented in this thesis has several directions for future work. The first involves generalizing or specializing the envelopes used in this work to function with other unique properties such as monotonicity or quasi-convexity. The upper-convex lower-concave can be relaxed to upper-quasi-convex lower-quasi-concave envelopes, and the methods proposed in this thesis can be directly applied to obtain quasi-convex sufficient conditions for considered problems. In addition, the choice of sparse nonlinear representation is problem-specific, and the domain knowledge should be incorporated. Having the least amount of shared decision variable between nonlinear basis functions is important to reduce conservativeness. The manipulation of algebraic equations can also change the shape of the nonlinear manifold. Exploring different representations will result in different scalability and performance.

Another direction is finding a set of problems where the solution of sequential convex optimization can be simplified. If there are either analytical solutions or approximate solutions without having to call the convex optimization solver. One of the limitations of sequential convex restriction is that the algorithm still needs to solve large-scale convex optimization problems, which could require a significant computational burden. While our approach can be applied to a wide range of applications with constraints that are sometimes difficult to handle, there could be a class of problems where the solutions to the convex subproblems are easy to obtain.

Lastly, the envelopes for nonlinear functions provide a loose estimate of the model.

Data-driven methods could be further studied for deriving the envelopes for nonlinearities. With the limited amount of data, there is inherent uncertainty in model estimation, and our approach could be combined with the estimated error to provide confidence in the model. The combined framework could address the questions regarding the robustness of the estimated model.

Appendix A

Nonlinear Envelopes

A.1 Upper-Convex Lower-Concave Envelopes

A.1.1 Upper-Convex Lower-Concave Envelope for Bilinear Function

A bilinear function can be bounded by the following concave envelopes with some ρ_1, $\rho_2 > 0$ and the nominal point $(x^{(0)}, y^{(0)})$ [61],

$$\begin{aligned} xy &\geq x^{(0)}y^{(0)} + y^{(0)}(x - x^{(0)}) + x^{(0)}(y - y^{(0)}) - \frac{1}{4}\left[\rho_1(x - x^{(0)}) - \frac{1}{\rho_1}(y - y^{(0)})\right]^2 \\ xy &\leq x^{(0)}y^{(0)} + y^{(0)}(x - x^{(0)}) + x^{(0)}(y - y^{(0)}) + \frac{1}{4}\left[\rho_2(x - x^{(0)}) + \frac{1}{\rho_2}(y - y^{(0)})\right]^2. \end{aligned} \tag{A.1}$$

The over-estimator is tight along $\rho_2(x-x^{(0)})-\frac{1}{\rho_2}(y-y^{(0)}) = 0$, and the under-estimator is tight along $\rho_2(x - x^{(0)}) + \frac{1}{\rho_2}(y - y^{(0)}) = 0$. Both over- and under-estimators are tight at the nominal point, $(x^{(0)}, y^{(0)})$.

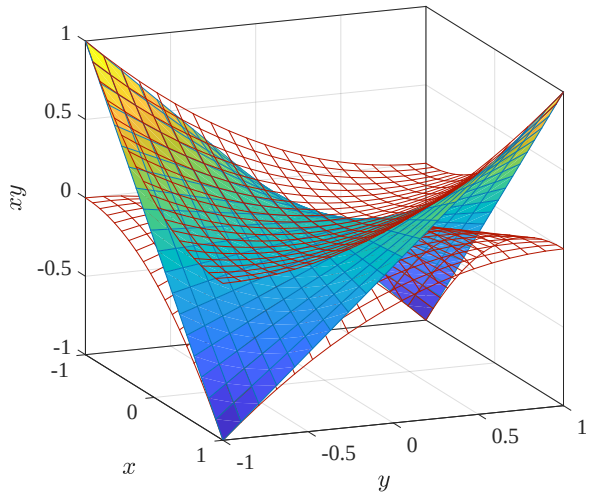

Figure A-1: Illustration of concave envelopes for a bilinear function.

A.1.2 Upper-Convex Lower-Concave Envelope for Unitary Quadratic Function

A unitary quad-ratic function can be bounded by the following quadratic concave envelopes for all x given the nominal point $x^{(0)}$ [61],

$$\begin{aligned} x^2 &\geq (x^{(0)})^2 + 2x^{(0)}(x - x^{(0)}) + (x - x^{(0)})^2 = x^2 \\ x^2 &\leq (x^{(0)})^2 + 2x^{(0)}(x - x^{(0)}) = 2x^{(0)}x - (x^{(0)})^2. \end{aligned} \tag{A.2}$$

A.1.3 Upper-Convex Lower-Concave Envelope for Trigonometric Function

Trigonometric functions can be bounded by the following quadratic concave envelopes for all θ given the nominal point θ_0,

$$\begin{aligned} \sin\theta &\geq \sin\theta^{(0)} + \cos\theta^{(0)}(\theta - \theta^{(0)}) - \frac{1}{2}(\theta - \theta^{(0)})^2 \\ \sin\theta &\leq \sin\theta^{(0)} + \cos\theta^{(0)}(\theta - \theta^{(0)}) + \frac{1}{2}(\theta - \theta^{(0)})^2, \end{aligned}$$

$$\begin{aligned} \cos\theta &\geq \cos\theta^{(0)} - \sin\theta^{(0)}(\theta - \theta^{(0)}) - \frac{1}{2}(\theta - \theta^{(0)})^2 \\ \cos\theta &\leq \cos\theta^{(0)} - \sin\theta^{(0)}(\theta - \theta^{(0)}) + \frac{1}{2}(\theta - \theta^{(0)})^2. \end{aligned}$$

A.1.4 Upper-Convex Lower-Concave Envelope for Logistic Function

A logistic function, $\sigma(x) = \frac{1}{1+e^{-x}}$, has the bounded second derivative of $\frac{\sqrt{3}}{18}$, and its quadratic concave envelope is

$$\sigma(x) \geq \sigma^{(0)} + \sigma^{(0)}(1-\sigma^{(0)})(x-x^{(0)}) - \frac{\sqrt{3}}{36}(x-x^{(0)})^2$$
$$\sigma(x) \leq \sigma^{(0)} + \sigma^{(0)}(1-\sigma^{(0)})(x-x^{(0)}) + \frac{\sqrt{3}}{36}(x-x^{(0)})^2.$$

where $x^{(0)}$ is the nominal point and $\sigma^{(0)} = \frac{1}{1+e^{-x^{(0)}}}$.

A.2 Upper-Concave Lower-Convex Envelopes

A.2.1 Upper-Concave Lower-Convex Envelope for Bilinear Function

A bilinear function can be outer-approximated by McCormick envelop [68]. Given the bounds, $\underline{x} \leq x \leq \overline{x}$ and $\underline{y} \leq y \leq \overline{y}$, the envelope is

$$\begin{aligned} xy &\geq \underline{x}y + x\underline{y} - \underline{x}\underline{y} \\ xy &\geq \overline{x}y + x\overline{y} - \overline{x}\overline{y} \\ xy &\leq \overline{x}y + x\underline{y} - \overline{x}\underline{y} \\ xy &\leq x\overline{y} + \underline{x}y - \underline{x}\overline{y}. \end{aligned} \tag{A.3}$$

A.2.2 Upper-Concave Lower-Convex Envelope for Trigonometric Function

Trigonometric functions can be bounded by the following quadratic envelopes provided in [30]. For all $x \in [-x^u, x^u]$, the envelopes are

$$\begin{aligned} \sin(x) &\leq \cos\left(\frac{x^u}{2}\right)\left(x - \frac{x^u}{2}\right) + \sin\left(\frac{x^u}{2}\right) \\ \sin(x) &\geq \cos\left(\frac{x^u}{2}\right)\left(x + \frac{x^u}{2}\right) - \sin\left(\frac{x^u}{2}\right), \end{aligned} \tag{A.4}$$

$$\begin{aligned} \cos(x) &\leq 1 - \frac{1 - \cos(x^u)}{(x^u)^2}x^2 \\ \cos(x) &\geq \cos\left(x^u\right). \end{aligned} \tag{A.5}$$

A.3 Formulations and Proofs for Chapter 4.1

A.3.1 Jacobian for System of Dynamical Equations

In this section, we derive the Jacobian of the system of equation and its inverse in Equation (2.4).

Jacobian for Explicit Time-discretization

The Jacobian for the system of equations, $F_{\text{explicit}}(\mathbf{x}, \mathbf{u}, \mathbf{w})$ in (4.8), evaluated at the nominal trajectory is given by

$$\frac{\partial F_{\text{explicit}}}{\partial \mathbf{x}} \bigg|_{(0)} = \begin{bmatrix} -I & \mathbf{0} & \dots & \mathbf{0} \\ A_1^{(0)} & -I & \mathbf{0} & \vdots \\ \mathbf{0} & \ddots & \ddots & \mathbf{0} \\ \mathbf{0} & \mathbf{0} & A_N^{(0)} & -I \end{bmatrix}, \tag{A.6}$$

where $A_t^{(0)} = I + h \cdot \frac{\partial f}{\partial x}\big|_{(x_{t-1}^{(0)}, u_t^{(0)}, w_t^{(0)})}$.

Lemma 15. The inverse of the Jacobian in (A.6) always exists and has the following closed-form representation,

$$\frac{\partial F_{\text{explicit}}}{\partial \mathbf{x}} \bigg|_{(0)}^{-1} = - \begin{bmatrix} I & \mathbf{0} & \dots & \mathbf{0} \\ A_{(1,0)}^{(0)} & I & \mathbf{0} & \vdots \\ \vdots & \ddots & \ddots & \mathbf{0} \\ A_{(N,0)}^{(0)} & \dots & A_{(N,N-1)}^{(0)} & I \end{bmatrix}, \tag{A.7}$$

where $A_{(i,j)}^{(0)}$ represents the linear sensitivity of the state at time step i with respect to the state at time step j. The sensitivity can be solved by applying the chain rule,

$$A_{(i,j)}^{(0)} = \prod_{t=j+1}^{i} \left(I + h \cdot \frac{\partial f}{\partial x}\Big|_{\left(x_{t-1}^{(0)}, u_t^{(0)}, w_t^{(0)}\right)} \right). \tag{A.8}$$

Lemma 15 can be checked by showing that multiplication of (A.6) and (A.7) is

an identity matrix.

Jacobian for Implicit Time-discretization

The Jacobian for the system of equations, $F_{\text{implicit}}(\mathbf{x}, \mathbf{u}, \mathbf{w})$ in (4.9), evaluated at the nominal trajectory is given by

$$\frac{\partial F_{\text{implicit}}}{\partial \mathbf{x}} \bigg|_{(0)} = \begin{bmatrix} -I & \mathbf{0} & \dots & \mathbf{0} \\ I & -A_1^{(0)} & \mathbf{0} & \vdots \\ \mathbf{0} & \ddots & \ddots & \mathbf{0} \\ \mathbf{0} & \mathbf{0} & I & -A_N^{(0)} \end{bmatrix}, \tag{A.9}$$

where $A_t^{(0)} = I - h \cdot \frac{\partial f}{\partial x}\big|_{(x_t^{(0)}, u_t^{(0)}, w_t^{(0)})}$.

Lemma 16. The inverse of the Jacobian in (A.9) always exists and has the following closed-form representation,

$$\frac{\partial F_{\text{implicit}}}{\partial \mathbf{x}} \bigg|_{(0)}^{-1} = - \begin{bmatrix} I & \mathbf{0} & \dots & \mathbf{0} \\ A_{(1,1)}^{(0),-1} & A_{(1,1)}^{(0),-1} & \mathbf{0} & \vdots \\ \vdots & \vdots & \ddots & \mathbf{0} \\ A_{(N,1)}^{(0),-1} & A_{(N,1)}^{(0),-1} & \dots & A_{(N,N)}^{(0),-1} \end{bmatrix}, \tag{A.10}$$

where $A_{(i,j)}^{(0)}$ represents the linear sensitivity of the state at time step i with respect to the state at time step j. The sensitivity can be solved by applying the chain rule,

$$A_{(i,j)}^{(0),-1} = \prod_{t=j}^{i} \left(I - h \cdot \frac{\partial f}{\partial x}\Big|_{\left(x_t^{(0)}, u_t^{(0)}, w_t^{(0)}\right)} \right)^{-1}. \tag{A.11}$$

Similar to explicit scheme, Lemma 16 can be checked by showing that multiplication of (A.9) and (A.10) is an identity matrix.

A.3.2 Residual Feedback Representation

The residual representation of the system involves the nonlinear residual function $g : (\mathbb{R}^n, \mathbb{R}^m) \to \mathbb{R}^n$,

$$\begin{aligned} \frac{d}{dt}x &= A(t)x + B(t)w + g(x,u,w) \\ g(x,u,w) &= f(x,u,w) - A(t)x - B(t)w \end{aligned} \tag{A.12}$$

where $A(t) = \frac{\partial f}{\partial x}\big|_{(x^{(0)},u^{(0)},w^{(0)})}$ and $B(t) = \frac{\partial f}{\partial w}\big|_{(x^{(0)},u^{(0)},w^{(0)})}$ are the Jacobians of the system dynamics evaluated at the nominal values. This representation is related to the Lur'e form in control [87, 54], which uses the sector bound to contain the nonlinearity. Similarly, we use upper-convex and lower-concave envelopes for bounding the nonlinearity.

The residual functions in (4.11) has the following representation for explicit scheme,

$$\boldsymbol{g}_{\text{explicit}}(\mathbf{x},\mathbf{u},\mathbf{w}) = \begin{bmatrix} \mathbf{0}_n \\ h \cdot g(x_0,u_1,w_1) \\ \vdots \\ h \cdot g(x_{N-1},u_N,w_N) \end{bmatrix}, \tag{A.13}$$

and for implicit scheme,

$$\boldsymbol{g}_{\text{implicit}}(\mathbf{x},\mathbf{u},\mathbf{w}) = \begin{bmatrix} \mathbf{0}_n \\ h \cdot g(x_1,u_1,w_1) \\ \vdots \\ h \cdot g(x_N,u_N,w_N) \end{bmatrix}, \tag{A.14}$$

where $g(x,u,w)$ is the nonlinear residual defined in (A.12) and $\mathbf{0}_n \in \mathbb{R}^n$ is a vector of zeros.

The worst-case contribution from the residual function over the domain $x \in$

$\mathcal{P}(x^u, x^\ell)$ and $w \in \mathcal{W}(\gamma)$ are

$$\begin{aligned} \boldsymbol{g}^u_{\mathcal{P},k}(\mathbf{u}, \mathbf{x}^u, \mathbf{x}^\ell) &= \max_{\mathbf{x}\in\mathcal{P}(\mathbf{x}^\ell,\mathbf{x}^u)} \max_{\mathbf{w}\in\mathcal{W}(\gamma)} \ \boldsymbol{g}^u_k(\mathbf{x}, \mathbf{u}, \mathbf{w}), \\ \boldsymbol{g}^\ell_{\mathcal{P},k}(\mathbf{u}, \mathbf{x}^u, \mathbf{x}^\ell) &= \min_{\mathbf{x}\in\mathcal{P}(\mathbf{x}^\ell,\mathbf{x}^u)} \min_{\mathbf{w}\in\mathcal{W}(\gamma)} \ \boldsymbol{g}^\ell_k(\mathbf{x}, \mathbf{u}, \mathbf{w}). \end{aligned} \tag{A.15}$$

A.3.3 Proof of Lemma 7

Proof. The necessary and sufficient condition for optimality for the projection problem in (4.15) is

$$(P_{\mathcal{B}_{t,i}}[x_t^{(0)}] - x_t^{(0)})^T(\tilde{x} - P_{\mathcal{B}_{t,i}}[x_t^{(0)}]) \geq 0, \ \ \forall \tilde{x} \in \mathcal{B}_{t,(i)},$$

for $i = 1, \ldots, s$. The condition, $L_t x_t + d_t < 0$, ensures that

$$(P_{\mathcal{B}_{t,i}}[x_t^{(0)}] - x_t^{(0)})^T(x_t - P_{\mathcal{B}_{t,i}}[x_t^{(0)}]) < 0, \ \ i = 1, \ldots, s.$$

Therefore, $x_t \notin \mathcal{B}_{t,(i)}$ for $i = 1, \ldots, s$. Therefore, the state x_t satisfies the safety constraints. □

Bibliography

[1] Matthias Althoff. Formal and compositional analysis of power systems using reachable sets. *IEEE Transactions on Power Systems*, 29(5):2270–2280, 2014.

[2] Liviu Aolaritei, Dongchan Lee, Thanh Long Vu, and Konstantin Turitsyn. A Robustness Measure of Transient Stability under Operational Constraints in Power Systems. *IEEE Control Systems Letters*, 2(4):803–808, oct 2018.

[3] Igor Averbakh and Yun-Bin Zhao. Explicit Reformulations for Robust Optimization Problems with General Uncertainty Sets. *SIAM Journal on Optimization*, 18(4):1436–1466, 2008.

[4] V Balakrishnan and S Boyd. On computing the worst-case peak gain of linear systems. *Systems & Control Letters*, 19(4):265–269, 1992.

[5] Stefan Banach. Sur les opérations dans les ensembles abstraits et leur application aux équations intégrales. *Fund. math*, 3(1):133–181, 1922.

[6] Somil Bansal, Anayo K Akametalu, Frank J Jiang, Forrest Laine, and Claire J Tomlin. Learning quadrotor dynamics using neural network for flight control. In *IEEE Conference on Decision and Control*, pages 4653–4660, 2016.

[7] Alberto Bemporad and Manfred Morari. Robust model predictive control: A survey. In A Garulli and A Tesi, editors, *Robustness in identification and control*, pages 207–226, London, 1999. Springer London.

[8] Mohamed Amin Ben Sassi, Romain Testylier, Thao Dang, and Antoine Girard. *Reachability Analysis of Polynomial Systems Using Linear Programming Relaxations*, pages 137–151. Springer Berlin Heidelberg, Berlin, Heidelberg, 2012.

[9] A. Ben-Tal and A. Nemirovski. Robust solutions of uncertain linear programs. *Operations Research Letters*, 25(1):1–13, aug 1999.

[10] Aharon Ben-Tal, Dick den Hertog, and Jean Philippe Vial. Deriving robust counterparts of nonlinear uncertain inequalities. *Mathematical Programming*, 149(1-2):265–299, feb 2014.

[11] Aharon Ben-Tal, Laurent El Ghaoui, and Arkadi Nemirovski. *Robust optimization*. Princeton University Press, 2009.

[12] Aharon Ben-Tal and Arkadi Nemirovski. On Tractable Approximations of Uncertain Linear Matrix Inequalities Affected by Interval Uncertainty. *SIAM Journal on Optimization*, 12(3):811–833, 2003.

[13] Dimitri P Bertsekas. *Nonlinear programming*. Athena Scientific, 1999.

[14] Dimitris Bertsimas, David B Brown, and Constantine Caramanis. Theory and applications of robust optimization. *SIAM review*, 53(3):464–501, 2011.

[15] Dimitris Bertsimas, Dessislava Pachamanova, and Melvyn Sim. Robust linear optimization under general norms. *Operations Research Letters*, 32(6):510–516, nov 2004.

[16] Hans Georg Beyer and Bernhard Sendhoff. Robust optimization - a comprehensive survey. *Computer Methods in Applied Mechanics and Engineering*, 196(33-34):3190–3218, 2007.

[17] Paul T Boggs and Jon W Tolle. Sequential quadratic programming. *Acta Numerica*, 4:1, 1995.

[18] Kim C Border. *Fixed point theorems with applications to economics and game theory*. Cambridge University Press, 1989.

[19] Luitzen Egbertus Jan Brouwer. Über abbildung von mannigfaltigkeiten. *Mathematische Annalen*, 71(1):97–115, 1911.

[20] Francesco Bullo. *Lectures on Network Systems*. http://motion.me.ucsb.edu/book-lns/, 2017.

[21] Richard H Byrd, Frank E Curtis, and Jorge Nocedal. An Inexact SQP Method for Equality Constrained Optimization. *SIAM Journal on Optimization*, 19(1):351–369, 2008.

[22] Richard H Byrd, Frank E Curtis, and Jorge Nocedal. An inexact Newton method for nonconvex equality constrained optimization. *Mathematical Programming*, 122(2):273–299, 2010.

[23] Giuseppe Calafiore and Laurent El Ghaoui. Ellipsoidal bounds for uncertain linear equations and dynamical systems. *Automatica*, 40(5):773–787, 2004.

[24] Eduardo F Camacho and Carlos Bordons Alba. *Model predictive control*. Springer science & business media, 2013.

[25] Nicholas Carlini and David Wagner. Towards evaluating the robustness of neural networks. In *IEEE Symposium on Security and Privacy*, pages 39–57, 2017.

[26] Y C Chen and A D Dominguez-Garcia. A Method to Study the Effect of Renewable Resource Variability on Power System Dynamics. *IEEE Transactions on Power Systems*, 27(4):1978–1989, 2012.

[27] Hyungjin Choi, Peter J. Seiler, and Sairaj V. Dhople. Propagating Uncertainty in Power-System DAE Models with Semidefinite Programming. *IEEE Transactions on Power Systems*, 32(4):3146–3156, jul 2017.

[28] Joe H Chow, G Peponides, P V Kokotovic, B Avramovic, and J R Winkelman. *Time-Scale Modeling of Dynamic Networks with Applications to Power Systems*, volume 46. Springer, 1982.

[29] Ignasi Clavera, Jonas Rothfuss, John Schulman, Yasuhiro Fujita, Tamim Asfour, and Pieter Abbeel. Model-based reinforcement learning via meta-policy optimization. In *Conference on Robot Learning*, pages 617–629, 2018.

[30] C. Coffrin, H. L. Hijazi, and P. Van Hentenryck. The QC Relaxation: A Theoretical and Computational Study on Optimal Power Flow. *IEEE Transactions on Power Systems*, 31(4):3008–3018, July 2016.

[31] Carleton Coffrin, Russell Bent, Kaarthik Sundar, Yeesian Ng, and Miles Lubin. PowerModels.jl: An Open-Source Framework for Exploring Power Flow Formulations. In *Power Systems Computation Conference (PSCC)*, June 2018.

[32] Andrew R Conn, Nicholas I M Gould, and Ph L Toint. *Trust region methods*, volume 1. Siam, 2000.

[33] Frank E Curtis, Travis C Johnson, Daniel P Robinson, and Andreas Wächter. An Inexact Sequential Quadratic Optimization Algorithm for Nonlinear Optimization. *SIAM Journal on Optimization*, 24(3):1041–1074, 2014.

[34] Thao Dang and Romain Testylier. Reachability analysis for polynomial dynamical systems using the Bernstein expansion. *Reliable Computing*, 17(1):1–24, 2011.

[35] Steven Diamond and Stephen Boyd. CVXPY: A Python-embedded modeling language for convex optimization. *Journal of Machine Learning Research*, 17(83):1–5, 2016.

[36] U Dini. Analisi infinitesimale, lezioni dettate nella r. *Universitá di Pisa (1877/78)*, 1877.

[37] Zhao Yang Dong, Jun Hua Zhao, and David J Hill. Numerical simulation for stochastic transient stability assessment. *IEEE Transactions on Power Systems*, 27(4):1741–1749, nov 2012.

[38] Asen L Dontchev and R Tyrrell Rockafellar. *Implicit functions and solution mappings*, volume 543. Springer, 2009.

[39] Iain Dunning, Joey Huchette, and Miles Lubin. JuMP: A Modeling Language for Mathematical Optimization. *SIAM Review*, 59(2):295–320, 2017.

[40] Krishnamurthy Dj Dvijotham, Robert Stanforth, Sven Gowal, Chongli Qin, Soham De, and Pushmeet Kohli. Efficient neural network verification with exactness characterization. In *Annual Conference on Uncertainty in Artificial Intelligence*, 2019.

[41] Laurent El Ghaoui and Hervé Lebret. Robust Solutions to Least-Squares Problems with Uncertain Data. *SIAM Journal on Matrix Analysis and Applications*, 18(4):1035–1064, 2003.

[42] Mahyar Fazlyab, Manfred Morari, and George J Pappas. Safety Verification and Robustness Analysis of Neural Networks via Quadratic Constraints and Semidefinite Programming. *arXiv preprint arXiv:1903.01287*, 2019.

[43] Monique Florenzano. *General equilibrium analysis: existence and optimality properties of equilibria*. Springer Science & Business Media, 2003.

[44] Virginie Gabrel, Cécile Murat, and Aurélie Thiele. Recent advances in robust optimization: An overview, jun 2014.

[45] Ian Goodfellow, Patrick McDaniel, and Nicolas Papernot. Making machine learning robust against adversarial inputs. *Communications of the ACM*, 61(7):56–66, jun 2018.

[46] Ian Goodfellow, Jonathon Shlens, and Christian Szegedy. Explaining and harnessing adversarial examples. In *International Conference on Learning Representations*, 2015.

[47] Nick Gould, Dominique Orban, and Philippe Toint. Numerical methods for large-scale nonlinear optimization, may 2005.

[48] LLC Gurobi Optimization. Gurobi optimizer reference manual, 2020.

[49] Hassan Hijazi, Carleton Coffrin, and Pascal Van Hentenryck. Convex quadratic relaxations for mixed-integer nonlinear programs in power systems. *Mathematical Programming Computation*, 9(3):321–367, 2017.

[50] IEEE PES Task Force on Benchmarks for Validation of Emerging Power System Algorithms. The Power Grid Library for Benchmarking AC Optimal Power Flow Algorithms. *arXiv:1908.02788*, Aug. 2019.

[51] Christian Jansson and Olaf Knüppel. *Numerical results for a self-validating global optimization method*. Technical Report 94-1, TU Hamburg-Harburg, 1994.

[52] Luc Jaulin. Nonlinear bounded-error state estimation of continuous-time systems. *Automatica*, 38(6):1079–1082, 2002.

[53] Kai Kellner, Thorsten Theobald, and Christian Trabandt. Containment Problems for Polytopes and Spectrahedra. *SIAM Journal on Optimization*, 23(2):1000–1020, 2013.

[54] Hassan K Khalil. Noninear Systems. *Prentice-Hall, New Jersey*, 2(5):1–5, 1996.

[55] Basil Kouvaritakis and Mark Cannon. Model predictive control. *Switzerland: Springer International Publishing*, 2016.

[56] Krishnamurthy, Dvijotham, Robert Stanforth, Sven Gowal, Timothy Mann, and Pushmeet Kohli. A Dual Approach to Scalable Verification of Deep Networks. *Annual Conference on Uncertainty in Artificial Intelligence*, 2018.

[57] Alexey Kurakin, Ian Goodfellow, and Samy Bengio. Adversarial examples in the physical world. *arXiv preprint arXiv:1607.02533*, 2016.

[58] Alex A Kurzhanskiy and Pravin Varaiya. Ellipsoidal techniques for reachability analysis of discrete-time linear systems. *IEEE Transactions on Automatic Control*, 52(1):26–38, 2007.

[59] Yann LeCun, Léon Bottou, Yoshua Bengio, and Patrick Haffner. Gradient-based learning applied to document recognition. *Proceedings of the IEEE*, 86(11):2278–2324, 1998.

[60] Dongchan Lee, Liviu Aolaritei, Thanh Long Vu, and Konstantin Turitsyn. Robustness against disturbances in power systems under frequency constraints. *IEEE Transactions on Control of Network Systems*, 6(3):971–979, 2019.

[61] Dongchan Lee, Hung D. Nguyen, Krishnamurthy Dvijotham, and Konstantin Turitsyn. Convex restriction of power flow feasibility sets. *IEEE Transactions on Control of Network Systems*, 6(3):1235–1245, 2019.

[62] Dongchan Lee and Konstantin Turitsyn. Robust Transient Stability Assessment via Reachability Analysis. In *Bulk power systems dynamics and control symposium (iREP)*, 2017.

[63] Dongchan Lee, Konstantin Turitsyn, Daniel K. Molzahn, and Line A. Roald. Feasible path identification in optimal power flow with sequential convex restriction. *IEEE Transactions on Power Systems*, 35(5):3648–3659, 2020.

[64] Dongchan Lee, Konstantin Turitsyn, Daniel K. Molzahn, and Line A. Roald. Robust ac optimal power flow with robust convex restriction. *IEEE Transactions on Power Systems*, 36(6):4953–4966, 2021.

[65] Dongchan Lee, Konstantin Turitsyn, and Jean-Jacques Slotine. Sequential convex restriction and its applications in robust optimization. *arXiv preprint arXiv:1909.01778*, 2019.

[66] Dongchan Lee, Konstantin Turitsyn, and Jean-Jacques Slotine. Robust model predictive control for nonlinear systems using convex restriction. *arXiv preprint arXiv:2003.00345*, 2020.

[67] Winfried Lohmiller and Jean-Jacques E Slotine. On contraction analysis for non-linear systems. *Automatica*, 34(6):683–696, 1998.

[68] Garth P McCormick. Computability of global solutions to factorable nonconvex programs: Part i—convex underestimating problems. *Mathematical programming*, 10(1):147–175, 1976.

[69] Federico Milano and Rafael Zarate-Minano. A Systematic Method to Model Power Systems as Stochastic Differential Algebraic Equations. *IEEE Transactions on Power Systems*, 28(4):4537–4544, nov 2013.

[70] Alexander Mitsos, Benoit Chachuat, and Paul I Barton. Mccormick-based relaxations of algorithms. *SIAM Journal on Optimization*, 20(2):573–601, 2009.

[71] Volodymyr Mnih, Koray Kavukcuoglu, David Silver, Alex Graves, Ioannis Antonoglou, Daan Wierstra, and Martin Riedmiller. Playing atari with deep reinforcement learning. *arXiv preprint arXiv:1312.5602*, 2013.

[72] Seyed-Mohsen Moosavi-Dezfooli, Alhussein Fawzi, and Pascal Frossard. Deepfool: A simple and accurate method to fool deep neural networks. In *IEEE Conference on Computer Vision and Pattern Recognition*, pages 2574–2582, 2016.

[73] Anusha Nagabandi, Gregory Kahn, Ronald S Fearing, and Sergey Levine. Neural network dynamics for model-based deep reinforcement learning with model-free fine-tuning. In *IEEE International Conference on Robotics and Automation*, pages 7559–7566, 2018.

[74] Jorge Nocedal and Stephen Wright. *Numerical optimization*. Springer Science & Business Media, 2006.

[75] Panagiotis N. Papadopoulos and Jovica V. Milanović. Probabilistic Framework for Transient Stability Assessment of Power Systems with High Penetration of Renewable Generation. *IEEE Transactions on Power Systems*, 32(4):3078–3088, jul 2017.

[76] Jaehyun Park and Stephen Boyd. General heuristics for nonconvex quadratically constrained quadratic programming. *arXiv preprint arXiv:1703.07870*, 2017.

[77] Adam Paszke, Sam Gross, Francisco Massa, Adam Lerer, James Bradbury, Gregory Chanan, Trevor Killeen, Zeming Lin, Natalia Gimelshein, Luca Antiga, Alban Desmaison, Andreas Kopf, Edward Yang, Zachary DeVito, Martin Raison, Alykhan Tejani, Sasank Chilamkurthy, Benoit Steiner, Lu Fang, Junjie Bai, and Soumith Chintala. Pytorch: An imperative style, high-performance deep learning library. In *Advances in Neural Information Processing Systems 32*, pages 8024–8035, 2019.

[78] Hugo N. Villegas Pico, Dionysios C. Aliprantis, and Elena C. Hoff. Reachability analysis of power system frequency dynamics with new high-capacity HVAC

and HVDC transmission lines. In *2013 IREP Symposium Bulk Power System Dynamics and Control - IX Optimization, Security and Control of the Emerging Power Grid*, aug 2013.

[79] R J Plemmons. M-matrix characterizations.I—nonsingular M-matrices. *Linear Algebra and its Applications*, 18(2):175–188, 1977.

[80] Ali Punjani and Pieter Abbeel. Deep learning helicopter dynamics models. In *IEEE International Conference on Robotics and Automation*, pages 3223–3230, 2015.

[81] James Blake Rawlings, David Q Mayne, and Moritz M Diehl. *Model Predictive Control: Theory, Computation, and Design*. Nob Hill Publishing, 2017.

[82] Moonkyung Ryu, Yinlam Chow, Ross Anderson, Christian Tjandraatmadja, and Craig Boutilier. Caql: Continuous action q-learning. In *International Conference on Learning Representations*, 2020.

[83] John Schulman, Yan Duan, Jonathan Ho, Alex Lee, Ibrahim Awwal, Henry Bradlow, Jia Pan, Sachin Patil, Ken Goldberg, and Pieter Abbeel. Motion planning with sequential convex optimization and convex collision checking. *The International Journal of Robotics Research*, 33(9):1251–1270, 2014.

[84] Gagandeep Singh, Timon Gehr, Matthew Mirman, Markus Püschel, and Martin Vechev. Fast and effective robustness certification. In *Advances in Neural Information Processing Systems*, pages 10802–10813, 2018.

[85] Gagandeep Singh, Timon Gehr, Markus Püschel, and Martin Vechev. An abstract domain for certifying neural networks. *Proceedings of the ACM on Programming Languages*, 3:1–30, 2019.

[86] Sumeet Singh, Anirudha Majumdar, Jean-Jacques Slotine, and Marco Pavone. Robust Online Motion Planning via Contraction Theory and Convex Optimization. *ICRA submission*, 2017.

[87] Jean-Jacques E Slotine, Weiping Li, et al. *Applied nonlinear control*. Prentice hall Englewood Cliffs, NJ, 1991.

[88] Vincent Tjeng, Kai Xiao, and Russ Tedrake. Evaluating Robustness of Neural Networks with Mixed Integer Programming. *International Conference on Learning Representations*, 2019.

[89] Pauli Virtanen, Ralf Gommers, Travis E. Oliphant, Matt Haberland, Tyler Reddy, David Cournapeau, Evgeni Burovski, Pearu Peterson, Warren Weckesser, Jonathan Bright, Stéfan J. van der Walt, Matthew Brett, Joshua Wilson, K. Jarrod Millman, Nikolay Mayorov, Andrew R. J. Nelson, Eric Jones, Robert Kern, Eric Larson, CJ Carey, İlhan Polat, Yu Feng, Eric W. Moore, Jake Vand erPlas, Denis Laxalde, Josef Perktold, Robert Cimrman, Ian Henriksen, E. A. Quintero,

Charles R Harris, Anne M. Archibald, Antônio H. Ribeiro, Fabian Pedregosa, Paul van Mulbregt, and SciPy 1. 0 Contributors. SciPy 1.0: Fundamental Algorithms for Scientific Computing in Python. *Nature Methods*, 17:261–272, 2020.

[90] Andreas Wächter and Lorenz T Biegler. On the Implementation of an Interior-Point Filter Line-Search Algorithm for Large-Scale Nonlinear Programming. *Mathematical Programming*, 106(1):25–57, 2006.

[91] Erik Weitenberg and Claudio De Persis. Robustness to noise of distributed averaging integral controllers in power networks. *Systems & Control Letters*, 119:1–7, 2018.

[92] Eric Wong, Frank Schmidt, Jan Hendrik Metzen, and J Zico Kolter. Scaling provable adversarial defenses. In *Advances in Neural Information Processing Systems*, pages 8400–8409, 2018.

[93] Y Zhang. General robust-optimization formulation for nonlinear programming. *Journal of Optimization Theory and Applications*, 132(1):111–124, 2007.

[94] Y. Zhang and J. Cortés. Characterizing tolerable disturbances for transient-state safety in power networks. *IEEE Transactions on Network Science and Engineering*, pages 1–1, 2018.